CHAPTER 3

NUMERICAL EXPERIMENTS

This chapter gives the collected results of numerical experiments with the elementary model, which is apparently the simplest but is at the same time adequate for the basic problem concerning the motion of a system of weakly coupled non-linear oscillators. In this chapter we shall mainly study the basic criterion of stochasticity according to the overlapping of resonances, and also some details of the structure of the motion of a system with divided phase space. In our opinion the experimental results obtained below form a sufficiently reliable basis for the theory of stochasticity developed in this paper. Further experiments with more complicated models will be presented in the next chapter.

3.1 General remarks

In the last chapter by means of semi-qualitative physical considerations we established the existence and estimated the position of the border of stochasticity for a one-dimensional non-linear oscillator under the action of external periodic perturbation. This is the main result given in this paper. Unfortunately, attempts at rigorous mathematical analysis of the problem have so far met with insurmountable difficulties, due mainly to the very complicated structure of the phase plane of the system (see Sections 2.8 and 3.3). Under these conditions it is natural to turn to experiments. In the present case, however, it is not necessary to carry out "real" experiments, i.e. to observe the motion of some kinds of real mechanical systems; furthermore, this is not so simple to do from a technical point of view, since conservative systems are what interest us most. Apparently the best approximation would be the motion of protons in colliding beam storage rings[80]. However, no such rings have yet been built**). A rather less suitable experiment (because of radiation damping) is the motion of electrons in a magnetic trap under ultra-high vacuum. Such experiments have been carried out[81-83] with interesting results, which will be discussed in Section 4.4. Of course, the charm of "real" experiments is that in investigating even the simplest question one may encounter a new fundamental law of nature by chance. However, if we limit ourselves a priori to so-called "constructive" physics*) (see Introduction), i.e. solely to the consequences of firmly established fundamental laws of nature, in the present case the laws of mechanics, a much simpler and in a sense more powerful method of investigation is what is known as numerical experimentation, which in the present case is taken to mean numerical integration of the equations of motion by a digital computer. Of course, one can consider the computer itself to be a specific mechanical system and calculating in it as a special case of a "real" experiment, exactly as, let us say, the motion of electrons in a magnetic trap can, in its turn, be considered as an analogue (electronic!) computer. Nevertheless, this "special" case (the computer) is sharply distinguished by its unusual, or one could say unlimited, flexibility, bearing in mind the principles of construction of the computer and ignoring the merely technical limitations of the present day. Of course the latter must be carefully taken into account; as in any experiment, they determine its ultimate possibilities. For the computer the main limitations are:

---

*) This apparently not very felicitous term is used to signify such wide areas of physics as, for instance, statistical physics or chemistry (see below) as distinct from the narrower and more specialized problems of technical and applied physics.

**) The author is happy to be wrong now on this point after the successful putting into operation of the first proton Intersecting Storage Rings (ISR) at CERN.

a) computation speed ($\sim 10^6$ operations per second for typical present-day computers;

b) operational memory size ($\sim 10^7$ bits);

c) number of (binary) digits of the mantissa, on which the computing accuracy depends, and also the degree of continuity of the quantities in the computer presentation (≈ 50).

The best type of dynamical system for computer experiments is a cascade, i.e. a transformation with discrete time. With the above-mentioned limitations one can confidently work in times $\sim 10^8$ steps (iterations), rising in individual cases to 10^{10} steps (Section 3.3). On changing over from a cascade to a flux, i.e. to differential equations, the situation deteriorates considerably, since in order to ensure reasonable accuracy one is obliged to take an extremely small integration step and the actual duration of the process under investigation is considerably reduced. The situation is extremely bad for the integration of equations in partial derivatives, especially many-dimensional ones; here the operational memory of the computer is utterly insufficient. In this connection we wish to draw attention to a computing system of a new type, "Illiac-4", now being installed at the University of Illinois (USA), which is a combination of 256 central processors of ordinary computers[86] [see also Ref. 87)]. For a certain class of problem, including the integration of equations in partial derivatives, the effective computation speed of this machine reaches 10^9 operations per second. This would be indeed an enormous step forward in the technique of numerical experimentation!

Thus we must turn to numerical experimentation. Of course, the laws obtained by this method must also somehow be derived by simple deduction from the equations of motion. The ergodic theory works in just this way. It is interesting to note that the difficulties occuring here are connected not only (and probably not so much) with proving the corresponding theorems, but also with formulating them. For, the more complicated the phenomenon the greater the quantity of increasingly intricate conditions that have to be introduced in order to ensure the "mathematical rigour" of the theorem. Therefore, in a number of cases the result can be obtained much faster by inductive means (as in fundamental physics), i.e. by means of generalization, extrapolation, analogy, check experiments, etc., with the specific aim of constructing an approximate theory and, what is more important, the whole system of notions and models connected with it, which enable us to approach the practical problems of applied physics. It is therefore natural for the main value attaching to experimentation in this region to be heuristic, i.e. it should help us to guess a correct approximate theory or at least to understand correctly, even though qualitatively, the fundamental features of the phenomenon concerned. Therefore, it is not necessary for us to integrate the very complex equations of motion of real mechanical systems, it is sufficient to examine the most simple models that are adequate for the main problem. It is evident that the correct choice of a model is also one of the main difficulties of such experimentation.

The conception under discussion is generally well-known and widely applied in such areas of "constructive" physics as oscillation theory, hydrodynamics, statistical mechanics and even chemistry*). Here we should like only to point out again two important aspects:

---

*) See for example the very interesting Nobel lecture of Mulliken[128] where he says in particular: "... I should like once more to express my conviction that the age of computational chemistry has already begun, when hundreds (if not thousands) of chemists will switch from laboratory work to computation for the study of newer and newer problems".

firstly, the need to combine experimentation ("real" or numerical) with analytical theory, even though semiqualitative, without which it is completely impossible to orientate oneself in the inexhaustible sea of phenomena of applied physics; secondly, any use of numerical experimentation is just a heuristic method and not simply a way of obtaining specific numerical data*).

In this connection it should be noted that perhaps the main advantage of numerical experimentation, apart from its simplicity and convenience (when there is a good computer available!) is the possibility of extremely "pure", i.e. fully controlled, organization of the experiment and extremely flexible variation of the conditions, unattainable in a "real" experiment. Furthermore, a computer offers wide scope for processing, including logical processing, of computation results, even without output from the machine, and these possibilities are beginning to be used also in "real" experiments, for instance by on-line computers. The main drawback of numerical experiment, better termed "apparatus" effect, which needs careful watching, consists of so-called "computation errors", which boil down to round-off "errors", i.e. connected with the finite number of mantissa digits in the computer. The space of all quantities in computer experiments can be said to be "quantized". This "apparatus" effect will be thoroughly discussed in Section 3.3.

Below we describe numerical experiments with the most simple models specially constructed for investigating the fundamental characteristics of stochasticity. In the next chapter we shall deal with some applications of the theory developed to more or less practical problems. The numerical experiments carried out in this connection may also be considered as a continuation of the experiments with the most simple models, although they are already considerably more difficult to interpret on account of the much greater complexity of the corresponding dynamical systems. This last remark applies also to the incomplete numerical experiments with the most simple many-dimensional system, described in Section 3.6.

Quite a number of papers have appeared recently on the subject of numerical experiments similar to those described in this and the subsequent chapters. Perhaps the closest results are those obtained by Hénon and Heiles[92] and Greene[47]. References to other papers are made in the course of our report.

In what follows, for the sake of brevity we shall replace the term "numerical experiment" by the term "experiment"; this will not lead to misunderstandings, since everywhere in this paper except in Section 4.4 we mention only numerical experiments.

The majority of the experiments described in this chapter (except for Section 3.6) were carried out on the BESM-6 at the Computing Centre of the Siberian Section of the USSR Academy of Sciences, in co-operation with Israelev.

---

*) There is a very interesting discussion of the heuristic role of the computer in an even wider class of so-called mathematical experiments, not necessarily connected with the integration of differential equations, in a paper by Ulam[93]. It is also extremely useful permanently to associate computer experimentation with the experimenter's theoretical conclusions. This continuous link between man and machine has even been given a special name, the "synergetic approach" [93,94]. It seems to us, however, that this is a typical experimental situation and the "synergetic approach" can be considered simply as a special case of "real" experiment.

3.2 Choice of model and processing of computation results

The detailed analysis made in the previous chapter showed that the phenomenon of stochasticity can be reduced, ultimately, to an elementary model (Section 2.4), which for convenience we will re-write again in the form:

$$\begin{aligned} \varphi' &= \{ \varphi + k \cdot f(\psi) \} \\ \psi' &= \{ \psi + \varphi' \} \end{aligned} \qquad (3.2.1)$$

where the brackets signify, as usual, the fractional part of the argument. The possibility of simplifying the problem in this way is due, in particular, to the fact that the elementary model describes the motion in the stochastic layer near the non-linear resonance separatrix, which is the "nucleus" of any stochasticity (Section 2.6). Therefore our basic experiments, described in this chapter, were carried out with the elementary model (3.2.1). Only in the last section shall we introduce the results of some experiments with a many-dimensional system. The model for these experiments, close to the elementary model, will be described there (Section 3.6).

The form of the function $f(\psi)$ in (3.2.1) ("force") was determined mainly by reasons connected with choosing the case that would be the simplest for computing while being non-trivial. Non-triviality signifies the presence of "islets" of stability in the stochastic component, or of quasi-resonances (Sections 2.8 and 3.5). An example of a trivial "force" is the function*)

$$f(\psi) = \psi - 1/2 \qquad (3.2.2)$$

for which stochasticity was rigorously proved recently by Oseledets and Sinai under the condition of local instability (Section 2.8).

The "saw" type "force" used below is of the same type:

$$f(\psi) = \begin{cases} \psi - 1/4 ; & \psi \leq 1/2 \\ 3/4 - \psi ; & \psi \geq 1/2 \end{cases} \qquad (3.2.3)$$

However, if we "smooth out" the peaks of the "saw" by the quadratic function:

$$f_{sm}(\psi) = \frac{1}{4} - \delta - \lambda \cdot (\psi - 1/2)^2 \qquad (3.2.4)$$

for $\psi \approx \frac{1}{2}$ and similarly for $\psi \approx 0$; 1, this "smoothed-out saw" is already a non-trivial "force", since these quadratic sections lead precisely to the formation of regions of stability (Section 3.5).

---

*) Trivial only in the stochastic region but not in the region of Kolmogorov stability (see Section 3.3).

In the majority of the experiments use was made of the most simple non-trivial "force":

$$f(\varphi) = \varphi^2 - \varphi + 1/6 \qquad (3.2.5)$$

Here the minimum number of multiplications was chosen and the linear term ($-\psi$) improves the smoothness (only the derivative is discontinuous); the coefficient 1/6 eliminates the constant drift ψ ($< f > = 0$), leaving only the diffusion.

For some control experiments an analytical "force" *) was used:

$$f(\varphi) = \frac{\sin 2\pi\varphi}{2\pi} \qquad (3.2.6)$$

Finally, for the study of stable regions use was made of the transformation:

$$\begin{aligned} \varphi' &= \varphi - \varphi^3 \\ \psi' &= \psi + \varphi' \end{aligned} \qquad (3.2.7)$$

which is essentially equivalent to the elementary model (3.2.1) (with $f = -\psi^3$), but does not contain the factor k **) and what is most important, makes it possible to avoid taking the fractional parts (for stable trajectories). As a result a record computation speed was achieved for the latter model -- 7 μsec per step (3.2.7), while the computing speed for model (3.2.1) with a "force" (3.2.5) was about 20 μsec per step. In order to achieve maximum computation speed the program was written in computer language. In particular, it was possible to fit all the main loop of the computing of transformation (3.2.1) proper in the fast registers of the BESM-6, which obviated the need for relatively slow access to the operational memory. Moreover, the normalization and round-off were suppressed, i.e. in fact fixed-point was used; this further increased the computation speed.

The main output data was a histogram of the distribution function of the trajectory in the phase plane, i.e. the number of times the trajectory entered each of the bins of the phase square. It is not given, as a rule, on account of its extreme cumbersomeness even for very rough subdivision of the phase plane (32 × 32 bins, 1024 numbers) ***). On the basis of the histogram a much more compact phase map can be constructed (see for example Figs. 3.3.1 and 3.3.2), which records only the fact of whether or not the trajectory enters each of the bins.

The finest division of the phase plane in order to obtain the histogram was 128 × 128 = 16384 bins. For a phase map it is not necessary to occupy a whole word of the machine memory for each bin, it is sufficient to use one binary digit[88]. This makes it possible to increase the number of bins to 512 × 1024 = 524288. With this number of bins the

---

*) The factor 2π in amplitude was introduced for easier comparison with (3.2.5).

**) The introduction of this factor into (3.2.7) is equivalent to the transformation $\varphi \to \varphi/\sqrt{k}$: $\psi \to \psi/\sqrt{k}$.

***) See also Section 3.6 where individual sections of similar histograms are given.

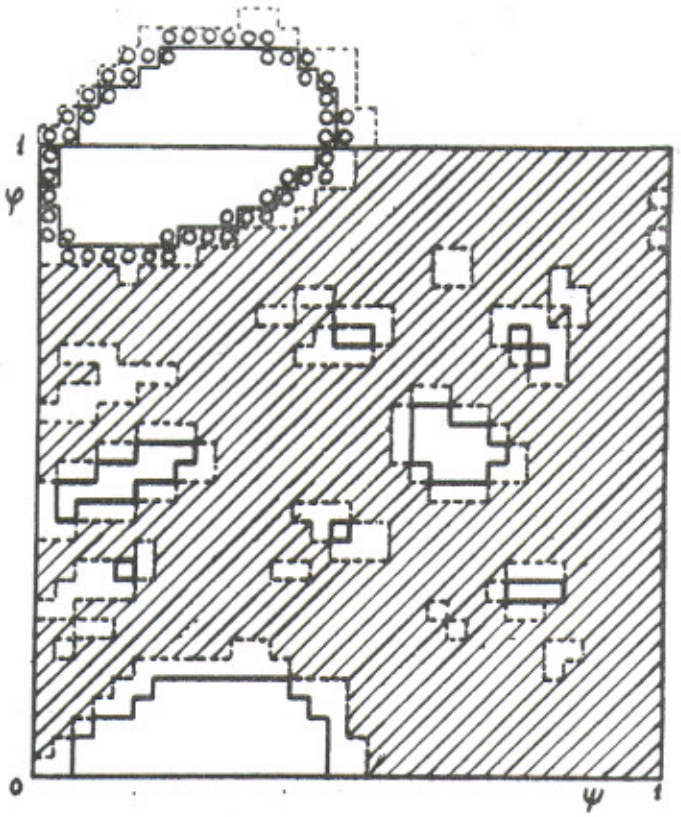

Fig. 3.3.1: Phase map of system (3.2.1) for "force" (3.2.5); divided into 32 × 32 bins: $k \approx 1$; $\varphi_0 = 0$; $\psi_0 \approx 0.765$; $t = 5 \times 10^6$ steps; the stochastic region is hatched; the bins completely free from the trajectory are shown by an unbroken line; between the unbroken and dotted lines are bins with considerably less density of trajectory (only part of the bin occupied by the stochastic component); the small circles represent the stable trajectory with initial conditions $\varphi_0 = 0$; $\psi_0 \approx 0.460$; $t = 5 \times 10^6$.

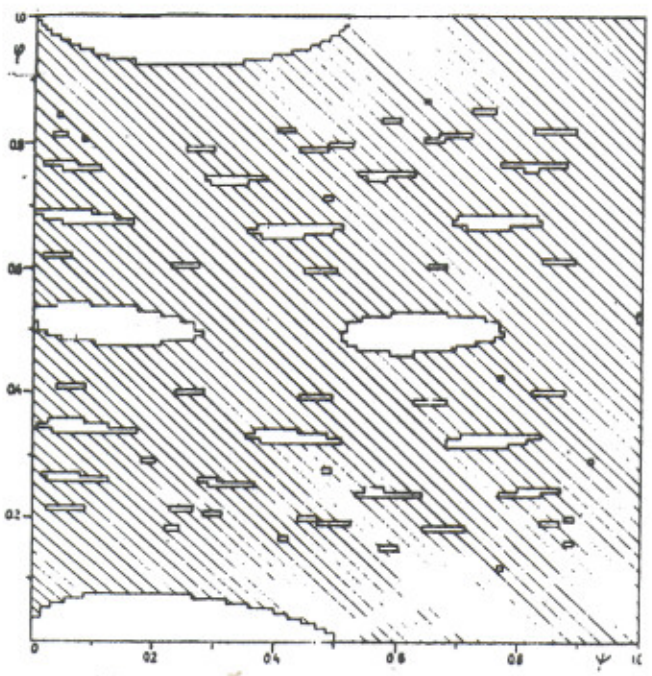

Fig. 3.3.2: The phase map for "force" (3.2.5): 128 × 128 bins; $k = 0.2$; $t = 5 \times 10^7$; the stochastic component is hatched.

output of even a phase map becomes impossible, and one has to limit onself to computing the empty and full bins and to the output of characteristic sections of the phase plane map (see for example Fig. 3.5.2). Let us note that all array dimensions for the distribution function and phase map were chosen equal to some power of two, which considerably simplifies programing in computer language. Some special processing methods will be described below.

3.3 Kolmogorov stability

Let us begin with a description of experiments on Kolmogorov stability. It should be recalled that this means the existence of non-resonant invariant tori[20], which for system (3.2.1) have the form of curves crossing the whole of the phase square along the axis ψ. In particular, for an unperturbed system ($k = 0$) they are simply straight lines: $\varphi = \text{const}$. According to the KAM theory (Section 2.2) this invariance does not, generally speaking, extend to the resonant regions, situated for transformation (3.2.1) in the vicinity of rational values of the momentum:

$$\varphi_p = \frac{r}{q} \tag{3.3.1}$$

r,q are integers. If the resonances of this system overlap, the non-resonant tori, and with them also the Kolmogorov stability, vanish.

According to the estimates in Section 2.7 under the condition:

$$\ell \leq 1 \tag{3.3.2}$$

overlapping of the resonances of the higher harmonics (of the first order) takes place for any $k \to 0$.

For "force" (3.2.5) $\ell = 0$ (discontinuity of the first derivative) and therefore it can be expected that there will be no Kolmogorov stability for any k. Figure 3.3.2 gives the phase diagram for $k = 0.2$. It will be seen that the stochastic component crosses the whole region along φ, leaving only isolated islets of stability. This in fact signifies the absence of Kolmogorov stability as determined above.

For smaller values of k, however, the region occupied by the trajectory is limited in φ, at least during the computation time $t_0 = 10^8$. Moreover, towards the end of the motion ($t \geq 0.7 \times t_0$), no diffusion at all can be observed to within the size of the phase bin ($\Delta\varphi = 1/128$).

For the other "force" (3.2.3) with the same smoothness parameter $\ell = 0$ the stochastic component remained limited in φ even for $k \approx 1$ during $t = 5 \times 10^8$.

At present it is not quite clear whether this means the existence of some region of Kolmogorov stability, i.e. incomplete overlapping of resonances, or a very small diffusion coefficient. It can be asserted only that the resonance regions occupy a considerable part of the phase plane, since out of ten randomly chosen initial conditions [for "force" (3.2.5), $k \approx 0.01$] it turned out that four lay inside resonances of high ($q \sim 100$) harmonics (motion limited in ψ), six fell in narrow ($\Delta\phi \sim 10^{-3}$) stochastic bands (probably destroyed separatrices) and there was not one case of Kolmogorov stability. A summary phase map is given in Fig. 3.3.3. The resonance regions can be clearly seen inside the stochastic bands. However,

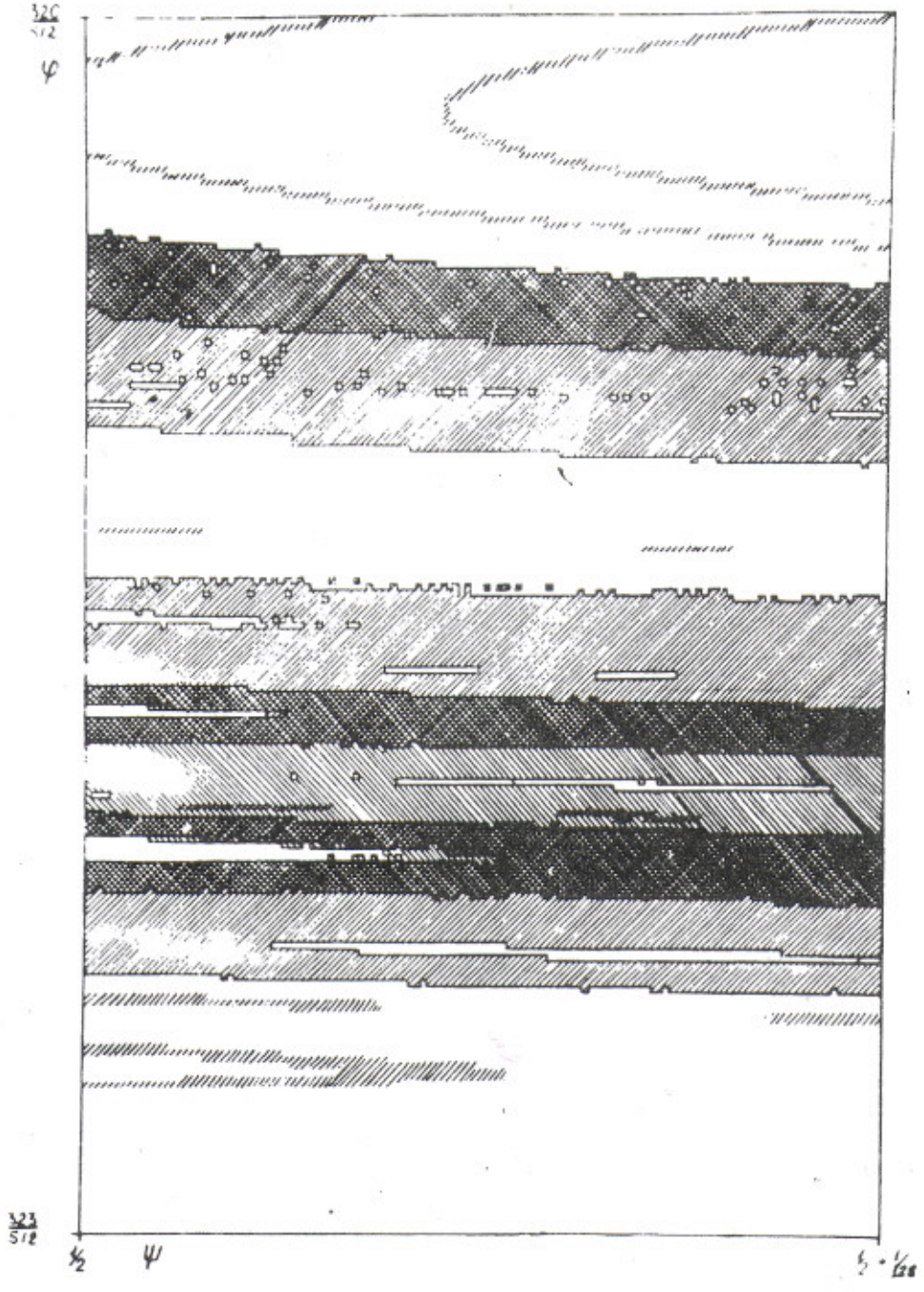

Fig. 3.3.3: Summary phase map of the motion of system (3.2.1) with a "force" (3.2.5) for different initial conditions $k \approx 0.01$; $t = 10^7$; the size of the given section of the phase plane $(\Delta\varphi,\Delta\psi)$ is $3/512 \times 1/128$; it is divided into 374×128 bins. The wide ergodic bands are hatched; the narrow regions (one or two bins wide) represent stable trajectories inside first order resonances.

the most interesting feature of the motion in our opinion is the overlapping stochastic bands with diffusion limited in φ. This shows especially clearly the extraordinarily complicated structure of the phase plane of the system under consideration, if moreover it is taken into account that the bin size $(\Delta\varphi,\Delta\psi)$ in Fig. 3.3.3 is approximately $(3 \times 10^{-5}) \times (6 \times 10^{-5})$.

A no less interesting case is illustrated in Fig. 3.3.4 *), which gives the phase map of the motion for "force" (3.2.3) and k = -1.145. Here the grey circles show the region of the phase space actually occupied by the trajectory of motion, and the black circles and crosses represent the periodical extension of the "grey" region along the axis ψ. Both regions overlap (the overlapping bins are represented by crosses), nevertheless the diffusion is limited by the "grey" region, at least during the computation time (3×10^6 steps). This shows that there are possibly very narrow gaps in the set of overlapping resonances of different harmonics. A similar hypothesis was discussed in Section 2.7.

It is possible to explain the stopping of the diffusion in a completely different way -- attributing it to so-called "cycling", i.e. the appearance of periodical motion because of the finite number of points of the computer phase space (see below). "Cycling" is facilitated by the fact that in some segments along φ the diffusion can be very slow (Section 2.7).

In order to verify the above assumptions, experiments were carried out with an artificially reduced number of mantissa digits. This was done by "cutting off" the lowest digits of φ and ψ after each step of the transformation. Some of the results of these experiments are given in Table 3.3.1, which gives the number of bins of the phase square (out of 16384) filled by the trajectory, depending on the number n of binary digits of the mantissa "cut off", for two values of the parameter k.

If gaps are the reason why the diffusion stops, then an increase of n should facilitate diffusion on account of "jumping" over these gaps; if the "cycling" is responsible, the opposite effect should be observed, since "cycling" appears more easily when there are less digits. From Table 3.3.1 it can be seen that the dependence of the diffusion on n is of a complicated and contradictory nature, and it is possible that both factors are operative. In any case this question requires further study.

Table 3.3.1

n	0	6	11	14	15	16	25
$k \approx 0.148$	6815	4528	11270	13807	6996	14427	
$k \approx 0.03$	1246					808	144

*) This drawing is borrowed from Ref. 76 where a similar problem was studied.

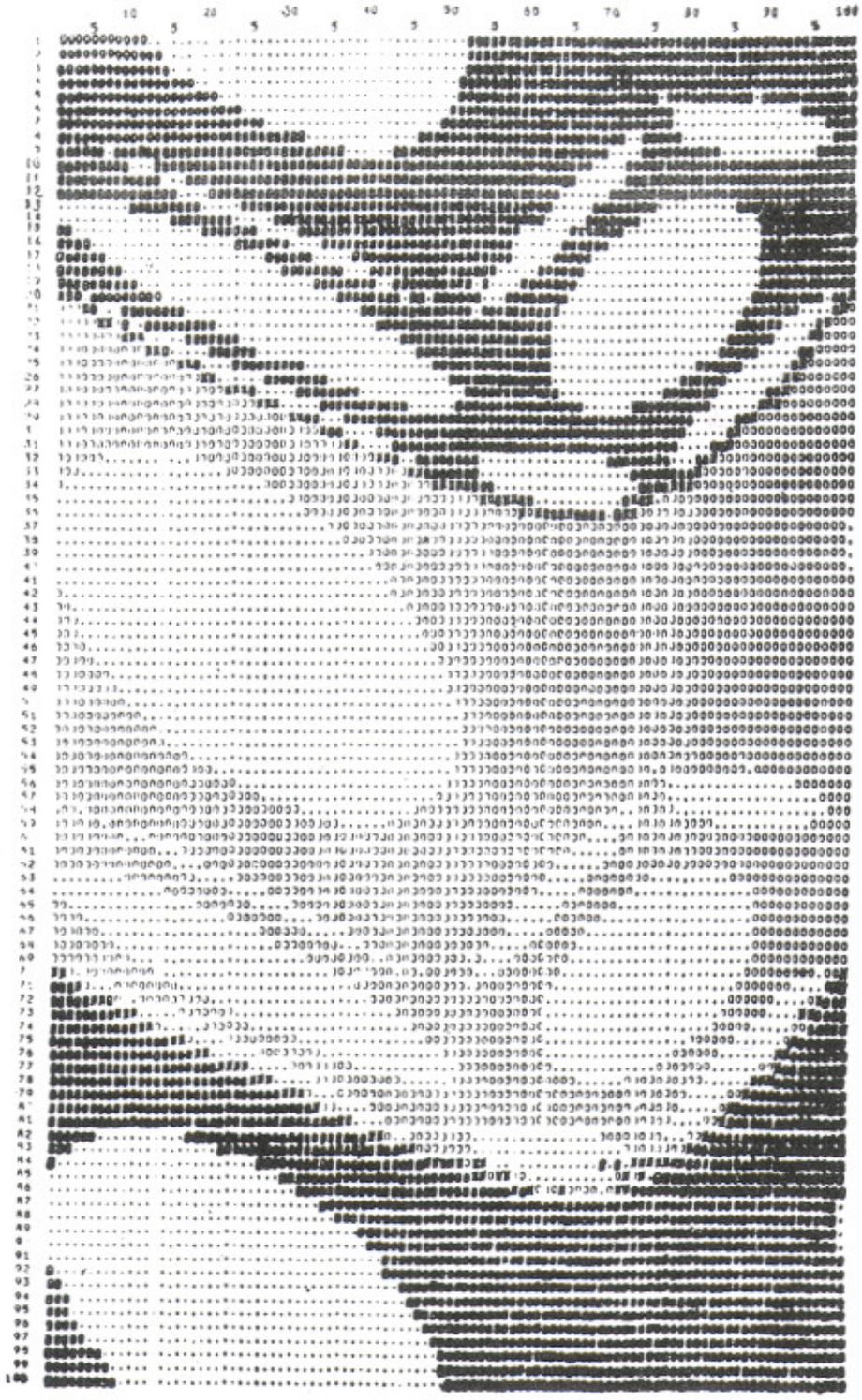

Fig. 3.3.4: Phase map of model (3.2.1) with a "force" (3.2.3): $k = -1.145$; $t = 3 \times 10^6$. The black circles and crosses represent the periodical extension along the axis φ of the region occupied by the trajectory and denoted by grey circles; bins common to both regions are marked by crosses.

Let us note that a similar effect of stopping the diffusion had also been observed earlier in numerical experiments by Courant[97] and Hine[98]. Thus the motion in this case is in a sense even more stable than could be expected from the first approximation (Section 2.7). Nevertheless one has the impression that in the case studied ($\ell = 0$) there is in fact no Kolmogorov stability outside the resonances, in accordance with the estimates of Section 2.7. According to the results of Ref. 76 the same apparently takes place for the case $\ell = 1$, whereas for $\ell = 2$ the results of this paper are not inconsistent with Kolmogorov stability, again in accordance with the results of Section 2.7

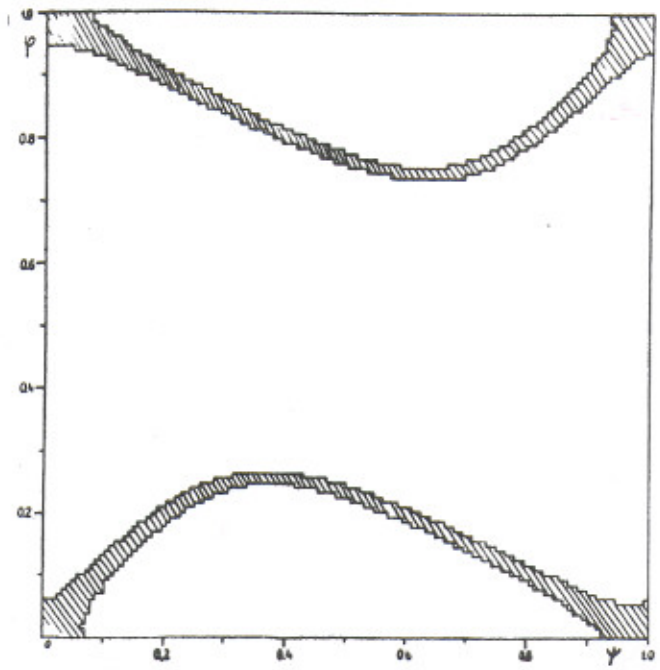

Fig. 3.3.5: Phase map for the analytical "force" (3.2.6): 128 × 128 bins; $k \approx 0.62$; $t = 10^7$. The hatched region represents the stochastic layer in the vicinity of the separatrix of the main resonance.

For purposes of comparison Fig. 3.3.5 gives the phase diagram of system (3.2.1) with an analytical force (3.2.6), for which the amplitude of the harmonics decreases exponentially. It can be seen that there remains only a small unstable band along the resonance separatrix (Section 2.8). Recent numerical experiments[184] seem to point in the direction of the former cause, i.e. the existence of extremely thin gaps of less than 10^{-12}, since for double precision computation the diffusion drops considerably.

It is inconvenient to use force (3.6.2) for numerical experiments, since it takes too long to compute the sine. It was therefore used only for the check experiments (see below).

Let us now return to the isolated stable regions which can be well seen in Figs. 3.3.1 and 3.3.2. They lie inside the resonances of various harmonics. The largest region of stability corresponds to the basic resonance $q = 1$, although in Fig. 3.3.2 one can distinguish stable regions of resonances of up to the fifth harmonic inclusive.

The reason for the increased stability of these regions is that the trajectories here are limited in ψ (see for example Figs. 3.3.1 and 3.3.6) and do not generally speaking cross

the singularity of the "force" $f(\psi)$. On the other hand, the KAM theory also applies, with some modification[77,176,78], to the internal region of the resonances. It leads to the conclusion that under specific conditions there exists a sufficiently small stable region around an elliptical point (around the periodical solution, in the general case). The size of the stable region is determined in the present case by the width of the stochastic layer in the vicinity of the separatrix. It can be estimated by the formulae in Section 2.6, or according to local instability (Section 2.4). In particular, the complete disappearance of the stable region in Fig. 3.3.1 corresponds to the transformation of the elliptical point of transformation (3.2.1) from a "force" (3.2.5) ($\psi_0 = \frac{1}{2} - 1/\sqrt{12} \approx 0.21$) into a hyperbolic point. This takes place under the condition $k > k_s = 4/(1 - 2\psi_0) \approx 7$ which can be considered as a form of stochasticity criterion (Ref. 47, Section 2.4). Since for the case in Fig. 3.3.1 $k = 1 \ll 7$, the stable region must be of a considerable size, determined in practice by the singularity $f(\psi)$ at the point $\psi = 0$. The same conclusion can be reached by considering the parameter of destruction of the separatrix $s_1 = \omega_1/\Omega_\phi$ (Section 2.6), where the perturbation frequency $\omega_1 = 2\pi$ and the phase oscillation frequency is obtained by linearizing transformation (3.2.1) at the point $\psi = \psi_0$ which gives: $\Omega_\phi = \sqrt{2k}$. Assuming that $s_1 \sim 1$ we obtain: $k'_s \sim 2\pi^2$. The relation $k'_s/k_s \sim 3$ characterizes the accuracy of the estimate: $s_1 \sim 1$.

A fundamental question arises: is the approximate border thus determined the same border of eternal stability whose existence follows from the KAM theory? In other words, is not the border of stability in Fig. 3.3.1 substantially displaced if the time of the motion is considerably increased?

Model (3.2.7) was chosen for carrying out this experiment. A similar experiment had been carried out earlier by Laslett[91] with the transformation:

$$\begin{aligned} q' &= q + \frac{13}{4}p \\ p' &= p + q'(q'-1) \end{aligned} \qquad (3.3.3a)$$

The motion of this system is similar to the motion in the stable region in Fig. 3.3.1 ["force" (3.2.5)]. The reason for choosing a more symmetrical transformation (3.2.7) was connected in particular with round-off errors (see below). Moreover, transformation (3.2.7) has a "real" border of stochasticity, i.e. it has a region of strong stochasticity determined by the overlapping of the resonances, while the border of stability for transformation (3.3.3a), as in Fig. 3.3.1, is determined by the destroyed separatrix. In the latter case there is some indeterminacy in establishing the distance to the border of stochasticity, since in any neighbourhood of the chosen initial conditions there are always destroyed separatrices of resonances of sufficiently high harmonics. Unfortunately, in Ref. 91 the position of the border of stochasticity was not determined at all, so that we can do no more than make a rough estimate of it according to the criterion of local stability (Section 2.4), which gives a value: $q_s \sim 0.5$. In this case the energy for the stable trajectory studied in Ref. 91 is approximately 200 times less than at the border of stochasticity, i.e. this trajectory lies far inside the region of Kolmogorov stability.

In order to find by experiment the approximate border of stochasticity in our case (in a short time) an auxiliary system was used:

$$\varphi'_{n+1} = \{\varphi'_n - 8(\psi'_n - 1/2)^3\}$$
$$\psi'_{n+1} = \{\psi'_n + \varphi'_{n+1}\} \qquad (3.3.3)$$

the phase map of which is given in Fig. 3.3.6 for $t = 5 \times 10^6$. The fractional parts here

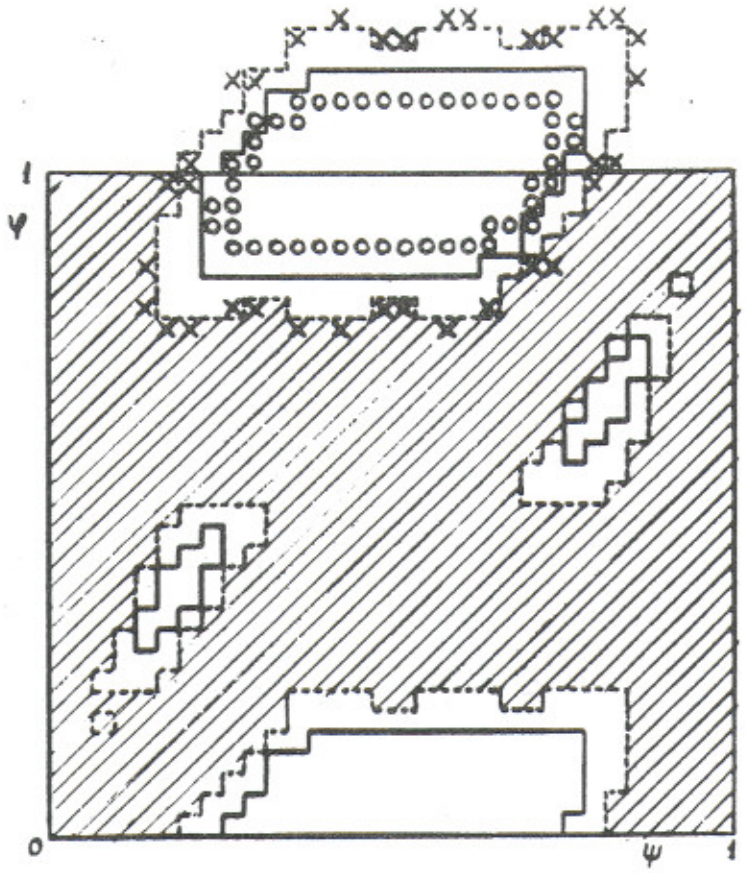

Fig. 3.3.6: The phase plane of system (3.3.3); the notation is the same as in Fig. 3.3.1; the ergodic trajectory corresponds to the initial conditions $\varphi'_0 = 0$; $\psi'_0 \approx 0.830$; the long computation trajectory $\varphi'_0 = 0$; $\psi'_0 = 0.735$ is represented by small circles; the crosses represent the other stable trajectory near the second order resonance: $\varphi'_0 = 0$; $\psi'_0 = 0.803$; for all three trajectories $t = 5 \times 10^6$.

are indispensable, since in the opposite case the trajectory in the stochastic region rapidly runs to infinity: $\phi_n \sim \psi_n \sim C^{(3^n)}$; $C > 1$. By computation this leads to overflow. The transformation coefficient 8 and the shift of ψ by $\frac{1}{2}$ were chosen with a view to convenient arrangement of the stable region in a standard phase square 1×1.

From Fig. 3.3.6 it follows that the border of stability lies somewhere in the interval $0.69 < \psi_s < 0.93$ ($\varphi = 0$). The more accurate measurements of Ref. 76 lead to the value $\psi_s \approx 0.80$ (for $t = 10^6$).

Let us note that the position of the border of stability cannot depend on the singularity of the "force" connected with taking the fractional part in (3.3.3) (discontinuity of the function $f(\psi)$). Indeed, the border in this case is clearly separated from the location of the singularities ($\psi = 0; 1$); therefore the latter can in no way influence the trajectories of the system that are located between the border and the singularities.

The stable (for $t = 5 \times 10^6$) trajectory, represented in Fig. 3.3.6 by crosses, lies precisely on the border. However, it is not continuous, i.e. it may be situated in "islets" of stability inside the stochastic region (see Section 3.5). This is just how it is in reality, according to Ref. 76. In this connection, a more "normal" trajectory was chosen for the long computation, marked in Fig. 3.3.6 by small circles, for which $\psi \approx -0.67$ ($\varphi = 0$). This is 12% less than the critical value for the phase and 40% less for the energy.

This trajectory was computed in $t = 10^{10}$ steps. After every 100 steps the position of the system was marked on a phase map with a minimum bin size [1/512 (in ψ) by 1/1024 (in ψ)]. The trajectory occupied 1876 bins, and this number did not change for $t > t_1 = 10^8$.

The latter value is of the order of magnitude expected, which can be estimated as

$$t_1 \sim \frac{L^2}{\nu} \qquad (3.3.4)$$

where L is the length of the trajectory (number of bins) and $\nu = 1/100$ is the frequency of output on to the phase plane. The estimate is based on the assumption that there is "random" intersection of the bin by the trajectory, so that out of L bins there may be one in which the length of the trajectory will be $\sim$ L times smaller than the average.

In order to reinforce the result obtained, the following additional processing proposed by Arnold was carried out. In the lower horizontal segment of the trajectory with minimum curvature (Fig. 3.3.6) a square was chosen with sides $2^{-18} \approx 4 \times 10^{-6}$. Exact values φ, ψ of all the points (about 100) entering this square during $t = 10^8$ were printed out at the beginning and end of the long computation. The values obtained were interpolated as a straight line by the least squares method, separately for the beginning and end of the long computation. The differences $\Delta\varphi$ between the co-ordinates of the points and of the interpolation line ($\Delta\psi = 0$), proportional to the distance of the points from this line, were plotted depending on time (Fig. 3.3.7) and on ψ (Fig. 3.3.8). The quantity $\Delta_r = 10^{-12}$ serves as the unit length along the axis $\Delta\varphi$ and is equal to the maximum round-off error.

In Fig. 3.3.8 no correlations are observed between $\Delta\varphi$, ψ, for example, due to the curvature of the trajectory or entry into a high order resonance. It can therefore be concluded that the scattering of the points is due to some "diffusion". The diffusion process can be especially clearly seen in Fig. 3.3.7. It may be due either to round-off errors or to the fact that we have not yet reached the region of eternal stability of the KAM theory. In order to check this last assumption the experiment was repeated for a trajectory lying considerably nearer to the fixed point ($\varphi = \psi = 0$) than the long computation trajectory (φ 1.7 times smaller, energy 2.9 times lower), and also for a trajectory lying further away (φ 11% larger, energy 23% higher). In both cases the diffusion coefficient turned out to be the same as for the long computation, so that the diffusion must be related to the effect of round-off errors.

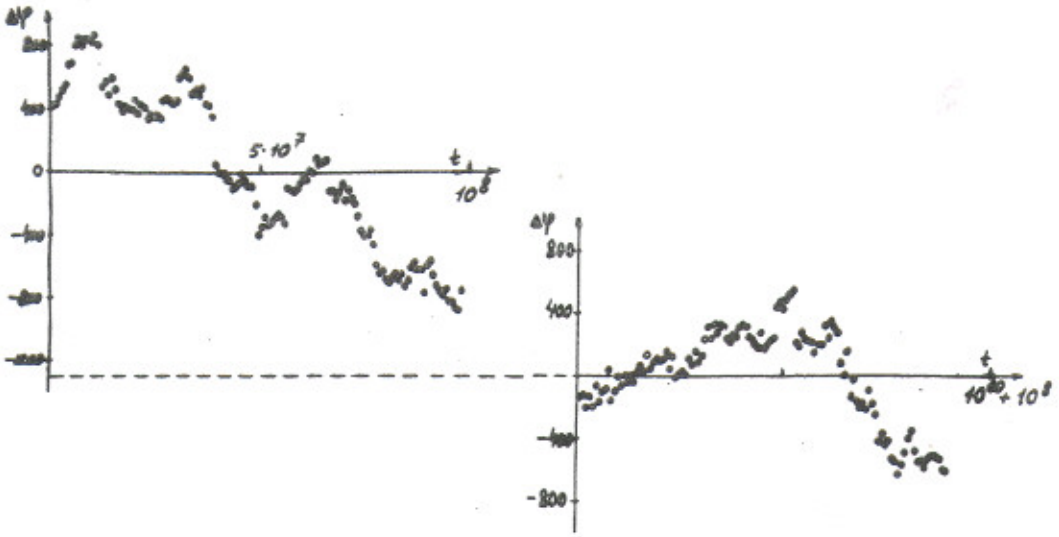

Fig. 3.3.7: Weak diffusion due to round-off for transformation (3.2.7): $\Delta\varphi$ is the deviation of the experimental points from the interpolation straight line in units of the maximum round-off error (space "quantum") $\Delta_r = 10^{-12}$; $\varphi_0 \approx -0.316$ (long computation); the points on the left relate to the beginning of the long computation and those on the right to the end.

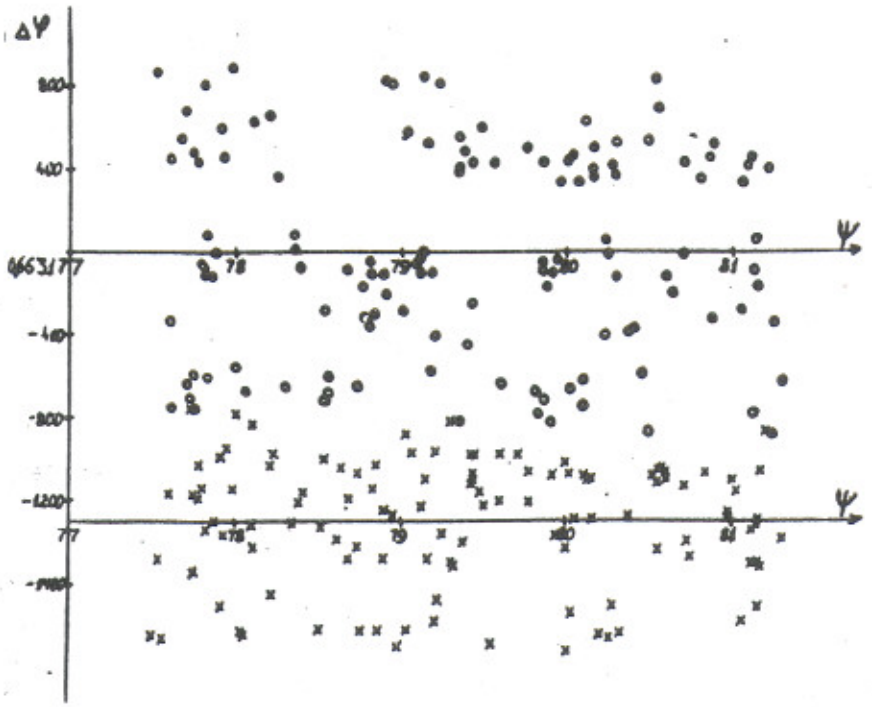

Fig. 3.3.8: Search for the correlation $\Delta\varphi$, ψ : O - the beginning of the long computation; × - the end of the long computation (see Fig. 3.3.7).

It thus appears very likely that the long computation trajectory lies in the region of eternal stability of the KAM theory. In other words, the strict border of stability for transformation (3.2.7) is somewhere in the interval:

$$0.67 < \psi_s < 0.80. \qquad (3.3.4a)$$

As already repeatedly noted [see for instance Refs. 89 and 90] the border of stability in the general case is not simply a line, but there is a whole transitional region of alternating stable and unstable layers of increasingly fine structure, corresponding to higher harmonic resonances. Some of the regions are characterized by a relatively long time of development of instability. So, for instance, according to the data of Ref. 76, when the computing time is increased from 3×10^5 to 10^6 the border shifts from $\psi = 0.88$ to $\psi = 0.80$, i.e. by approximately 10%.

This transitional region for the transformation in question (3.2.7) was thoroughly studied recently in Ref. 184 using double precision computation. It was found that both boundaries of the region are rather sharp: the upper one is at $\psi \approx 0.62$ ($\psi = 0$) where the trajectory's "lifetime" (up to running away to infinity) drops from $t_\ell \sim 100$ steps down to $t_\ell \sim 1$ in $\Delta\psi \sim 2 \times 10^{-6}$; the lower boundary is at $\psi \approx 0.52$, as compared with $\psi < 0.56$ according to (3.3.4a) [76], where the lifetime increases steeply from $t_\ell \sim 3 \times 10^4$ up to $t_\ell \sim 10^6$ in $\Delta\psi \sim 3 \times 10^{-3}$. The latter must lie very close to the border of KAM eternal stability since a stable trajectory was found (certainly in the region of Kolmogorov stability in $\Delta\psi \approx 8 \times 10^{-3}$ only. This trajectory proved to be stable with an accuracy better than 10^{-20} (in ψ) during the computation time $t = 10^7$.

Although the example we have studied of a trajectory stable for such a long time is (of necessity!) unique, it gives grounds for hoping that the position of the strict border of stability according to the KAM theory can in fact be estimated in order of magnitude by means of the relatively simple stochasticity criteria obtained in the present paper (Chapter 2). In any event this correspondence has been observed in all (about 100) cases of computation for a time $t \sim 10^7$.

The accuracy of this assertion is determined by the residual diffusion in Fig. 3.3.7, which can be explained by round-off errors (see below). Let us note that this diffusion does not contradict the KAM theory, since the round-off errors are equivalent to some rough (with a great number of fine discontinuities) perturbation, which is inadmissible for the theory.

The residual diffusion coefficient is (see below): $D \approx 4 \times 10^{-27}$. In Ref. 91 this estimate was considerably reduced on account of the use of double precision computation: $D \approx 1.6 \times 10^{-61}$. However, in the experiments in Ref. 91 there was systematic accumulation of round-off errors (drift): $V_q = dq/dt \approx 1.3 \times 10^{-31}$. This value should be compared to $\sqrt{D} \approx 6 \times 10^{-14}$ in our case, so that the accuracy achieved in Ref. 91 is all the same considerably greater. It is true that the trajectory chosen in Ref. 91 apparently lies substantially further from the border of stochasticity and was computed in a considerably shorter time ($t \sim 10^7$). In this connection let us note that the increase in accuracy does not necessarily compensate for the reduction in the time of motion, since instability may develop according to an exponential law (see Section 3.6).

From Fig. 3.3.7 it can be seen that there is a conspicuous stopping of diffusion after $t \sim 10^8$. This is apparently explained, at least in part, by "cycling", i.e. the appearance of periodicity of the motion. "Cycling" necessarily occurs sooner or later as a result of the finite number of points (S) of the phase plane in the computer presentation. The maximum possible time until "cycling" begins is obviously: $T_c = S$, after which one of the previous points of the trajectory is necessarily reached and consequently an exact repetition of the motion begins. In the case under consideration S is determined by the area of the ring along the trajectory, the width of which (d) depends on the scattering of the points in Fig. 3.3.7: $S = L \cdot d \approx 2 \times 10^{12} \times 1600 \approx 3 \times 10^{15}$, where $L \approx 2 \times 10^{12}$ is the perimeter of the trajectory in units of maximum round-off error $\Delta_r = 10^{-12}$ which is the computer space "quantum".

In order to obtain a more realistic estimate of the quantity T_c we shall assume that the round-off is characterized by "random" diffusion with a coefficient D_0 (see below). Then the probability of the trajectory arriving in one of the previous points in a step is equal to the relative density of occupation of the phase space by the trajectories: $\omega(t) = t/L \cdot d(t)$, where $d(t) \approx 2\sqrt{2 D_0 t}$. The beginning of the "cycling" is determined (on the average) from the condition: $\int_0^{T_c} \omega \, dt = 1$; this gives

$$T_c \approx (3L\sqrt{2D_0})^{2/3} \tag{3.3.5}$$

Putting here the experimental value obtained below*) $D_0 \approx 4 \times 10^{-3}$, we obtain: $T_c \approx 6 \times 10^7$. This does not contradict the data of Fig. 3.3.7, but it also does not prove that the limitation of the diffusion is necessarily due to the "cycling". This question will be discussed further a little later on.

Let us note that in the stochastic case $L \cdot d \sim L^2 \sim S = 10^{24}$, and $T_c \sim \sqrt{S} \sim 10^{12}$, so that "cycling" is completely insignificant. The diffusion coefficient can be determined from the mean displacement $(\Delta\varphi)_\tau$ between the points in Fig. 3.3.7, which are separated by an interval of time τ:

$$D_{exp} = \frac{\overline{(\Delta\varphi)_\tau^2}}{2\tau} \tag{3.3.6}$$

The results of the computation of D_{exp}, for all three trajectories (see above) are given in Table 3.3.2, which also gives the mean values of the diffusion coefficients for all the trajectories. Moreover, it gives the experimental root-mean-square errors, which satisfactorily agree with the expected values. The variance between different values of D_{exp}, including those for various τ, does not substantially exceed the statistical errors. The least probable are three small values of D_{exp} for $\tau = 10^8$ (probability $\sim 6\%$). However, if rejecting the end of the long computation, which is possible, corresponds to "cycling" and is therefore insignificant, the probability of the two remaining cases is increased to 16%, which is no longer a substantial deviation.

---

*) Here and in what follows all lengths are in units of Δ_r.

Table 3.3.2

τ	Long computation $\varphi_0 = -0.316$		$\varphi_0 = -0.187$	$\varphi_0 = -0.350$	$< D_{exp} >$
	Beginning	End			
10^6	3.2×10^{-3}	3.5×10^{-3}	5.5×10^{-3}	4.3×10^{-3}	$(4.1 \pm 0.9) \times 10^{-3}$
10^7	5.7×10^{-3}	2.8×10^{-3}	2.4×10^{-3}	1.5×10^{-3}	$(3.1 \pm 1.6) \times 10^{-3}$
10^8	4.7×10^{-3}	1.1×10^{-3}	0.9×10^{-3}	1.0×10^{-3}	$(1.9 \pm 1.9) \times 10^{-3}$

The distribution of large values of $(\Delta\varphi)_\tau$ was also studied. At the beginning of the long computation they agree well with the normal law, and at the end there are two jumps, the probability of which is $\sim 10^{-2}$. The latter may also signify the "cycling" effect at the end of the long computation. If this case is refused, one has the impression that the accumulation of round-off "errors" indeed follows a diffusion law.

The same result is obtained from an additional series of experiments with artificial reduction of the number of mantissa digits by 2, 4, 8, 12, 16 binary digits out of 40. The mean diffusion coefficient of this series is $< D > = (5.6 \pm 1.2) \times 10^{-3}$, which agrees well with the results in Table 3.3.2.

When 20 digits were "cut off" "cycling" was observed for $t \approx 10^6$. If estimate (3.3.5) is applied here, we obtain $T_c \approx 6000$, i.e. almost 200 times less than the value observed. This result can be explained, for example, by the strong correlations of neighbouring values φ, ψ. If this really is the main cause, strong correlation of approximately 200 neighbouring values can be expected. This hypothesis is partly confirmed below when the diffusion coefficient is calculated. If it is applied to the long computation, "cycling" can be expected only when $t \sim 10^{10}$, i.e. only at the very end of the long computation. Then there must be some other reasons for the limitation of the diffusion after $t \sim 10^8$, which can be clearly seen in Fig. 3.3.7. The question as a whole requires further study.

It should be pointed out that according to the results in Table 3.3.2 if there is any change in the diffusion coefficient it decreases rather than grows with τ. Hence it follows, in particular, that within the limits of statistical fluctuations there is no permanent drift, i.e. no systematic accumulation of errors. Let us write the upper limit of possible drift in the form: $V_\varphi = d(\Delta\varphi)/dt \lesssim \sqrt{D_{exp}/t} \approx 6 \times 10^{-6}$ (in units of Δ_r).

The absolute value of the diffusion coefficient $D_{exp} \approx 4 \times 10^{-3}$ (Table 3.3.2) does not correspond at all to the expected value for random errors (Δ). The latter can be calculated according to the formula: $D_r = <\Delta^2>/2$. The quantity $<\Delta^2>$ depends on the round-off algorithm. In our case the lowest digits of the product were simply rejected, which corresponds to a random quantity of Δ, uniformly distributed in the interval $(-\Delta_r, \Delta_r)$. Since in one step of the transformation (3.2.7) there are two multiplications*), $D_r = <\Delta^2> = 1/3$, i.e. it is approximately 80 times greater than the experimental value. This discrepancy may signify

*) Since we used fixed-point arithmetic (Section 3.2) there was no round-off when doing addition.

strong correlation of neighbouring errors. Let us assume, for example, that the correlation decreases according to an exponential law: $\rho = e^{-n/n_0}$, where n is the number of steps. Using expression (2.10.5b) for the diffusion coefficient taking into account the correlations, we obtain: $n_0 \approx 80$.

Let us now have a closer look at the accumulation of random errors, limiting ourselves to the most simple case of interest to us in fixed-point arithmetic. In this case the error is determined simply by the lowest digits of the product. But this operation is similar to one of the standard kinds of pseudo-random number generator (Ref. 95, 96, see also Section 4.7). Thus, the problem of round-off error accumulation is brought mainly to the study of various pseudo-random number generators. The specific mechanism of such a generator depends on the computation algorithm. In the present case the generator turns out to be rather poor, judging by the value of the correlation cited above. Precisely such a generator has not been studied, as far as we know, but similar ones containing the squaring operation in fact give poor results[95]. If our transformation contained the operation of multiplying by a constant, we should obtain a generator of the type of system (2.3.3), which is stochastic, with an enormous constant $k \sim \Delta_r^{-1}$. Various tests of this generator show that it gives random numbers (usually called pseudo-random) of very good quality (Section 4.7). Accordingly, in this case the accumulation of errors must take place according to a random law. This last result is confirmed, apparently, by the data of Ref. 91 on the investigation of transformation (3.3.8a), which contains just such multiplication by a constant. The "error diffusion" in this case agrees with the merely random diffusion[91].

A slightly more complicated question is that of constant drift, which was observed in Ref. 91 ($V_q \sim q \cdot \Delta_r \sim 10^{-31}$), but is absent in our experiment. There are apparently two most important differences between the two experiments:

i) We used fixed-point arithmetic while Laslett[91] used floating-point numbers;

ii) Our transformation (3.2.7) is symmetrical with respect to the sign of φ, ψ, in contrast to Laslett's transformation (3.3.3a).

Asymmetrical round-off was used in both experiments: $\langle \Delta \rangle = \Delta_r/2 \neq 0$, but for fixed-point arithmetic this is equivalent to a constant "force" in the equation for the "momentum", which only slightly displaces the trajectory of the system; in the case of floating-point arithmetic this "force" is proportional to the "velocity", i.e. it becomes "dissipative". To be more precise, the "force" is proportional to the velocity modulus if, as is the case for the majority of present-day computers, a negative number is represented in a complementary code. But in such a case, for symmetrical oscillations the mean "dissipation" vanishes and for asymmetrical ones it remains.

The most radical means of preventing drift is to introduce symmetrical round-off, which is provided for in the majority of computers but requires additional time. Another method is to change over to fixed-point arithmetic, if the algorithm of the problem permits. This considerably increases the computing speed also, particularly if double precision is used.

3.4 Stochasticity

In this section we will discuss the experimental results relating to the behaviour of the elementary model (3.2.1) in the region of stochasticity, i.e. when $k \gg 1$.

Is the motion in this case really stochastic?

Let us begin with K-entropy (Sections 2.3 and 2.4). For the experimental determination of K-entropy Sinai's equation[17] was used:

$$h = \overline{\lim_{l \to 0} \ln (l'/l)} \tag{3.4.1}$$

where l, l' is the length of the transverse vector (Section 2.4) before and after the transformation respectively, and averaging is carried out along the trajectory of the main motion. We chose $l = 10^{-7}$, so that for the largest value of $k = 10^3$ the value $l' \sim 10^{-4} \ll 1$. Numerical calculation of transformation (3.2.1) was carried out for two trajectories, the initial points of which were $\vec{l}$ apart, and after each step of the transformation the length of the transverse vector ($\vec{l}$) was brought to the initial value of $l = 10^{-7}$ without changing its direction.

An analytical estimate of the K-entropy is given by expression (2.4.21), which can be made more accurate for the elementary model, on the basis of Sinai's equation (2.4.19):

$$h = \langle \ln \lambda_a^+ \rangle \tag{3.4.2}$$

where λ_a^+ is the projection of λ^+ in the direction of the asymptote, which generally speaking is not identical with the direction of the extension eigenvector (θ^+), if the latter turns (Section 2.4.8).

However, for large kf' the direction of the eigenvector hardly changes, as can be easily verified by using expression (2.4.14) or (2.8.4):

$$\operatorname{tg} \theta^+ \approx 1 - 1/kf' \tag{3.4.3}$$

A narrow phase region near the stable phase region (2.4.7) is an exception:

$$-4 < k \cdot f'(\psi) < 0 \tag{3.4.4}$$

the probability of entering which is $\sim 1/k$. In the main region the variation of $\theta^+ \sim 1/k$.

Let us note also that the regions of the values (sectors) θ^+, θ^- do not overlap for any kf'. Indeed, it follows from (2.8.4) that the full range of variation of θ^+ is:

$$0 < \operatorname{tg} \theta^+ < 2 \tag{3.4.5}$$

and the range of variation of θ^- is precisely complementary to (3.4.5). In the majority of cases the contraction vector is directed almost along the axis ψ:

$$\operatorname{tg} \left(\frac{\pi}{2} - \theta^- \right) \approx - \frac{1}{kf'} \tag{3.4.6}$$

Hence it follows that the asymptote practically all the time makes an angle of $\sim 1/k$ with the direction of the extension vector, only occasionally (with a probability of $\sim 1/k$) deviating by an angle of ~ 1. In this case one can put approximately: $\lambda_a \approx \lambda^+$ with an accuracy of $\sim 1/k$. In fact the accuracy of this equality is even better, since the ratio λ_a/λ^+ varies both ways and partially compensates for the deviations. Let us explain in this connection that λ_a is an oblique projection of λ^+ along the eigenvectors, which are generally speaking non-orthogonal (Section 2.4).

Thus the K-entropy can be estimated according to the formula:

$$h \approx \langle \ln \lambda^+ \rangle \tag{3.4.7}$$

where the averaging is carried out over ψ, and in the stable region (3.4.4) one should put $\lambda^+ = 1$. Let us note that it would be incorrect simply to exclude all the stable phase region (3.4.4) from the mean (3.4.7), since according to the data of the next section the stochastic trajectory occupies almost all this region except for a very small fraction of "islets" of stability.

The K-entropy was calculated for a "force" of two forms: (3.2.5) and (3.2.6). In the first case the integral (3.4.7) can be calculated to the end and gives:

$$h = \left[H\left(\frac{k}{2}+1\right) + H\left(\frac{k}{2}-1\right) \right] / k$$
$$H(x) = x \ln\left(x + \sqrt{x^2-1}\right) - \sqrt{x^2-1} \tag{3.4.8}$$

In the case of force (3.2.6) an explicit estimate can be obtained, if use is made of the approximate expression (2.4.6):

$$\lambda^+ = \left|\frac{kf'}{2}\right| \pm 1 + \sqrt{\left|\frac{kf'}{2}\right|^2 \pm |kf'|} \approx$$
$$\approx kf' \pm 2 \pm \frac{1}{|kf'|} \tag{3.4.9}$$

where the sign is identical with the sign of f'. Limiting ourselves to the first term only, the accuracy of the K-entropy estimate again will be a little better than $\sim 1/k$, since the contributions from the subsequent terms almost counterbalance each other. For force (3.2.6) we obtain:

$$h \approx \int_0^1 d\psi \cdot \ln |k \cos 2\pi\psi| = \ln \frac{k}{2} \tag{3.4.10}$$

A similar estimate for force (3.2.5) gives:

$$h \approx (\ln k) - 1 \tag{3.4.11}$$

The results in Table 3.4.1 enable us to compare the experimental values of the K-entropy with the various estimates. As already noted above, the initial distance between the trajectories was chosen as $\ell = 10^{-7}$. Increasing it to 10^{-3} changes the experimental value h from 3.615 to 3.72 [k = 100.2; force (3.2.5)]. The usual number of steps when calculating the K-entropy according to formula (3.4.1) was $t = 10^4$. Reducing this figure to 10^3 leads to a change in the K-entropy from 4.234 to 4.242 [k = 142.0; force (3.2.6)].

The results in the table show the very good agreement between the experimental values of the K-entropy and the analytical estimates, even the most simple ones [(3.4.10), (3.4.11)]. This also shows indirectly that when $k \gg 1$ (in fact, when $k \gtrsim 10$, see table) the stochastic component occupies practically all the phase plane of system (3.2.1).

Table 3.4.1

k	"Force" (3.2.5)			"Force" (3.2.6)		
	Exp. value	Estimates		Exp. value	Estimates	
		(3.4.8)	(3.4.11)		(3.4.7)	(3.4.10)
6.21	0.958	0.909	0.826	1.157	1.133	1.133
14.0	1.654	1.655	1.639	1.949	1.949	1.948
25.0	2.241	2.225	2.219	2.537	2.526	2.526
50.0	2.914	2.913	2.912	3.227	3.219	3.219
100.2	3.615	3.608	3.607	3.914	3.914	3.914
142	3.938	3.955	3.956	4.234	4.263	4.263
200	4.308	4.288	4.288	4.603	4.605	4.605
1000	5.926	5.908	5.908	6.206	6.215	6.215

This result is confirmed by direct experimental verification of the ergodicity of transformation (3.2.1). In itself ergodicity is a weak property, completely insufficient for stochasticity. However, when there is the additional condition of local instability of motion almost everywhere, as is the case for our model (3.2.1) from (3.4.4) when $k \gg 1$, the establishment of ergodicity is decisive evidence of stochasticity, according to the latest results of Anosov[31] and Sinai[34,17].

A rough check of the ergodicity was made by a phase map with the smallest bins (512 × 1024 = 524288 bins). From the results in Tables 3.4.2 and 3.4.3 it follows that for sufficiently large k the trajectory in fact goes through all the phase plane bins*). From the analysis made in the next section it will be seen that the stochastic component may nevertheless not occupy all the phase plane, but the area of the stable regions (and their dimensions) decreases, generally speaking exponentially with the growth of k, and for special values of k proportionally to k^{-2}.

*) With regard to the last three cases in Table 3.4.3, see next section.

Table 3.4.2

"Force" (3.2.5)

k	4	8	16	32
Number of empty bins	42038	60	0	0
Fraction of the area $\times 10^5$	8000	11.4	0	0

Total number of phase plane bins = 512 × 1024 = 524288

Table 3.4.3

"Force" (3.2.6)

k	3.67	4.78	5.88	8.64	10.5	23.1	37.7	50.3
Number of empty bins	48958	10292	1681	24	0	45	8	4
Fraction of the area $\times 10^5$	9300	1900	320	4.6	0	8.6	1.5	0.76

Total number of phase plane bins = 524288

A finer check of the ergodicity consists in investigating the uniformity of the occupation of the phase space by the stochastic trajectory. For this the phase square was subdivided into $N_1 = 128 \times 128 = 16384$ bins and the number of times the trajectory entered each of the bins (n_i) was calculated. The criterion of uniformity used was the variance: $D = \langle (n_i - M)^2 \rangle$, where $M = \langle n_i \rangle = t/N_1$ is the mean value of the number of entries, t is the time of motion (number of steps) and averaging is carried out over all the bins. The predicted value of D is: $D/M = 1 \pm \sqrt{2/N_1} = 1 \pm 0.011$; the last term gives the root-mean-square deviation. The experimental value for force (3.2.5) when $k = 16$, $t = 10^7$, is $D/M = 1.017$. The probability of such a deviation is about 12%.

Finally the stochasticity was further checked by watching the process of occupation of the phase plane bins by the trajectory. For random motion for not too long a time there must remain a certain number of empty bins (N_0), which can be calculated according to the standard Poisson distribution:

$$N_0 = N_2 \cdot e^{-u} \pm \sqrt{N_0} \qquad (3.4.12)$$

where $N_2 = 512 \times 1024 = 524288$ is the total number of phase plane bins. The results of this experiment are given in Table 3.4.4. It should be pointed out that in the present case $M = t/5N_2$, since output on to the phase plane was carried out every fifth step.

Table 3.4.4

t, steps	10^7	2×10^7	3×10^7	4×10^7	5×10^7
Number of empty bins, experiment	11531	258	6	1	0
Expected number of empty bins for random occupation	11500 $\pm$ 107	251 $\pm$ 16	5.8 $\pm$ 2.4	0.12 $\pm$ 0.35	2.5×10^{-3} $\pm$ 0.05

To sum up, it can be said that the motion of the elementary model (3.2.1) when $k \gg 1$ really appears to be "random". The question arises as to whether finally this is the result of round-off errors or, in other words, special properties of the "quantized" space of the computer. In our opinion this is not so, for the following reasons. To begin with, round-off "errors" are in no event random and are determined by an exact and invariable algorithm of the computer. The latter forms a kind of dynamical system, which in its turn is open to the question of whether it is stochastic or not. This depends on the computation algorithm; in the typical case, when there is multiplication in the algorithm, the round-off is apparently stochastic. But even in this case its influence is negligible for a stable system (Section 3.3). Even if round-off "errors" were not accumulated diffusely but systematically, which is possible in some cases[91], they would be considerable only in an interval of time $\sim \Delta_r^{-1} = 10^{12}$. Therefore round-off can have an important effect only under the condition of local instability, which in itself already signifies stochasticity. In other words, the influence of round-off "errors" is not the cause of stochasticity but its effect. Let us note, however, that these "errors" can substantially sharpen the transition to stochasticity and, in particular, make it considerably less sensitive to the initial conditions. This is due to the fact that at the moment when local instability appears, the original dynamical system (3.2.1) immediately becomes much more complex, since it begins to be "sensitive to" the round-off algorithm. As an excuse, we can only say that probably something like this happens in Nature, too; this was thoroughly discussed in Section 2.13.

Finally, it should be mentioned that motion in "quantized" space may possibly have exclusive properties, since the measure of such space in relation to continuous space is zero, and all the theorems of the ergodic theory are valid except for zero measure. It seems to us, however, perfectly improbable that two sets of zero measure and of a completely different nature could be identical.

In spite of all the above optimistic remarks in connection with the purity of numerical experiments, further study (both experimental and analytical) of the characteristics of the "quantized" space of the computer is certainly desirable.

3.5 Intermediate zone of the system with divided phase space

In the previous section it was established that for sufficiently large k the motion of the elementary model really satisfies all the tests for stochasticity. Let us now study the

intermediate zone ($k \sim 1$) which also gives us a better understanding of the mechanics of stochasticity.

The main feature of the intermediate zone are the "islets" of stability, or quasi-resonances, penetrating a long way into the stochastic region and apparently existing for any $k \to \infty$ (Section 2.8). Furthermore, the intermediate zone extends deep into the region of Kolmogorov stability. This is revealed, first of all, by the fact that the observed border of stochasticity depends on the time of motion, and near the border there is a region of very slow diffusion. The corresponding results are given in Section 3.3 and we shall not return to this question. Moreover, the whole region of Kolmogorov stability is penetrated by stochastic layers of resonances, which is of considerable importance for the many-dimensional system (Section 2.12). Some experiments with the simplest many-dimensional system will be described in the next section.

In this section we shall restrict ourselves to investigating the quasi-resonances in the intermediate zone. As was shown in Section 2.8, the largest quasi-resonance corresponds to special values of k, lying in the intervals (2.8.8) and (2.8.9) and to the period $T = 1$.

An example of such a quasi-resonance is given in Fig. 3.5.1 for $k \approx 60$; $t = 10^8$. The size of the stable trajectory ($\Delta\varphi \approx \Delta\psi \approx 1/32$) lying, to judge from its improper form, rather near to the boundary of the stable region, agrees well with estimate (2.8.10): $\Delta\varphi \sim \Delta\psi \sim 2/k \approx 1/30$ [$f' = 2$ for "force" (3.2.5)]. The relative area of the stable region is in this case $(4/kf')^2 \sim 10^{-3}$ (2.8.10).

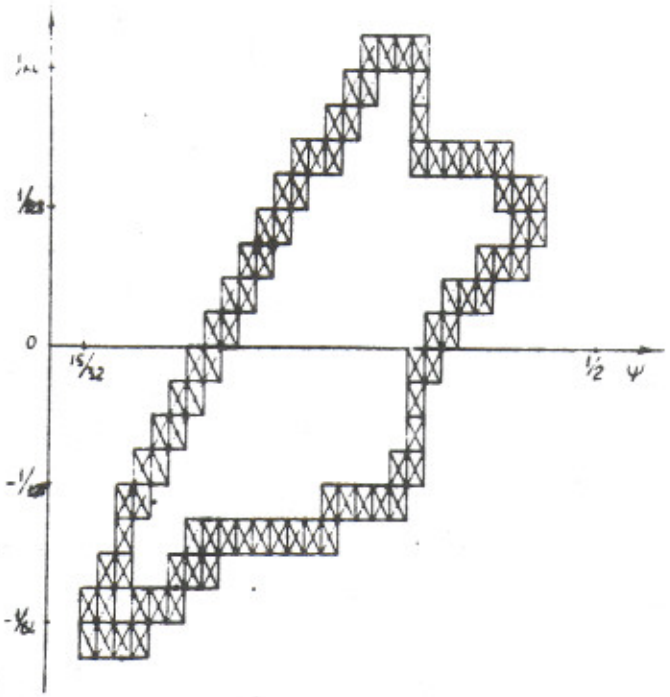

Fig. 3.5.1: An "islet" of stability for a special value of $k = 60.1993377$; $\varphi_0 = 0.01$; $\psi_0 \approx 0.483$; $t = 10^8$; size of bin $(1/512) \times (1/1024)$; the picture does not contradict the ideally thin curve corresponding to an absolutely stable trajectory.

For values of k outside the intervals of (2.8.8) the area of the stable regions decreases considerably faster, as seen from Table 3.4.2 (see previous section). The table gives the number of phase plane bins not occupied by the stochastic component, depending on k.

The phase map for one such case is given in Fig. 3.5.2 ["force" (3.2.5); k = 8; $t = 10^8$]. Two "islets" of stability can be clearly seen. More detailed analysis shows (see below) that there is also a third "islet", denoted in Fig. 3.5.2 by a dotted line. It is narrower than a phase plane bin and therefore remained unnoticed. The period of motion in this case is T = 3, and the figures on the phase diagram show the sequence of motion. Two "islets" (1,2) lie in the stable phase region (3.4.4) and one of them (1) strongly spreads out in the direction of the extension (see Section 3.4). The third islet (3) lies in an unstable region in ψ and strongly spreads out in the direction of the contraction.

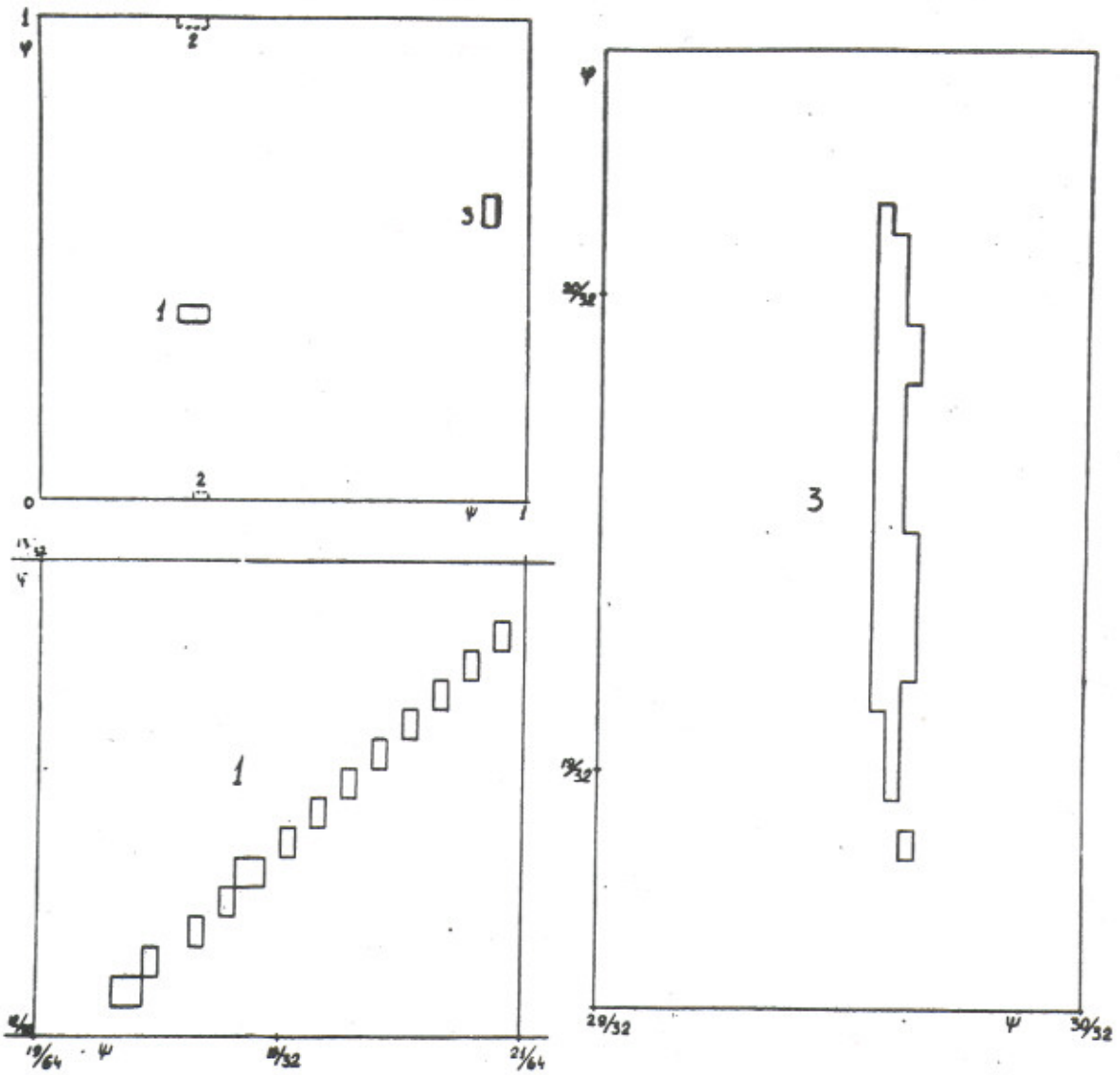

Fig. 3.5.2: "Islets" of stability in the stochastic region ["force" (3.2.5)]: k = 8; $t = 10^8$; T = 3. The figures show the sequence of motion. "Islets" (1,2) lie in the stable phase region, and islet (1) spreads strongly in the direction of the extension (in the unstable region). "Islet" (3) is situated in the unstable region and spreads strongly in the direction of the contraction.

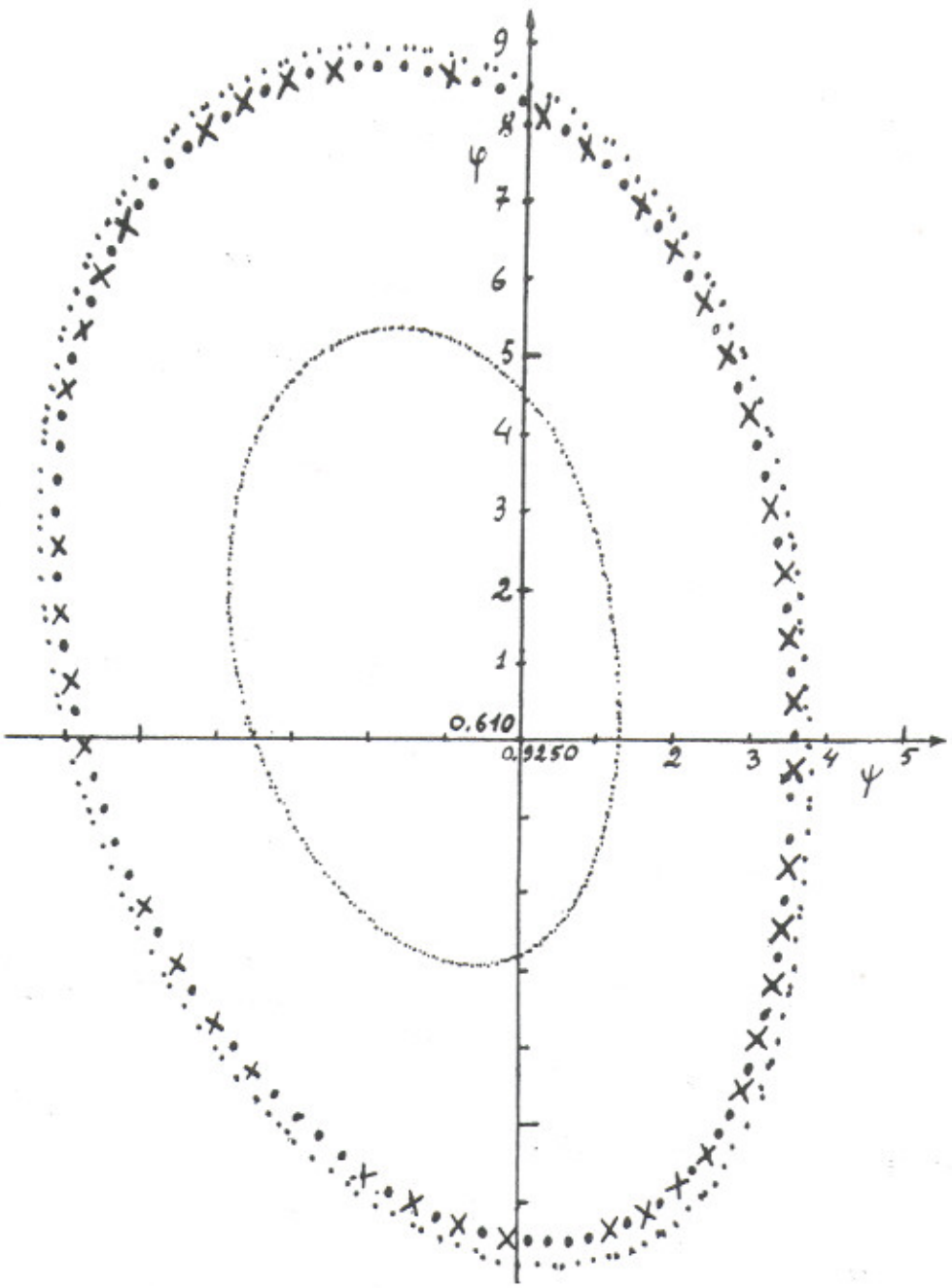

Fig. 3.5.3: The stable trajectories inside the second order resonance, situated in a narrow region (3) (Fig. 3.5.2): $k = 8$: $t = 2 \times 10^7$; for the middle trajectory the dots correspond to the end of the computation, the crosses to the beginning; the scale along the axes differs by a factor of 10 and the figures give the last decimal digit of the numbers in the centre of the diagram.

Figure 3.5.3 shows three trajectories inside one of the "islets" (3), which were in fact used to establish the existence of three stable regions for the case presented in Fig. 3.5.2. The dots in Fig. 3.5.3 denote the values obtained after computation lasting $t = 2 \times 10^7$ steps (for the middle trajectory). A striking feature is their regularity, which becomes still more remarkable if it is noted that they agree with a high degree of accuracy (better than 10^{-4}) with the values obtained right at the beginning of the computation, denoted in Fig. 3.5.3 by crosses. They coincide in both coordinates, which may indicate that they fall in the vicinity of a second order resonance of a very high harmonic ($q = 108$). The dimensions of the "islets" agree in order of magnitude with the estimates of Section 2.8 [(2.8.16), (2.8.14)]. Thus for "islet" (3) Fig. 3.5.2 gives: $\Delta\varphi \approx 0.04$; $\Delta\psi \approx 0.003$, and the formulae of Section 2.8 give the estimates: $\Delta\varphi \sim 0.1$; $\Delta\psi \sim 0.01$ ($T = 2$), if expression (3.4.11) is used for the K-entropy of the "force" (3.2.5).

The case considered partly confirms Sinai's hypothesis (see Section 2.5) that the stable phase region may "damage" the stochasticity also outside this region. However, it is the dimensions and over-all area of the stable regions that are important. From the results in Table 3.4.2 it can be seen that the last quantity rapidly vanishes with the growth of k within the limits of accuracy of the experiment, when the minimum distinguishable size on the phase plane is $\sim 10^{-3}$.

A negligible fraction of the stable regions may be due to the specific form of the "force" (3.2.5). Indeed, for this force there is only one stable phase region (3.4.4) near $\psi = \frac{1}{2}$. It is not possible for there to be a periodical solution ($T > 1$) lying entirely in region (3.4.4), which may lead to a considerable decrease in the number of stable regions. In order to test this assumption the experiment was repeated with "force" (3.2.6). In this case there are two stable phase regions $\psi \approx \frac{1}{4}; \frac{3}{4}$, so that the above-mentioned limitation drops.

The results of this experiment are given in Table 3.4.3 and Fig. 3.5.4. With the exception of the last three values of k, lying just on the left-hand border of the stable interval (2.8.8) for all the remaining (unspecialized) k values the area of the stable regions very rapidly decreases with the growth of k. The law of decrease agrees in order of magnitude with estimate (2.8.20), which for "force" (3.2.6) can be written more specifically in the form:

$$S^{(2)}(k) \sim \left(\ln \frac{k}{2}\right)^{-1} \cdot \exp\left[-3\left(\ln \frac{k}{2}\right)\left(\sqrt{\frac{\pi k}{2}} - 1\right)\right] \qquad (3.5.1)$$

Here we used expression (3.4.10) for the K-entropy of the "force" (3.2.6). Estimate (3.5.1) is shown in Fig. 3.5.4 by a continuous line. It is very sensitive to the quantity $\omega_0(k)$. Therefore for the other "forces" the k values of the experimental points in Fig. 3.5.4 are converted according to ω_0: $k_{eff} = 4/\pi\omega_0$ [see (2.8.12)].

According to the results of Section 2.8, a fraction of the stable regions is sensitive to the value of the parameter $\gamma = \omega_0 \cdot e^h$. When $\gamma > 1$, the number of quasi-resonances of the first type and their over-all area formally diverge (Section 2.8), i.e. the fraction of stable regions can be expected to be considerable. For "force" (3.2.8) $\gamma = 2/e < 1$, as

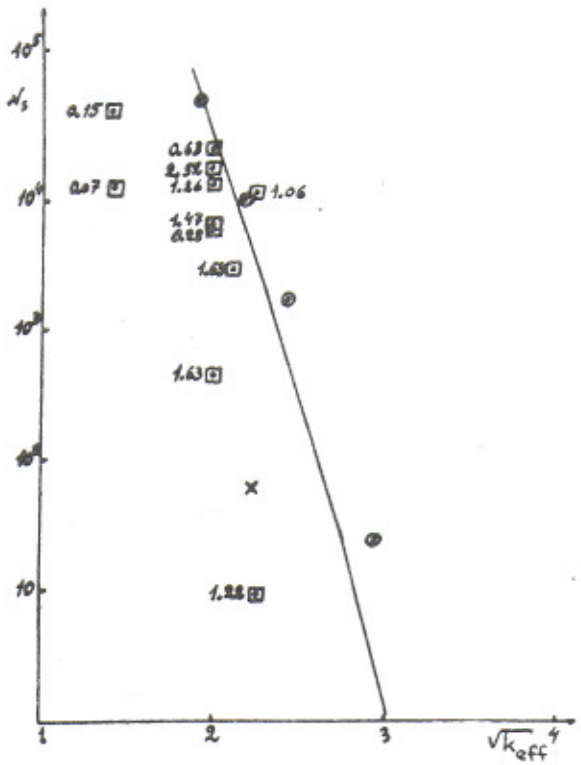

Fig. 3.5.4: The dependence of the number of stable bins of the phase plane (N_s) on the parameter k_{eff} for various cases: ⊙ - force (3.2.6); $\gamma = 0.63$; × - force (3.2.5); $\gamma = 0.74$; ⊡ - force (3.2.3) and (3.2.4); the values of γ are indicated near the dots; the continuous line is an analytical estimate according to formula (3.5.1).

also for force (3.2.6): $\gamma = 2/\pi$. Precisely for this reason a special "force" of the "smoothed out saw" type (3.2.3), (3.2.4) was constructed, for which any values of γ depending on the parameters δ, λ, and k are possible:

$$\gamma = \begin{cases} 2\xi_1 k \cdot (\lambda/e)^{\gamma\xi_1}; & k \le 2/\lambda\xi_1 \\ \frac{4}{\lambda}\left(\frac{\lambda}{e}\right)^{\gamma\xi_1}; & k \gg 2/\lambda\xi_1 \end{cases} \qquad (3.5.2)$$

$$\xi_1 = \frac{1}{2\lambda} - \sqrt{\frac{1}{4\lambda^2} - \frac{\delta}{\lambda}}; \quad e = 2.71\ldots$$

The results of the experiments with "force" (3.2.3), (3.2.4) are also given in Fig. 3.5.4, the value of the parameter γ being indicated next to the experimental points. Contrary to expectations, the stable area in the case of $\gamma > 1$ proves to be even smaller than estimate (3.5.1). A possible explanation of this interesting result in terms of the mutual destruction of quasi-resonances under overlapping is given in Section 2.8.

Apparently this can also explain the fact that the experimental results are of the same order of magnitude as estimate (3.5.1), at least for "force" (3.2.6), which takes into account quasi-resonances for the second type only. However, if quasi-resonances of the first type are significant only when $\gamma > 1$, the total number and area of quasi-resonances of the third type are already divergent for any γ (Section 2.8). It is evident that they, like the quasi-resonances of the first type for $\gamma > 1$, mutually destroy each other when they overlap.

In spite of the fast reduction of the area of the quasi-resonances with the growth of k, it is not out of the question that their total number is unlimited, and they form an everywhere dense set of stable trajectories (Sinai's hypothesis, Section 2.5). The estimates of Section 2.8 give precisely this result; however, they are not sufficiently accurate, so this question still remains open.

In spite of all the experimental results given above, there is still some doubt as to whether the whole system of stable regions is so fine that it escapes observation (like one of the stable regions in Fig. 3.5.3). It seems to us that the answer to this question is given by the following gross experiment. We have in all about 100 cases of computation with $k \gg 1$. A stable region was not entered in any of them, in spite of the quite different initial conditions.

3.6 An example of weak instability of a many-dimensional system

In this section we shall give a brief description of the first attempt to observe Arnold diffusion for a two-dimensional non-autonomous oscillator, given by the transformation:

$$\begin{aligned} I_1' &= I_1 - \varphi_1^9 + \mu_0 \varphi_2 \\ I_2' &= I_2 - \varphi_2^9 + \mu_0 \varphi_1 \\ \varphi_1' &= \varphi_1 + I_1' \\ \varphi_2' &= \varphi_2 + I_2' \end{aligned} \qquad (3.6.1)$$

It is easy to see that this model is an extension of the elementary model to the two-dimensional case. The choice of $f(\phi) = -\varphi^9$ is due to the desire to have more resonances with conservation of the analyticity of the force (see below).

Numerical experiments on Arnold diffusion were carried out together with Keil*) and Sessler**) on the CDC-6600 computer at CERN, in Geneva[76]. Model (3.6.1) was chosen after many preliminary experiments.

Before going over to the experiments themselves let us obtain some simple analytical relations for model (3.6.1) which will be useful later on.

If $|\varphi_i^9| \ll 1$ and $|\mu_0 \varphi_i| \ll 1$, transformation (3.6.1) can be approximately replaced by the differential equations:

$$\begin{aligned} \dot{I}_i &\approx -\varphi_i^9 + \mu_0 \varphi_j \\ \dot{\varphi}_i &\approx I_i \end{aligned} \qquad (3.6.2)$$

with the conserved Hamiltonian***)

---

*) E. Keil, CERN, Geneva, Switzerland.

**) A. Sessler, Lawrence Radiation Laboratory, University of California, Berkeley, California, USA.

***) We thus ignore the external perturbation, whose effect in fact turns out to be very weak (see below).

$$H = \frac{1}{2}(I_1^2 + I_2^2) + \frac{1}{10}(\varphi_1^{10} + \varphi_2^{10}) - \mu_0 \varphi_1 \varphi_2 \qquad (3.6.3)$$

In view of the sharp dependence of the potential energy on the co-ordinate φ, it can be considered approximately that the unperturbed motion ($\mu_0 = 0$) takes place in a rectangular potential well; it is characterized by the frequency:

$$\omega \approx \frac{\pi}{2\sqrt{5}} \varphi_0^4 \qquad (3.6.4)$$

and spectrum:

$$\varphi_{2n+1} \approx \frac{8}{\pi^2}(-1)^n \varphi_0 \cdot (2n+1)^{-2} \qquad (3.6.5)$$

The last expression is valid for harmonics that are not too high: $n \leq 10$, while an approximation to a rectangular potential well is valid.

In approximation (3.6.3) there are only coupling resonances: $m\omega_1 = n\omega_2$, the effect of which can lead only to an energy exchange between oscillators, while the total energy H (3.6.3) is conserved. Since the latter depends also on the coupling energy $H_i = -\mu_0\varphi_1\varphi_2$, the maximum value of the amplitude of one of the oscillators, say φ_{10}, is reached under the condition $\mu_0\varphi_{10} = \varphi_{20}^9$ or:

$$10 \cdot H_2 = H_i \qquad (3.6.6)$$

where $H_2 = \varphi_{20}^{10}/10$; $H = H_1 + H_2 + H_i$.

Variation of the total energy of the system H is possible on account of the external resonances:

$$m\omega_1 + n\omega_2 = 2\pi \qquad (3.6.7)$$

where we took into consideration only the first harmonic of the external perturbation with a frequency of 2π, since under the condition $\varphi^9 \ll 1$ assumed above, $\omega \sim \varphi^4 \ll 2\pi$ (3.6.4). From the shape of the spectrum (3.6.5) it follows that maximum amplitude corresponds to one-dimensional resonance $n = 0$ (or $m = 0$), and $\omega_2 \approx 0$, whence the minimal oscillation harmonic necessary for an external resonance is equal to: $m \approx 2\pi/\omega_0$ where ω_0 is the maximum value of the frequency for given initial conditions.

Let us now turn to a description of the numerical experiments.

The largest part of the computing programme, including the rather laborious data processing, was written in FORTRAN. However, the main loop for computing transformation (3.6.1) proper is written in the symbolic operating code of the CDC 6600 (ASCENT) in order to obtain the maximum computation speed*). We managed to place the whole of this loop in the instruction stack of the CDC 6600's central processor, thus eliminating the relatively slow reference to the operative memory. Moreover, advantage was taken of the possibility of two parallel multiplications in the CDC 6600. As a result it proved possible to reduce the

*) The possibility of combining these two languages was in our opinion a considerable advantage of the compiler of the CERN computer.

time for the computation of one step of transformation (3.6.1) to 9 μsec in spite of the large number of multiplications. The processed computation data was put out periodically after a specific number of steps and included, in particular, a map of the two-dimensional projection of the four-dimensional phase space of the system onto the plane (φ_1,φ_2) (see, for example, Fig. 3.6.4), and also part of a histogram near the edge of the distribution function of the trajectory $f(\varphi_1,\varphi_2)$ (see, for example, Fig. 3.6.5). The purpose of this processing was to find out whether the edge of the distribution was sharp or smooth. It is easy to see that the latter indicates that there are no invariant tori, i.e. that there is some instability of motion. Indeed in the one-dimensional case the phase trajectory is an ellipse and its projection onto the axis φ leads to the singularity $f(\varphi) \propto |\varphi - \varphi_0|^{-\frac{1}{2}}$ near the edge of the distribution. For a two-dimensional system with $\mu_0 = 0$ the distribution function occupies a rectangle in the plane (φ_1,φ_2) with a similar singularity around the edge (Fig. 3.6.7). If $\mu_0 \neq 0$, but there are invariant tori, the singularity is conserved, but now with a more complicated outline, reflecting the configuration of an invariant torus (Fig. 3.6.9). Finally, if the edge of the distribution becomes smooth, this points to the destruction of the invariant tori and their transformation into a layer of some thickness (in four-dimensional space, Fig. 3.6.5).

First of all it is necessary to determine the region of one-dimensional stability (3.6.1) when $\mu_0 = 0$. This can be done as in Section 3.3, by one trajectory, the initial point of which certainly lies in the region of stochasticity. In order to prevent the trajectory from drifting into "infinity", i.e. the computer's overflow, it is necessary to limit the phase plane of the system by taking the fractional part (Section 3.2), which is equivalent to periodical boundary conditions. In the present case a square was used: $-1 \leq I, \varphi < 1$. The phase map of the system for $t = 10^6$ is given in Fig. 3.6.1, where the circles mark the bins occupied by the trajectory. For $I_0 = 0$ the initial phase φ_0 should lie in the interval (-0.78, +0.78). The accuracy of this value of the interval is determined by the bin size of the phase map and is about +2.5%.

Let us compare this result with the theoretical estimate, which it is easiest to obtain from an analysis of the local stability (Section 2.4): $K_0 = -9\varphi_0^8 < -4$, whence: $\varphi_0 < 0.9$, which is very close to the numerical result given above.

As noted in Section 3.3, at the border of stochasticity in the intermediate zone the instability develops very slowly and therefore the border of stochasticity observed depends on the time of motion. The value given above for the stable interval relates to $t = 10^6$. When $t = 2 \times 10^5$ the border of stochasticity shifts outwards by approximately 4% (along φ_0). It is not out of the question that when $t > 10^6$ it shifts inwards again a little, although according to the KAM theory there is certainly a border of eternal stability (see Section 3.3 and below).

Probably the most interesting experiment with model (3.6.1) is the unique case of very weak instability which was observed when: $\mu_0 \approx 0.00115$; $I_{10} = I_{20} = 0$; $\varphi_{10} = 0.375$; $\varphi_{20} = 0.721$. Figure 3.6.2 shows the time dependence of the increase (ΔS) of the area (S) of the above-mentioned two-dimensional projection (φ_1,φ_2) of the trajectory of motion in a linear and logarithmic scale.

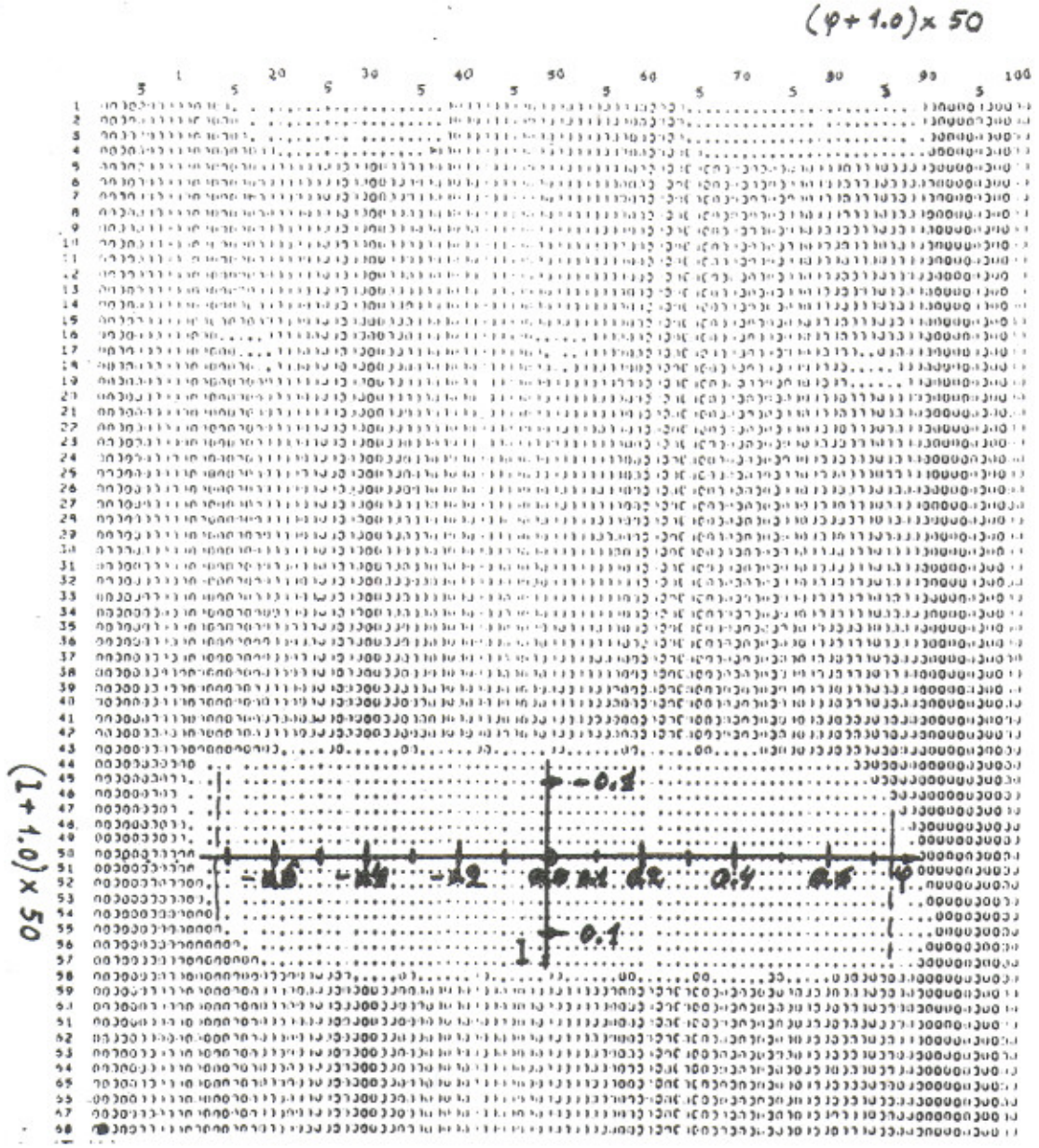

Fig. 3.6.1: The region of one-dimensional stability for model (3.6.1); $\mu_0 = 0$; $t = 10^6$.

Phase maps of the projection of the motion on to the plane (ψ_1, ψ_2) are given in Figs. 3.6.3 and 3.6.4; the first of them relates to the beginning of the motion ($t = 10^7$ steps), and the second to the very end ($t = 3.648 \times 10^8$), when the trajectory emerges into the region of one-dimensional instability. A histogram of the distribution in the latter case is given in Fig. 3.6.5, where it is clearly seen that its border is smooth and consequently some instability takes place.

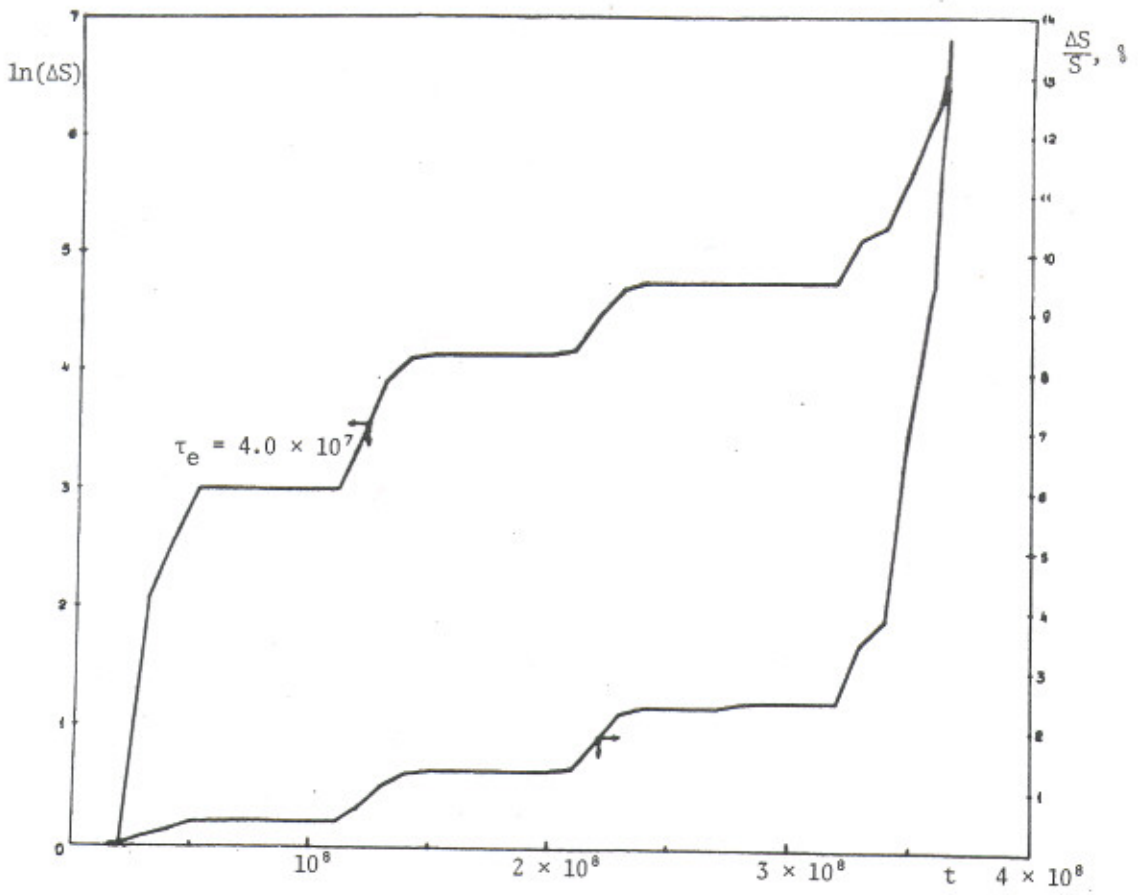

Fig. 3.6.2: An example of the weak instability of a two-dimensional non-autonomous oscillator (3.6.1): $\mu_0 \approx 0.00115$; $\varphi_{10} \approx 0.375$; $\varphi_{20} \approx 0.722$; $I_{10} = I_{20} = 0$; S is the area of projection of the motion on to the plane (φ_1, φ_2); ΔS is the increase of S in the process of motion; τ_e is the rise-time.

The law of the development of the instability in time is surprising. First of all it is striking that the increase of the area (ΔS) takes place in portions. This, however, may be due to the finite size of the phase plane bin; so, for example, the first "step" in Fig. 3.6.2 corresponds to 19 bins only, and the whole area S comprises about 5,000 bins. An analysis of the phase maps, which were put out periodically in $\Delta t = 10^7$, shows that the

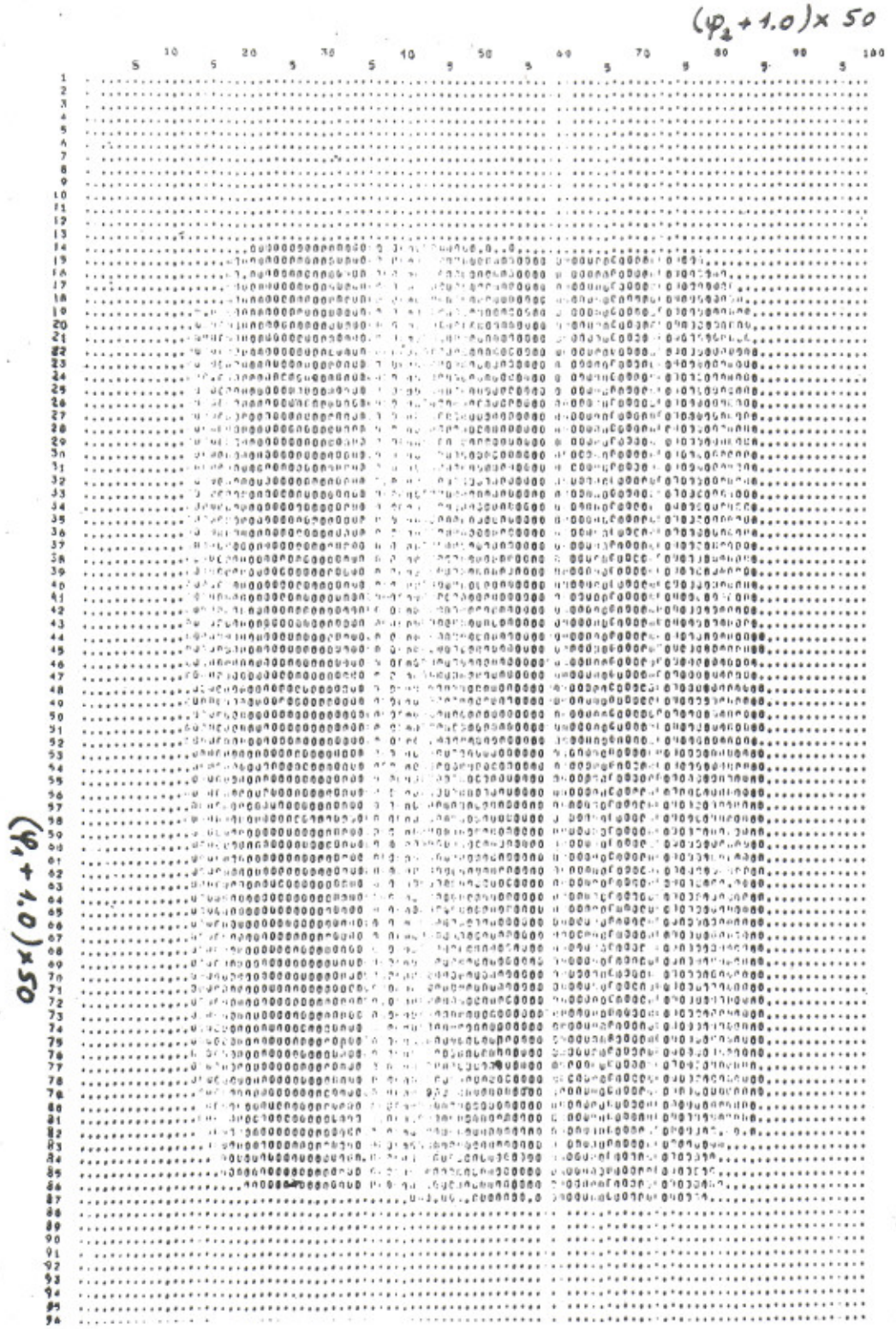

Fig. 3.6.3: Phase map of the case in Fig. 3.6.2 near to the beginning of the computation: $t = 10^7$. The circles mark the bins occupied by the trajectory and the dots give the coordinate network.

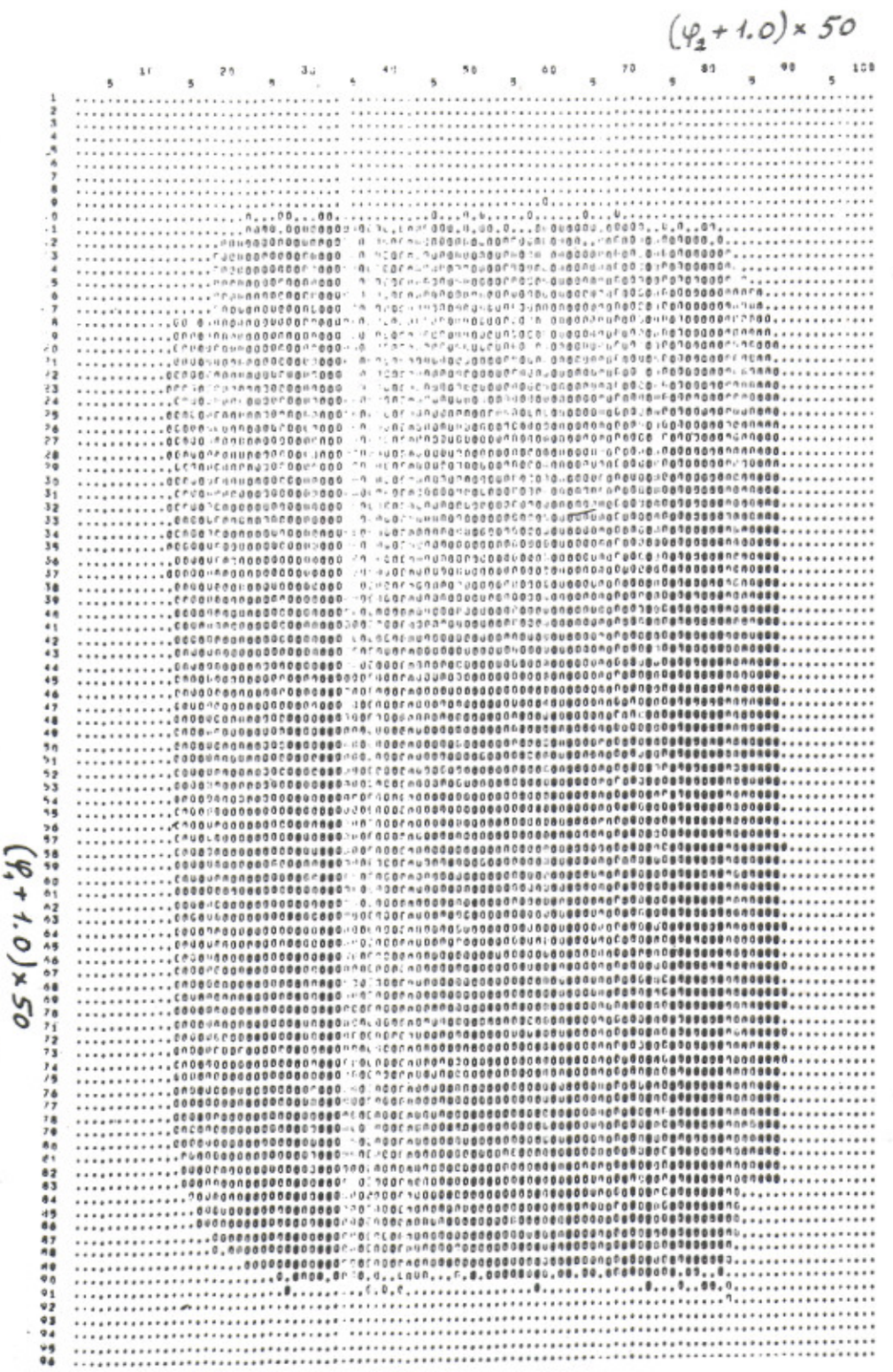

Fig. 3.6.4: Phase map of the case in Fig. 3.6.2 near to the end of the computation: $t = 3.648 \times 10^8$. The circles mark the bins occupied by the trajectory and the dots give the coordinate network.

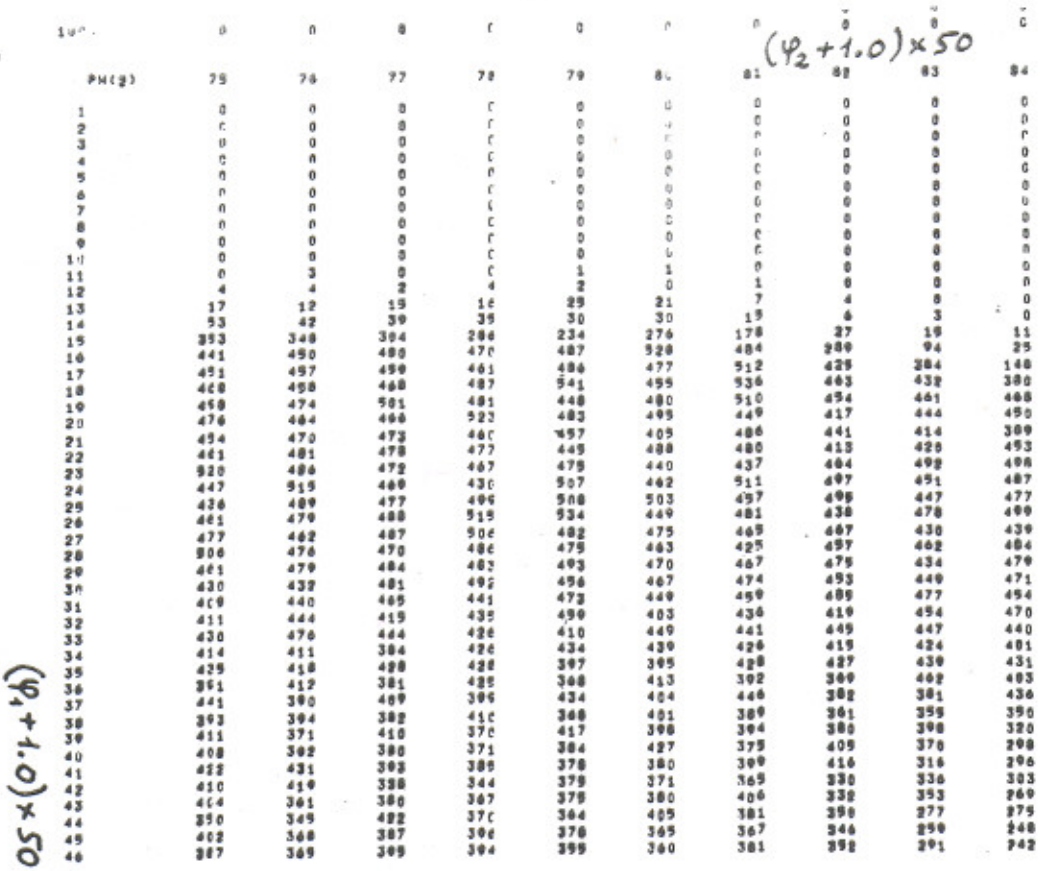

Fig. 3.6.5: Part of the histogram of the distribution of the projection of the trajectory on to the plane (φ_1, φ_2) for the case in Fig. 3.6.2: $t = 3.648 \times 10^8$.

increase in the area occurs smoothly along the whole perimeter, which shows the rapid energy exchange between the two degrees of freedom. Measurement of the local instability shows that this exchange takes place already in $t \sim 10^3$ (see Table 3.6.1).

The most surprising thing in Fig. 3.6.2 is the unexpected steep rise of the curve $\Delta S(t)$ at the end of the computation. The data of the phase maps show that almost immediately after the beginning of the rise, the energy exchange between the oscillators ceases and the increase in S is on account of only one of them.

On the whole the function $\Delta S(t)$ is exponential rather than linear or proportional to $\sqrt{t}$. If the last sharp rise is excluded, the dependence $\Delta S(t)$ agrees best with a linear function, although one certainly cannot exclude the possibility (because of large experimental errors) of a dependence like $\Delta S \propto \Delta\varphi_0 \propto \sqrt{t}$, corresponding to ordinary diffusion ($\Delta\varphi_0 \ll \varphi_0$). In the latter case the mean diffusion coefficient is: $D_\varphi = d(\Delta\varphi_0)^2/dt \sim 2 \times 10^{-13}$.

If it is assumed that there is a linear law S(t), the mean rate of development of instability is: $V_\varphi = d(\Delta\varphi_0)/dt \sim 4 \times 10^{-11}$. However, this case appears unlikely. As far as we know, the only mechanism leading to a linear law is connected with the so-called microtron resonance (Section 2.4). However, this contradicts the local instability of motion discovered experimentally (see below).

The weak instability discovered cannot be explained by the computer round-off errors. Indeed, the relative error of single round-off in the CDC-6600 does not exceed $\varepsilon_0 = 2^{-47} \approx 10^{-14}$. Even if it is considered that all the errors accumulate one way, then the error of one step (for φ) is: $\varepsilon_1 = 4\varepsilon_0 < \varphi^3 > + 2\mu_0 \varepsilon_0 < \varphi^2 > + \varepsilon_0 \approx \varepsilon_0$, and for the whole computation: $\varepsilon_N < \varepsilon_0 \times 10^9 \approx 10^{-5}$, which is considerably less than the size of a phase bin $\Delta\varphi = 2 \times 10^{-2}$. As a check the trajectory of system (3.6.1) with the interaction "switched off" ($\mu_0 = 0$) was computed during $t = 10^8$. Figures 3.6.6 and 3.6.7 give the phase map and distribution histogram respectively. The stability of motion in this case is evident. Similar results are also obtained with the interaction "switched on" (even though $\mu_0 \approx 0.00915$) for special initial conditions, for example for $\varphi_{10} = 0.375$; $\varphi_{20} = 0.522$ (Figs. 3.6.8 and 3.6.9; $t = 5 \times 10^7$).

The mechanism of weak instability is most probably connected with Arnold diffusion along one of the strong resonances. In this case the motion must be locally unstable. In order to check this assumption two trajectories very close together at the beginning ($\Delta I = 0$; $\Delta\varphi \sim 10^{-10}$) were computed simultaneously and the distance between them was calculated depending on time (divergence of the trajectories). Figure 3.6.10 shows the divergence in phase; it does not contradict the exponential law with a rise-time $\tau_e = h^{-1} \approx 10^3$, where h is the K-entropy of the system. Approximately the same result is obtained for the momentum divergence of the trajectories.

Nevertheless the question is in fact more complex than it may appear at first glance. In Fig. 3.6.11 the data of Fig. 3.6.10 are plotted in a log-log scale and do not contradict (especially $\Delta\varphi_2$) the linear divergence of the trajectories. The latter can be explained as a simple frequency shift of the non-linear oscillations.

It is evident that the chosen interval $t = 3000$ is too short for any firm conclusion for the given value of the perturbation $\mu_0 = 0.00115$. An example of local instability when there is greater perturbation is given in Fig. 3.6.12. There is no doubt here as to the exponential nature of the divergence of the trajectories (on the average). Let us point out that the law of variation is identical for all four quantities (ΔI_{12}; $\Delta\varphi_{12}$). The exponential divergence continues up to $\Delta I \sim I_0 = 3.4 \times 10^{-3}$. The subsequent insignificant increase of ΔI is explained, probably, by phase oscillations in the coupling resonances.

For weak instability ($\mu_0 = 0.00115$) additional measurements of the local stability were made for different initial conditions in the interval: $0.5 < \varphi_{0i} < 0.75$ ($I_{0i} = 0$) and $t = 10^5$. In 11 cases out of 26 clearly expressed local instability was observed. An example of instability is given in Fig. 3.6.13, where $\Delta \equiv \Delta I$. The difference ΔI increases by more than 10 orders and reaches $\Delta_{max} \sim 10^{-3}$ (initial trajectory shift $\Delta I \sim \Delta\varphi \sim 10^{-14}$). The K-entropy in this case is $h \approx 2.5 \times 10^{-4}$, i.e, four times less than in Fig. 3.6.10. Figure 3.6.14 gives an example of a trajectory which was interpreted as stable. In spite of the great dispersion of the points the non-exponential character of the dependence $\Delta I(t)$ can be fairly well seen. Moreover, in contrast to Fig. 3.6.13, here the motion is explicitly regular (strong periodic excursions of the points upwards), which is incompatible with stochasticity. But there is an especially sharp discrimination between stable and unstable cases by the maximum value of ΔI at the end of computation. For example, in Fig. 3.6.14 the final value of $\Delta I \approx 3 \times 10^{-11}$, i.e. it differs by more than seven orders from the unstable case in Fig. 3.6.13. Such a clear discrimination can always be achieved, provided the computing time substantially exceeds the characteristic time for the development of instability: $ht \gg 1$.

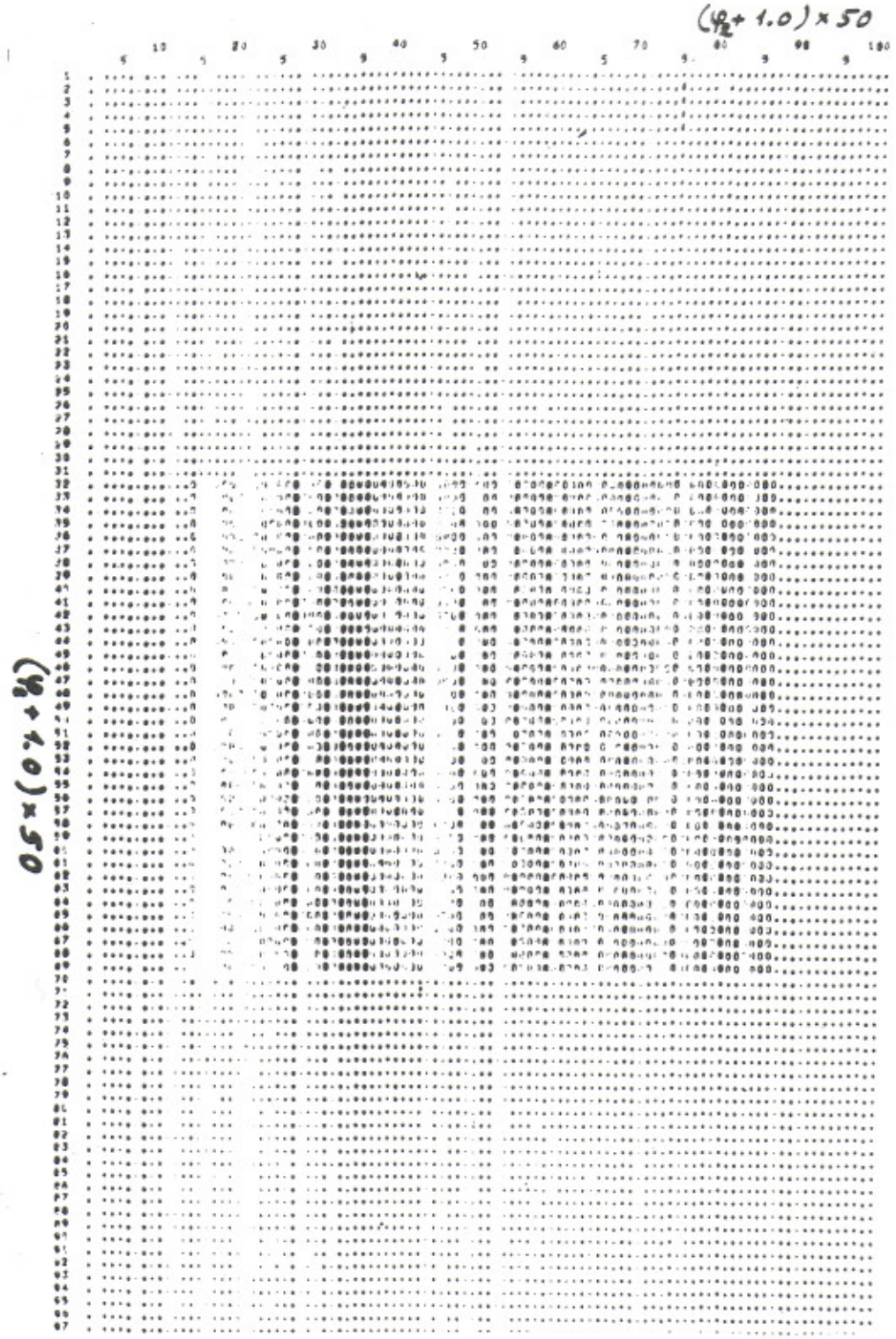

Fig. 3.6.6: Check experiment: the same as Fig. 3.6.3, except that $\mu_0 = 0$; $t = 10^8$.

$(\varphi_2 + 1.0) \times 50$

PH(2)	83	84	85	86	87	88	89	90	91
1	0			0		0	0	0	0
2	0			0		0	0	0	0
3	0			0		0	0	0	0
4	0			0		0	0	0	0
5	0			0		0	0	0	0
6	1			0		0	0	1	0
7	0			0		0	0	0	0
8	0			0		0	0	0	0
9	0			0		0	0	0	0
10	0			0		0	0	0	0
11	0			0		0	0	0	0
12	0			0		0	0	0	0
13	0		0	0		0	0	0	0
14	0		0	0	0	0	0	0	0
15	0			0		0	0	0	0
16	0			0		0	0	0	0
17	0			0		0	0	0	0
18	0			0	0	0	0	0	0
19	0			0		0	0	0	0
20	0			0		0	0	0	0
21	0			0		0	0	0	0
22	0			0		0	0	0	0
23	0			0		0	0	0	0
24	0			0		0	0	0	0
25	0			0		0	0	0	0
26	0			0		0	0	0	0
27	0		0	0	0	0	0	0	0
28	0			0	0	0	0	0	0
29	0			0	0	0	0	0	0
30	0			0		0	0	0	0
31	0			0		0	0	0	0
32	424	453	547	737	803	0	0	0	0
33	257	247	302	419	513	0	0	0	0
34	230	210	267	356	427	0	0	0	0
35	182	2	244	299	364	0	0	0	0
36	174	186	229	325	371	0	0	0	0
37	176	185	223	295	361	0	0	0	0
38	171	179	215	299	361	0	0	0	0
39	180	181	212	299	356	0	0	0	0
40	175	185	225	298	36	0	0	0	0
41	166	182	217	310	351	0	0	0	0
42	171	185	22	288	359	0	0	0	0
43	160	1 6	218	314	346	0	0	0	0
44	176	193	217	277	309	0	0	0	0
45	168	174	209	314	346	0	0	0	0
46	178	187	227	271	364	0	0	0	0
47	161	168	22	317	345	0	0	0	0
48	169	174	225	277	343	0	0	0	0
49	171		208	317	347	0	0	0	0
50	176	193	217	277	376	0	0	0	0
51	179	178	21	314	391	0	0	0	0
52	177	197	232	276	369	0	0	0	0

$(\varphi_1 + 1.0) \times 50$

Fig. 3.6.7: Check experiment: the same as Fig. 3.6.5, except that $\mu_0 = 0$; $t = 10^8$.

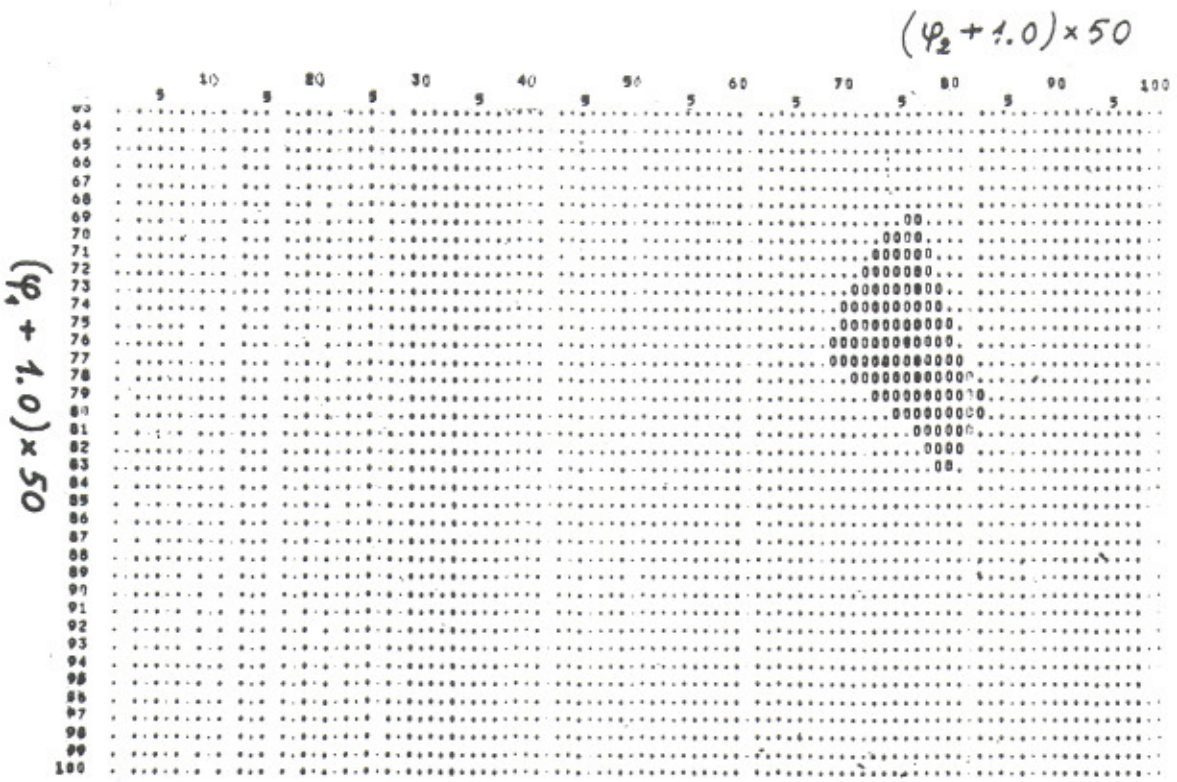

Fig. 3.6.8: Phase map of the stable region of system (3.6.1): $\mu_0 \approx 0.00915$; $\varphi_{10} \approx 0.375$; $\varphi_{20} \approx 0.522$; $I_{10} = I_{20} = 0$.

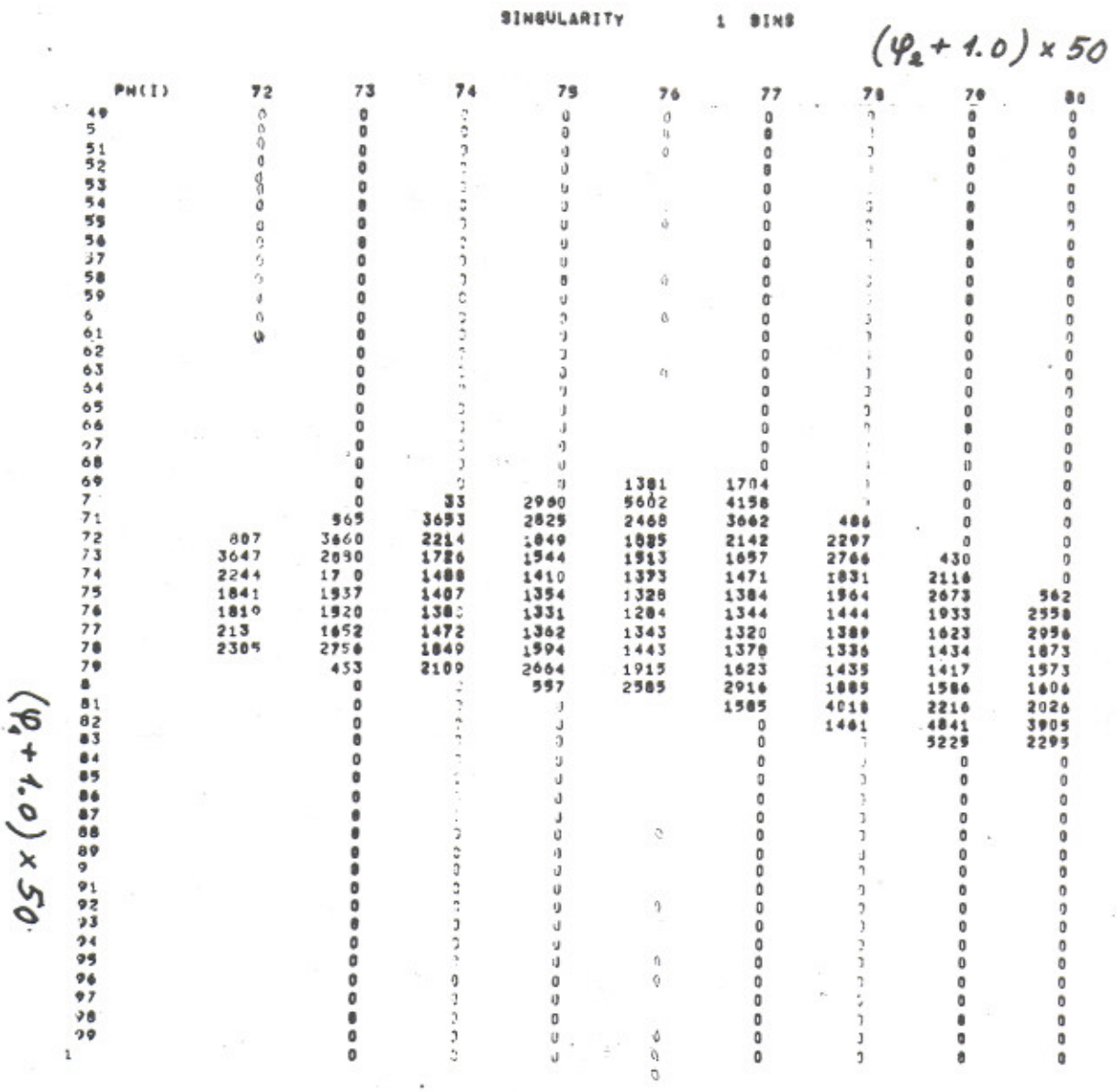

Fig. 3.6.9: Histogram of the distribution of the stable trajectory in Fig. 3.6.8.

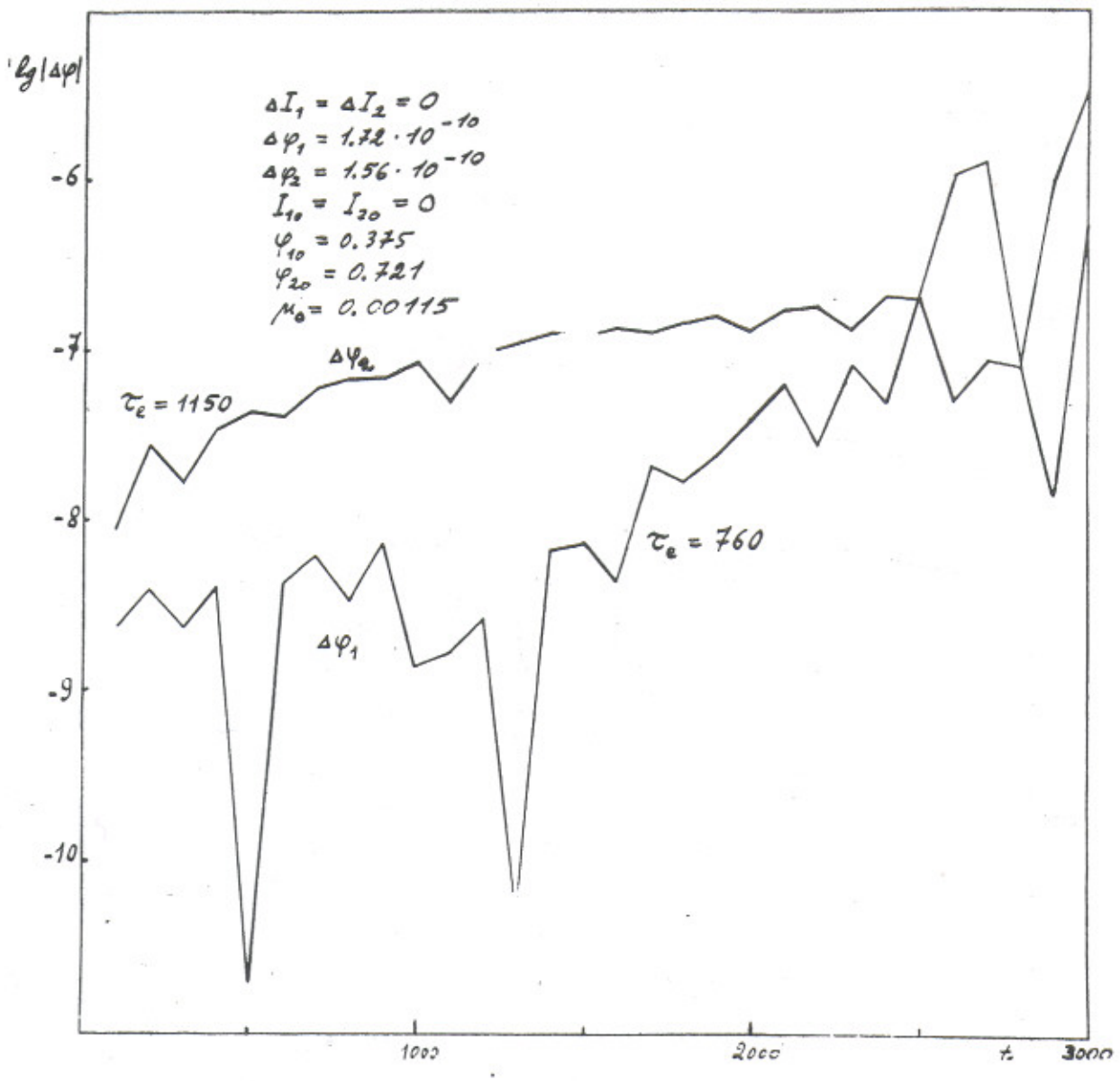

Fig. 3.6.10: Local instability of motion for the case in Fig. 3.6.2: τ_e is the mean rise-time.

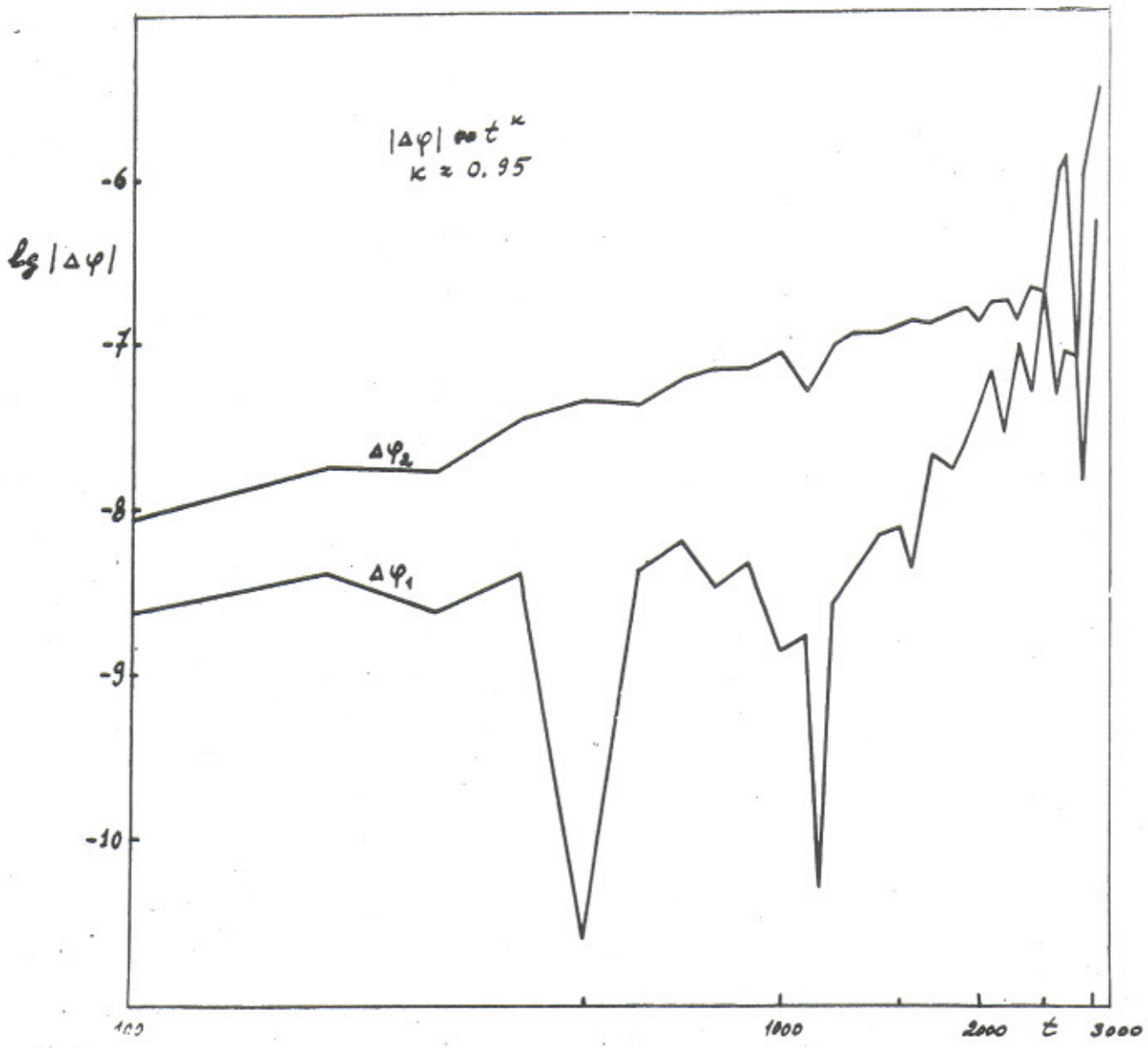

Fig. 3.6.11: The same as in Fig. 3.6.10, but in a log-log scale.

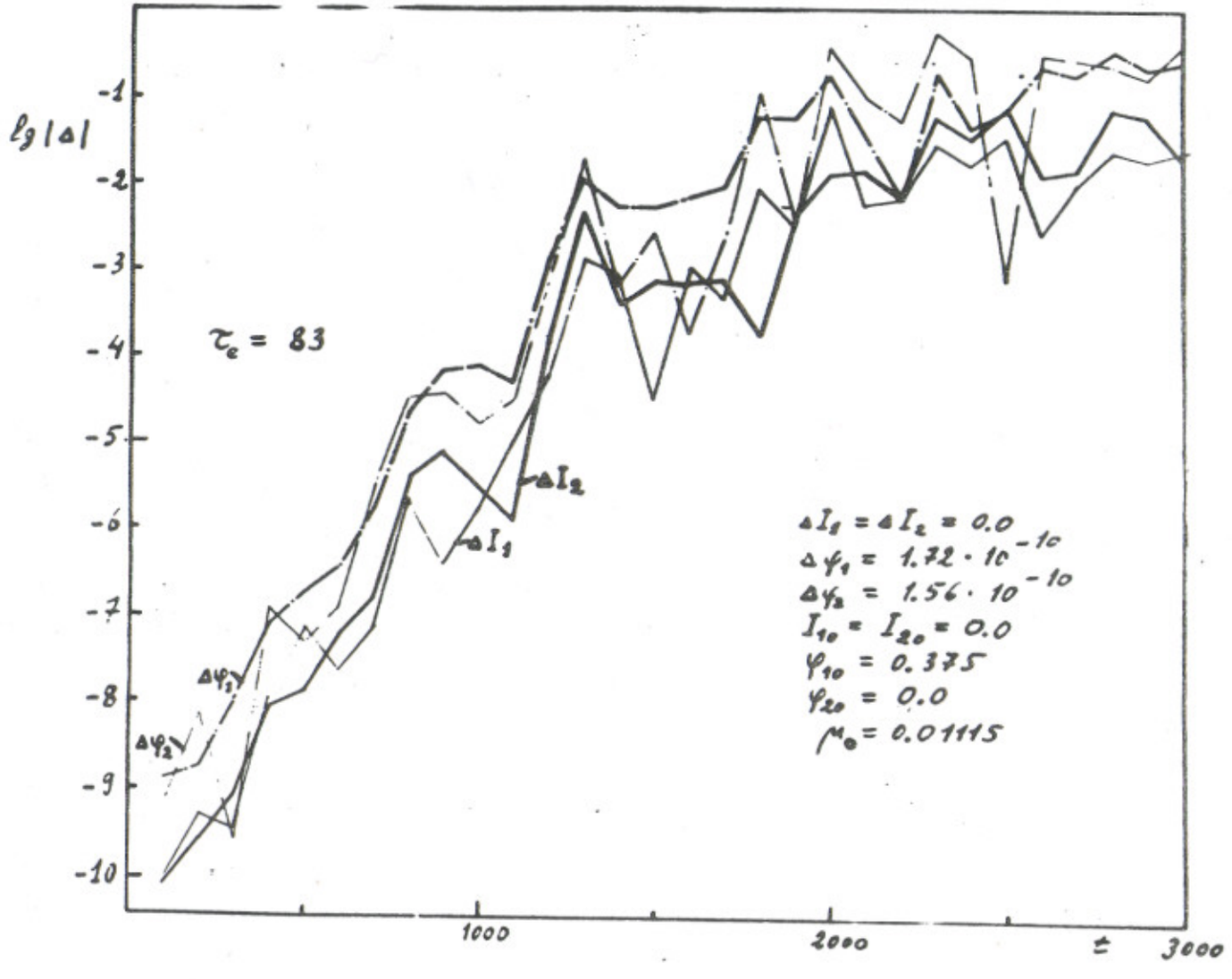

Fig. 3.6.12: Local instability of motion for model (3.6.1); τ_e is the mean rise-time; $\mu_0 \approx 0.011$.

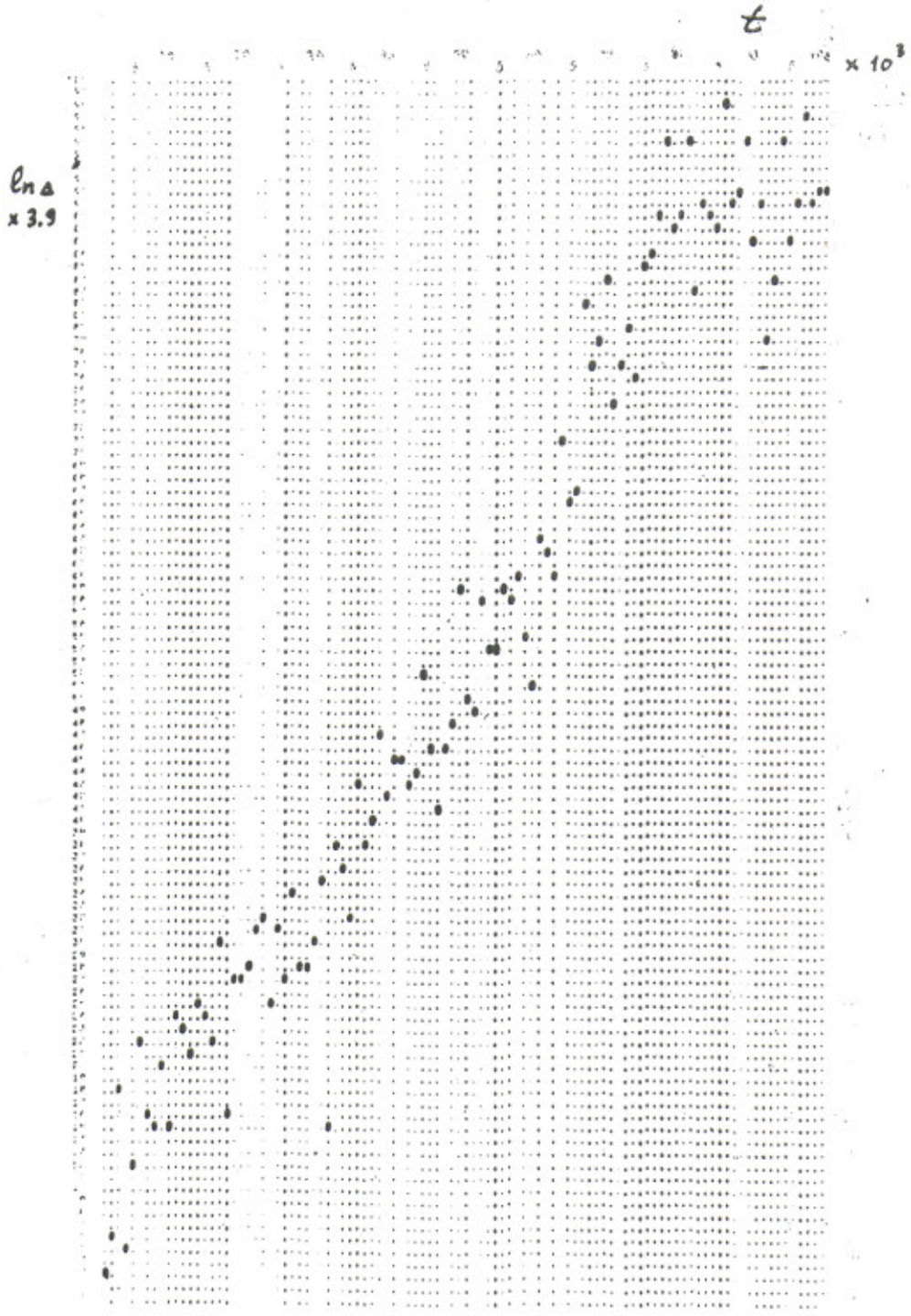

Fig. 3.6.13: Local instability for the case in Fig. 3.6.2, except that $\varphi_{10} \approx 0.555$; $\varphi_{20} \approx 0.745$; $\Delta \equiv \Delta I_1$: the motion is unstable.

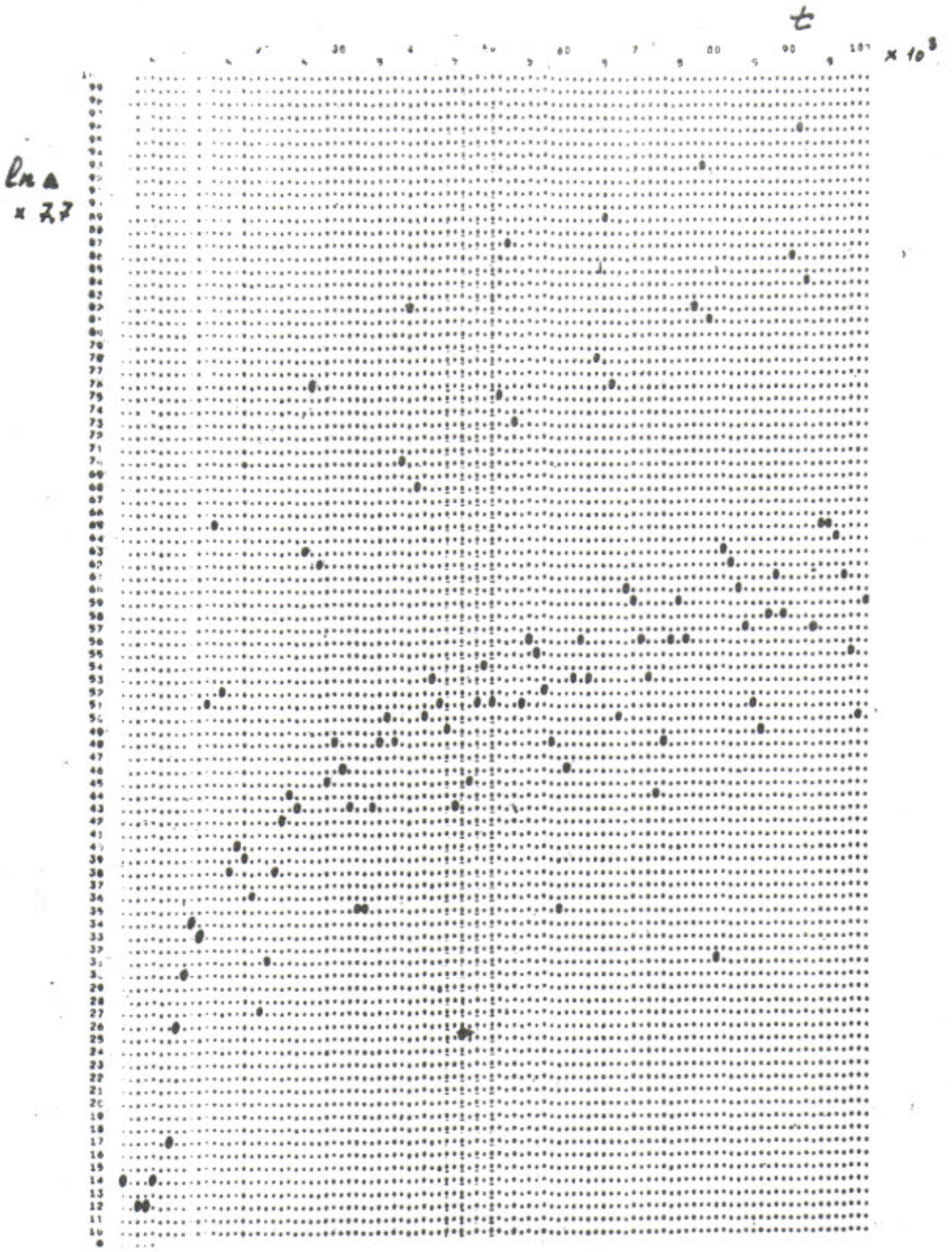

Fig. 3.6.14: The same as Fig. 3.6.13, except that: $\psi_{10} \approx 0.670$; $\psi_{20} \approx 0.640$; the motion is stable.

A summary of the results on local instability is given in Table 3.6.1. The numbers in the first column show the computation sequence for a random choice of φ_{10}, φ_{20}. All the unstable cases are grouped at the end of the table in order of decreasing K-entropy (the mean values of the K-entropy for two momenta and two phases are given). The values of the K-entropy are clearly divided into five groups, as shown in the table. The last column gives the mean values of the K-entropy per group. The different groups correspond, apparently, to resonances of different harmonics. The difference of the resonances according to their magnitude shows that the overlapping is slight. This result is also confirmed by the value of the relative fraction of unstable initial conditions, which according to the data of the table is: $\delta = 11/26 \approx 43\%$.

Table 3.6.1 illustrates once more the clear discrimination between stable and unstable cases according to the values Δ_{max} and thus the applicability of the method of investigating local instability.

Unfortunately the available experimental data does not make it possible unequivocally to link the discovered weak instability with Arnold diffusion, nor does it contradict such a hypothesis. Let us demonstrate this, using estimate (2.12.22). The main expression (2.12.29) is inapplicable in the present case because of a big difference in frequencies for an external resonance (see below). Let us choose coupling resonances as guiding resonances, and external resonances as perturbing resonances. The harmonic number of the latter is determined from (3.6.7) and (3.6.4) and is equal to (2.12.23):

$$\frac{mn'}{n_0} + \frac{2n'}{n_0} \approx \frac{8\sqrt{5}}{n_0 \varphi_0^4} \qquad (3.6.8)$$

Further, $\varepsilon \sim \mu_0/\varphi_0^8$ (3.6.1); $\alpha \sim 1$; $\varphi_0 \approx 0.7$. In view of the marked uncertainty of the estimate of the Arnold diffusion coefficient, let us use its experimental value, given above: $D_\varphi \sim 2 \times 10^{-13}$ and estimate the unknown parameter n_0 instead. As a result we obtain $n_0 \approx 3.5$ which does not contradict the expected value $n_0 \sim 10$ (see beginning of section).

Nevertheless, one cannot completely exclude the possibility that the observed weak instability is some complex one-dimensional effect. In particular, stability of motion when $\mu_0 = 0$ (Figs. 3.6.6 and 3.6.7) does not exclude this possibility either, since negative coupling energy may lead to an increase in the amplitude of the oscillations when $\mu_0 \neq 0$ (3.6.3).

It is obvious that this phenomenon calls for much more detailed experimental investigation. It seems to us that even a single case of weak instability which has in fact been observed shows that the problem as a whole is sufficiently interesting and important. Another case of possible Arnold diffusion will be discussed in Section 4.4.

Table 3.6.1

N	φ_{10}	φ_{20}	I		φ		$\langle h \rangle \times 10^2$
			Δ_{max}	$\langle h \rangle \times 10^2$	Δ_{max}	$\langle h \rangle \times 10^2$	
1.	0.711	0.656	2.10^{-10}		5.10^{-9}		
2.	0.680	0.618	10^{-11}		2.10^{-8}		
3.	0.596	0.733	3.10^{-10}		3.10^{-8}		
4.	0.619	0.625	6.10^{-11}		4.10^{-9}		
6.	0.517	0.615	5.10^{-11}		2.10^{-9}		
7.	0.610	0.580	9.10^{-11}		6.10^{-9}		
8.	0.672	0.642	8.10^{-11}		2.10^{-8}		
11.	0.560	0.588	3.10^{-10}		2.10^{-8}		
12.	0.589	0.503	3.10^{-10}		5.10^{-9}		
15.	0.601	0.648	4.10^{-11}		6.10^{-9}		
17.	0.531	0.726	2.10^{-10}		10^{-8}		
19.	0.538	0.714	9.10^{-11}		2.10^{-8}		
21.	0.670	0.640	7.10^{-11}		2.10^{-8}		
23.	0.681	0.606	5.10^{-10}		2.10^{-8}		
26.	0.574	0.560	2.10^{-10}		10^{-8}		
5.	0.587	0.744	2.10^{-1}	1.2	9.10^{-1}	1.2	1.1
14.	0.516	0.734	2.10^{-1}	1.2	9.10^{-1}	1.1	
9.	0.744	0.533	10^{-1}	1.2	9.10^{-1}	0.9	
18.	0.750	0.598	10^{-1}	1.0	9.10^{-1}	1.1	
24.	0.628	0.553	7.10^{-2}	1.0	9.10^{-1}	1.1	
16.	0.682	0.560	7.10^{-2}	0.9	9.10^{-1}	0.9	
13.	0.522	0.556	4.10^{-2}	0.54	9.10^{-1}	0.54	0.54
10.	0.535	0.512	3.10^{-2}	0.33	9.10^{-1}	0.31	0.32
20.	0.747	0.658	3.10^{-1}	0.15	9.10^{-1}	0.15	0.14
22.	0.554	0.556	7.10^{-2}	0.13	9.10^{-1}	0.13	
25.	0.555	0.745	5.10^{-2}	0.025	7.10^{-2}	0.025	0.025

CHAPTER 4

SOME APPLICATIONS

This last chapter of the present paper is devoted to some applications taken from the most varied regions of mechanics. Their choice is rather arbitrary and merely reflects current success in the application of the developing theory of stochasticity to specific problems. Some of them have been completely solved right up to the stage of practical application (Sections 4.1, 4.2, 4.7), and others have only been formulated (Section 4.3). In some cases numerical experiments were used, which may also be regarded as further proof of the general theory (Sections 4.1, 4.2, 4.6). In our opinion the questions of special interest are those connected with Arnold diffusion in the Solar System (Section 4.5); however, here there is still a great deal that is unknown.

4.1 Fermi stochastic acceleration

The stochastic method of acceleration is generally connected with the name of Fermi, who proposed one of the variants of such acceleration as an explanation of the origin of cosmic rays[99]. A little earlier (in 1948) a similar proposal for ordinary (terrestrial) accelerators was made by Burstein, Veksler and Kolomensky[100]. However, this paper was not published and remained little known until 1955[100]. At the present time there are a large number of papers devoted to the various aspects of statistical acceleration in plasma [see for example the review by Tsytovich[101]]. However, there is a question that has not been clarified in any of these papers and in fact has not even been posed: under what conditions is the motion of particles in plasma, accelerators, etc., stochastic? Is Fermi acceleration always possible? Clarification of the latter question by means of numerical experimentation in the simplest one-dimensional model was undertaken by Ulam[102] with a negative result. From the point of view of the present paper this result is perfectly natural, since for stochasticity of the motion, special conditions have to be fulfilled which are more strict the simpler the system. For the above-mentioned one-dimensional Fermi acceleration model the question was clarified in co-operation with Zaslavsky in a paper[103] of which we will also give an account. To complete the picture let us recall that the condition of stochastic acceleration in plasma were explained a little later by Zaslavsky, Sagdeev and Filonenko[104,105].

As already mentioned, in Ref. 102 the simplest case of Fermi acceleration was investigated: the motion of a light particle between two parallel infinitely heavy and absolutely elastic plane walls, one of which is motionless and the other oscillating according to a given law. Numerical computation of the motion of such a particle[102] gave a negative result: acceleration was practically not observed. The velocity of the particle sometimes reached three to four times the velocity of the wall and in the majority of cases was of the order of velocity of the wall, whereas according to the Fermi mechanism the mean velocity of the particle should grow infinitely in proportion to the time[99].

Let the wall oscillate according to a "saw-shaped" law, so that its velocity varies linearly with the time during each half-period. Further, let the minimum distance between the walls be l and the amplitude of the oscillations of one of them a. Then the motion of the particle is described by the following exact set of difference equations:

$$v_{n+1} = \pm v_n + V(\psi_n - 1/2) \tag{4.1.1}$$

$$\psi_{n+1} = \frac{1}{2} - 2\frac{v_{n+1}}{V} + \sqrt{\left(\frac{1}{2} - \frac{2v_{n+1}}{V}\right)^2 + \frac{4v_{n+1}}{V}\varphi_n} \tag{4.1.2}$$

$$\left(v_{n+1} > \frac{V\psi_n}{4}\right)$$

$$\psi_{n+1} = 1 - \psi_n + 4\frac{v_{n+1}}{V}\,; \quad \left(v_{n+1} \le \frac{V}{4}\psi_n\right) \tag{4.1.3}$$

$$\varphi_n = \left\{ \psi_n + \frac{\psi_n(1-\psi_n) + l/4a}{4v_{n+1}/V} \right\} \tag{4.1.4}$$

Here v_n is the velocity of the particle after the n^{th} collision; $V/4$ is the amplitude of the velocity of the wall; ψ_n is the phase of the oscillations of the wall at the moment of collision varying from 0 to $\frac{1}{2}$ when the wall moves in one direction and from $\frac{1}{2}$ to 1 when the reverse motion occurs. The brackets { ... } denote, as usual, the fractional part of the argument. The plus sign in (4.1.1) corresponds to formula (4.1.2) in the previous step, and the minus sign to formula (4.1.3).

As will be seen from what follows, an interesting case is:

$$l \gg a\,; \quad v_n \gg V \tag{4.1.5}$$

Then the set (4.1.1) - (4.1.4) takes the form:

$$v_{n+1} = v_n + V(\psi_n - 1/2)$$
$$\psi_{n+1} \approx \varphi_n \approx \left\{ \psi_n + \frac{lV}{16a\,v_{n+1}} \right\} \tag{4.1.6}$$

This transformation is of the same type as the basic model (2.1.11). According to the results of Section 2.4 the stochasticity parameter can be determined as: $K \approx (d\psi_{n+1}/d\psi_n) - 1$ (2.4.4) and is equal to:

$$K \approx -\frac{\ell}{16a}\cdot\left(\frac{V}{v}\right)^2 \tag{4.1.7}$$

whence the border of stochasticity (2.4.7):

$$\frac{v_1}{V} \sim \frac{1}{8}\sqrt{\frac{\ell}{a}} \tag{4.1.8}$$

The stochastic region thus covers the interval 0-v_1. In order to obtain considerable acceleration ($v \gg V$) it is necessary to fulfil the rather unexpected condition:

$$a \ll \ell \tag{4.1.9}$$

Under the condition $\Delta v/v \sim V/v \ll 1$ the kinetic equation takes the form of an FPK equation (Section 2.10):

$$\frac{\partial f(v,t)}{\partial t} = \frac{\partial}{\partial v}\left(\mathcal{D}(v)\cdot\frac{\partial f(v,t)}{\partial v}\right) \tag{4.1.10}$$

where the diffusion coefficient in velocity is (2.10.12):

$$\mathcal{D}(v) = \frac{1}{2}\frac{\langle(\Delta v)^2\rangle}{\Delta t} \simeq \frac{1}{48}\cdot\frac{vV^2}{\ell} \tag{4.1.11}$$

As a boundary condition it was proposed in Ref. 103 to use the condition of the absence of flux at the border of stochasticity:

$$\mathcal{D}\frac{\partial f}{\partial v}\Big|_{v=v_1} = 0 \tag{4.1.12}$$

This condition, of course, is not exact, since there is a transitional zone, but it makes it possible to obtain an approximate solution of Eq. (4.1.10). In particular, the steady-state distribution ($\partial f/\partial t = 0$) proves to be simply uniform: $f(v,t) \to v_1^{-1}$.

In order to check the degree of approximation of such a solution, the exact set of difference equations [(4.1.1) - (4.1.4)] was computed during $n = 10^5$ collisions with the

following parameter values: $a = 1$; $V = 4$; $v_0 = 0$. In order to reduce the effects of the finite number of digits the mantissae of the quantities ℓ and V were chosen in the form of a set of random numbers. The result of the numerical experiment was a distribution function F(v,t) proportional to the particle sojourn time in a given interval of velocity. The relation between f and F is given by the expression:

$$F(v,t) = \frac{1}{t}\int_0^t f(v,t)\,dt \qquad (4.1.13)$$

Figure 4.1.1a gives a typical steady-state distribution function for $t >> t_r$, where the relaxation time is $t_r \sim v_1^2/2D \sim 24 v_1 \ell/V^2 \sim 10^6$ (for the case in Fig. 4.1.1a: $\ell/a = 10^4$; $v_1 \approx 50$); along the x-coordinate the particle velocity is plotted in units of the maximum wall velocity. The arrow denotes the maximum velocity reached by the particle during 10^5 collisions. The distribution function is cut off rather sharply near the border of stochasticity $v_1 \approx 50$ (4.1.8), illustrating the accuracy of the boundary condition (4.1.12). The fluctuations in the distribution function in the stochastic region are determined by the number of independent particle transitions through the whole acceleration region: $N \sim t/t_r$. For the fluctuations we obtain the estimate:

$$\left|\frac{\Delta F}{F}\right| \sim N^{-1/2} \sim \sqrt{\frac{\ell}{10\,a\,n}} \qquad (4.1.14)$$

When $\ell/a = 10^4$ (Fig. 4.1.1a) $\Delta F/F \sim 1/10$

Figure 4.1.1b illustrates the validity of the stochasticity criterion $|K|^{-\frac{1}{2}} \sim 0.5$ (4.1.8) for various ℓ/a. Let us note that the particle penetrates quite far (particularly when there are small ℓ) into the transitional zone*).

A further interesting experiment was carried out by Israelev. He investigated the local stability of transformation (4.1.1) to (4.1.4) by the method of returning to the initial point. In other words, for various initial conditions $n = 10^4$ forward collisions were computed, and then by means of an inverse transformation the same number of backward collisions. A stable trajectory should then almost return to the initial point. Table 4.1.1 gives some results of this experiment for the case when $\ell/a = 2500$ ($v_1 \approx 25$).

The first number in each box (v_0) gives the initial value of the velocity, the third (v_n) the final value after $n = 10^4$ collisions in one direction, and the second (v_{2n}) after the reversal. Four regions are represented in the table. The first (I) is the wide stable region with high velocities ($v > v_1$); the fourth (IV) is the wide stochastic region ($v < v_1$). The most interesting are the two narrow regions (II,III) at the border of stochasticity, one

---

*) Considerable penetration of the trajectory behind the border of stochasticity is explained by the fact that the transformation under consideration is not smooth so that the region of stability does not actually exist (compare Section 3.3).

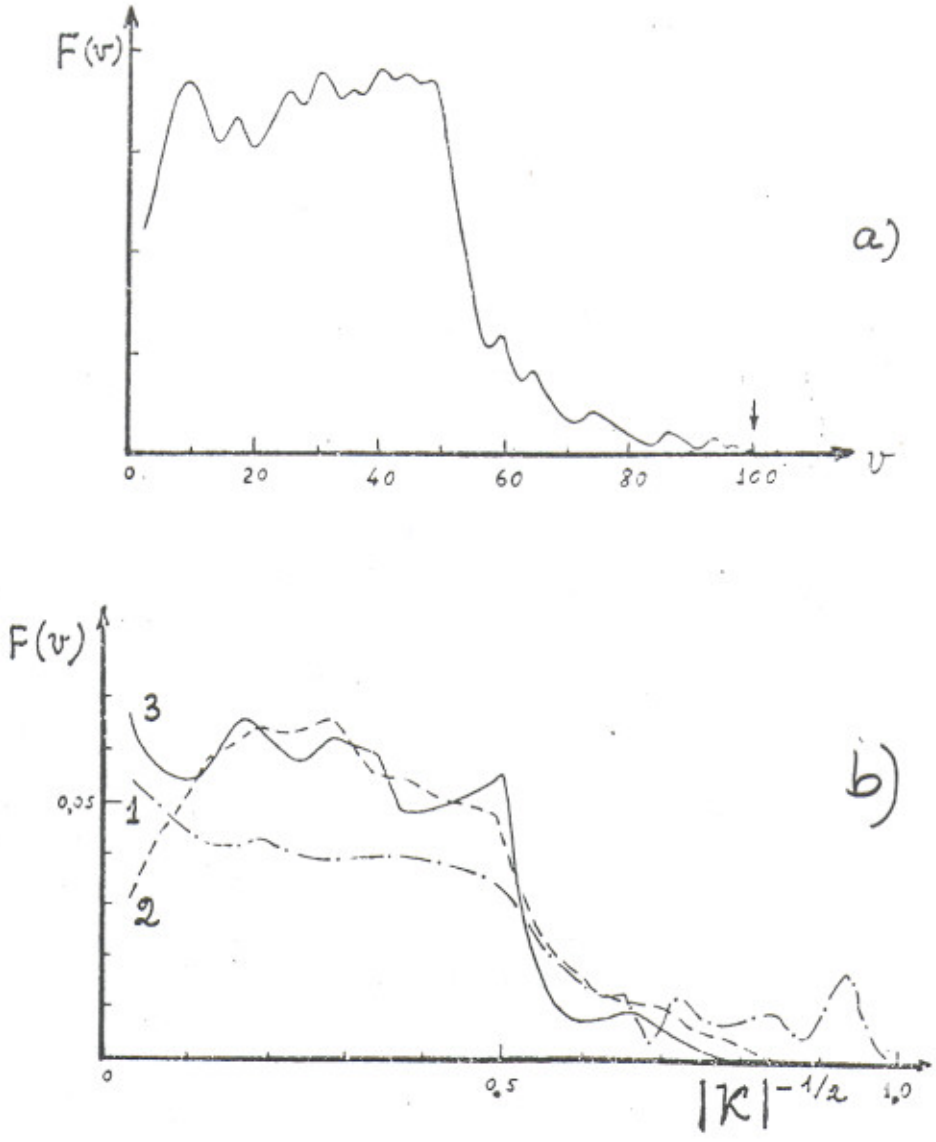

Fig. 4.1.1. Distribution function for Fermi one-dimensional stochastic acceleration: a) particle velocity v in units of maximum wall velocity (V = 4); $\ell/a = 10^4$; b) particle velocity expressed through stochasticity parameter K : 1 - $\ell/a = 400$; 2 - $\ell/a = 10^4$; 3 - $\ell/a = 4 \times 10^4$.

of which (III) is stable and the other (II) unstable. This again proves the connection between local instability and stochasticity, and also the complex structure of the transitional zone (Section 3.3).

For stable trajectories the values v_0 and v_{2n} agree with a relative accuracy of $\sim 10^{-8}$. The divergence is determined first of all by round-off errors, to which for transformation (4.1.1) to (4.1.4) are also added the errors of the square root computations.

Table 4.1.1

	I Stability	II Instability	III Stability	IV Instability
v_0	100.135814	28.0140073	27.0832487	25.4038022
v_{2n}	100.135814	78.9256083	27.0832485	78.1138416
v_n	101.653879	22.2647118	27.9428866	25.3236604
v_0	50.1389432	28.0139073	26.0341874	19.8875432
v_{2n}	50.1389430	23.8698307	26.0341874	41.5012536
v_n	49.2778544	32.8258519	27.0211406	19.5240320
v_0	29.0538478	28.0039973	25.4501387	10.1569183
v_{2n}	29.0538476	34.1160266	25.4501454	18.8937993
v_n	30.0626340	43.5787423	26.1233959	19.7363339

If it is considered that the latter are of the same order as the round-off and are also symmetrical, the relative accuracy of the reversal can be estimated as (see Section 3.3): $2\Delta_r \cdot \sqrt{nN/3} \sim 10^{-8}$, where $N \sim 10$ is the number of operations in one step of transformation (4.1.1) to (4.1.4); $\Delta_r = 2^{-36}$ and the factor 2 takes into account the mean value of the mantissa (floating point arithmetic). This estimate agrees with the observed accuracy of the reversal except in the last case in region III, which probably indicates weak instability near the border of stochasticity.

To sum up it can be said that in the one-dimensional case the Fermi acceleration process essentially depends on the fulfilment of the stochasticity conditions.

If we now turn to the case of two or more dimensions the situation changes substantially. In particular, Sinai showed[106] that for elastic collisions of disks or balls stochasticity always occurs. This result follows directly from the simple fact that, as can be easily shown, in this case strong local instability of motion always arises (Section 2.13). Of course rigorous proof of stochasticity is considerably more complicated[106]. It applies also to the general case of the collision of bodies with a convex surface[189]. This latter condition is exactly that which ensures local instability of motion. At the same time the presence of concave sections of the surface may lead to the appearance of regions of stability. A modification of the case of the motion of a particle between walls, considered above, can serve as a simple example, if one of the walls is made concave and the many-dimensional problem studied. It is clear that the transverse motion in this case will be stable*), and consequently the border of stochasticity will remain the same as for the plane

*) If the curvature radius is larger than the distance between walls.

walls. In the case of a convex wall the transverse motion is always unstable and the border of stochasticity disappears.

As already noted above, a stochastic accelerator (stochatron) was proposed in Ref. 100. However, in this paper it was assumed that the phase of the accelerating voltage should be random, but this is not so simple to realize in practice. We see now that this requirement is actually superfluous. In this respect the Fermi mechanism[99] is much closer to the ideas of the present paper than the processes studied in Refs. 100 and 101.

Stochastic acceleration at a fixed frequency was first applied, apparently, by Volosov et al. for pre-heating plasma in the stellarator[107,108]. The stochasticity criterion for this case was obtained in Ref. 107.

Below we give the derivation of a similar criterion for the ordinary accelerator, to which the original proposal referred[100], but working at a fixed frequency ω_0. In a short kick approximation the equation of motion of the particle in such an accelerator can be written in the form:

$$\begin{aligned} W_{n+1} &= W_n + eV_0 \cos\varphi_n \\ \varphi_{n+1} &= \varphi_n + T\omega_0 \end{aligned} \qquad (4.1.15)$$

where T,W are the period of revolution and total energy of the particle, and V_0 is the amplitude of the accelerating voltage. According to the general theory (Section 2.4) the criterion of stochasticity is determined by the relation:

$$K_0 = \left| eV_0\omega_0 \frac{dT}{dW} \right| \gtrsim 4 \qquad (4.1.16)$$

Developing the expression for dT/dW in the usual way[5], we obtain an estimate of the maximum energy of the stochatron in the form:

$$\frac{W_{max}}{eV_0} \sim \frac{\omega_0}{\omega} \cdot \left| \frac{1-\alpha\gamma^2}{\gamma^2-1} \right| \qquad (4.1.17)$$

Here ω is the rotation frequency of the particle in the accelerator, γ is the relativistic factor, $\alpha \approx Q^{-2}$ is the momentum compaction factor, and Q the number of betatron oscillations per turn. From this last expression it can be seen, in particular, that stochasticity is always absent near the critical energy: $\gamma = \alpha^{-\frac{1}{2}} \approx Q$. However, as a result of the "infiltration" of the particle into the transitional zone (see for example Fig. 4.1.1) more or less slow crossing of this region is possible.

To complete the picture, let us note that the ordinary microtron[7] works just at the border of stochasticity (4.1.17) so that, for instance, raising the accelerating voltage inevitably makes it go over to stochastic conditions.

Going back to the stochastic heating of plasma[107,108], let us note that its effectiveness can be even greater than follows from the simple theory[103,107]. In particular, instead of uniform distribution in velocity, in the real system maximum density can be expected to appear near the border of stochasticity, i.e. near the maximum energy, due to the capture of the particles in the stable regions owing to the presence of dissipation. This effect has apparently been actually observed in the experiments by Volosov's group.

In conclusion let us make some remarks concerning high-frequency heating and the confinement of plasma in magnetic traps. This method has become increasingly popular recently; in particular, a separate section was devoted to it at the Third Conference on Plasma Physics and Controlled Fusion (Novosibirsk, 1968; see also Ref. 109). Since this concerns rather dense plasma, the alternating field is equivalent to the oscillating wall, so that it is necessary to take into account effects connected with the border of stochasticity. On the one hand these effects can lead to the limitation of the maximum temperature of the heating. On the other hand, for instance for high frequency confinement in magnetic traps, they may in fact considerably impair the confinement on account of the increase in the longitudinal velocity of the particles.

4.2 Dynamics of the lines of force of the magnetic field in the stellarator

The objective of this section is to make some calculations, or rather estimates, of the conditions of stability of the motion of a single particle in a magnetic field of the stellarator or levitron type.

In general it can be considered that the magnetic moment of a particle is conserved with a sufficient degree of accuracy (see Section 4.4), so that the important thing is the stability of the drift trajectories of the particle. Further, limiting oneself to a region sufficiently far away from the separatrix, for the overwhelming majority of untrapped particles the deviation of the drift trajectories from the lines of force of the magnetic field can be neglected[110]. Thus it is necessary to investigate, as is usual, the stability of the lines of force, which can be regarded as trajectories of a dynamical system, namely an oscillator, since the main feature of a stellarator field is the finite velocity of the rotation (ω) of the lines of force in a plane perpendicular to the magnetic field.

This oscillator is subject to various perturbations (inaccuracies of manufacture, race-tracks, toroidality, etc.) with a period equal to the perimeter of the stellarator. The main danger comes from the resonances. They can be controlled in two ways.

Firstly, one can choose the "frequency" ω far away from all the resonant values, as is generally done in charged particle accelerators. For this it is necessary, however, for the oscillator to be almost linear, i.e. for the "frequency" ω to depend weakly on the rotation radius (r) and for all the stellarator region of interest to us to be outside the resonances. Such stellarator fields are possible (for instance, a double helical field with a large pitch) but apparently undesirable, if only because the size of the separatrix then decreases considerably*).

---

*) Let us note, however, that a double helical field with a small pitch makes it possible to eliminate the most dangerous central resonance by the proper choice of the value of $\omega(0)$ [111] (see note on p. 178).

Another known means of controlling resonances is to make the oscillator non-linear, i.e. to make its "frequency" depend on the rotation radius (on the amplitude): $\omega = \omega(r)$.

The numerous papers on research into resonant perturbations in the stellarator (see for instance Refs. 110, 112, and 113) may give the impression that an increase in non-linearity ($d\omega/dr$) always leads to increased stability. Similar hopes also existed in the initial design stage of strong focusing accelerators. In reality, however, the situation is different. Although non-linearity does stabilize resonances (Section 1.6) it leads also to the appearance of new instabilities. The most dangerous of them is apparently stochastic instability (Chapter 2). As far as we know, stochastic processes of this kind as applied to a stellarator were first studied by Sagdeev and Zaslavsky[86]. Below we will make a more thorough examination of the destruction of the internal region of the magnetic field of the stellarator, according to Ref. 89.

As an unperturbed system let us choose a straight n-helical magnetic field created by 2n conductors with a current J in each, wound with a pitch of $2\pi/\alpha$ on the surface of a cylinder with a radius a. Let us relate the toroidality of the real stellarator to the perturbations. Let us assume that the equations of "motion" of the lines of force have the form[115]:

$$\frac{ds}{dz} = 2\varepsilon_n s^{\frac{n}{2}} \cdot \sin n\theta; \quad \theta = \varphi - \alpha z; \quad s = \left(\frac{r}{a}\right)^2;$$
$$\frac{d\varphi}{dz} = \varepsilon_n s^{\frac{n}{2}-1} \cdot \cos n\theta; \quad \varepsilon_a = \frac{4J}{ca H_z} \qquad (4.2.1)$$

where H_z is the strength of the longitudinal field and r, φ, z the cylindrical co-ordinates. For (4.2.1) to be correct it is necessary, generally speaking, for both quantities εa, $s \ll 1$. However, the estimates by order of magnitude will also be correct in a wider region, in fact everywhere except in the immediate vicinity of the separatrix. The same remark also applies to the other strong inequalities. The quantity $s = (r/a)^2$, canonically conjugated to the angle φ was chosen as a variable. In accordance with Ref. 115 let us introduce the dimensionless "frequency" ω by the formula $\bar{\varphi} = \alpha\omega z$, where $\bar{\varphi}$ is the mean angle of rotation.

The mean rotation of the lines of force, which is also the main factor for the stability of the stellarator field, is rather similar to the betatron oscillations in an alternating gradient accelerator or to the stability of the Kapitsa pendulum[172,173].

Let us assume that the perturbations (constant in time) are described by the same equations as the main field (4.2.1), but with their own parameters ε_1, n_1, α_1. Let us further assume that the perturbation is a set of short uncorrelated "kicks", i.e. the parameters ε_1, n_1, α_1 are constant over a length ℓ (correlation length) satisfying the inequality:

$$a \ll \ell \ll (n_1\alpha_1)^{-1} \qquad (4.2.2)$$

There is a similar formulation of the problem, for instance, in the stability calculations for a strong-focusing accelerator[5]. As a result of the closure of the stellarator, any perturbation will be periodic with a period L (perimeter of the stellarator).

Let us first consider a single "kick" at the point z = 0. From Eqs. (4.2.1) under condition (4.2.2) we find:

$$\Delta S = 2\varepsilon_1 n_1 S^{\frac{n_1}{2}} \ell \sin n_1\varphi$$
$$\Delta\varphi = \varepsilon_1 n_1 S^{\frac{n_1}{2}-1} \ell \cos n_1\varphi \qquad (4.2.3)$$

The first equation determines the displacement of the magnetic surface, depending on the angle φ in the region of the perturbation. The latter changes under the action of the perturbation [the second equation in (4.2.3)] and also as a result of the rotation with a "frequency" ω, by a quantity $\alpha L\omega$ (per period). As a result, the action of the perturbation under consideration can be described by means of the following set of difference equations, similar to the basic model (Section 2.1):

$$S_{N+1} = S_N\left(1 + \frac{2\zeta_N}{n_1}\sin\psi_N\right)$$
$$\psi_{N+1} = \psi_N + \alpha L n_1 \omega(S_{N+1}) + \zeta_N \cos\psi_N \qquad (4.2.4)$$
$$\psi_N = n_1\varphi_N; \quad \zeta_N = \ell\varepsilon_1 n_1^2 S_N^{\frac{n_1}{2}-1}$$

Under specific conditions (see Section 2.2) the difference equations (4.2.4) can be replaced by the differential equations:

$$\dot{S} = \frac{2}{n_1}\zeta S \sin\psi$$
$$\dot{\psi} = \alpha L_1(\omega - \omega_p) + \zeta\cos\psi \qquad (4.2.5)$$

Here $L_1 = n_1 L$; $\omega_p = 2\pi m/\alpha L_1$ ($m = 0, 1, \ldots$) [110] is the resonant value of the "frequency" ω *); the dot denotes differentiation with respect to the "time" N. Everywhere in what follows, s denotes the parameter of the magnetic surface, i.e. we shall ignore its small deviations from the cylinder[115]. The phase frequency of the oscillations (4.2.5) is:

$$\Omega_\varphi^2 = \ell\alpha L s\omega'\zeta; \quad \omega' \equiv \frac{d\omega(s)}{ds} \qquad (4.2.6)$$

Let us note that the frequency Ω_φ is here measured in units of $(\alpha L)^{-1}$.

*) The resonances of the higher approximations: $\omega^{(p)} = (2\pi m/\alpha L \pm pn)/(n_1 \pm pn)$; $p = 1, 2, \ldots$ [113] have an additional small factor of the form $\left[(\varepsilon/\alpha)\cdot s^{n/2-1}\right]^p$ and can be important only near the separatrix.

Let us first estimate the stabilization of the resonances by non-linearity, as was done in Section 1.6. In the linear case ($\omega' = \Omega_\phi = 0$), system (4.2.5) determines the resonant (unstable) bands of the width:

$$\alpha L_1 (\Delta\omega)_\Lambda = 2\xi \tag{4.2.7}$$

At the same time the non-linear width of the resonance (size of the separatrix) is: $\alpha L_1 (\Delta\omega)_H \sim \Omega_\phi$. According to Section 1.6 the stabilization condition can be written in the form: $(\Delta\omega)_H \gtrsim (\Delta\omega)_\Lambda$ or (squared) *):

$$\xi \lesssim \frac{\alpha L_1 s \omega'}{2} = \frac{n-2}{2} \alpha L \omega = \frac{n-2}{2} \cdot \overline{\varphi}_L \tag{4.2.8}$$

where $\overline{\varphi}_L = \alpha L \omega$ is the total rotation angle of the line of force around the stellarator, and we used the relation: $\omega_s \propto s^{n-2}$ [115])

The stochasticity parameter for system (4.2.5) is:

$$K = 2\alpha L s \omega' \xi \cos\varphi = \Omega_\phi^2 \cos\varphi \tag{4.2.9}$$

Let us determine the border of stochasticity from the condition: $K_0 = \Omega_\phi^2 = 4$. This choice of border is confirmed, in particular, by the results of the numerical computation given in the previous section (Fig. 4.1.1). The condition of stability of the motion thus takes the form:

$$\xi \lesssim \frac{2}{\alpha L s \omega'} = \frac{2}{(n-2)\overline{\varphi}_L} \tag{4.2.10}$$

The last expression is exactly the opposite of (4.2.8). This means that the permissible perturbation reaches a maximum in the region:

$$\varphi_L = \frac{2}{n-2} \sim 1 \; ; \quad \xi_{max} \sim 1 \tag{4.2.11}$$

The formulae given above are directly applicable only when $n > 2$. For a double helical field one should assume that [115]): $(n-2)\,\overline{\varphi}_L \to \Delta\overline{\varphi}_L$; the latter is the difference between the rotation angles at the axis of the stellarator and at the radius r under consideration.

If the condition of non-linear stabilization of the resonance (4.2.8) is violated, the line of force withdraws into the wall in a time (number of turns):

---

*) The stabilization condition of the resonance in the centre of the stellarator ($\omega_p = 0$) has a different form: $\xi \lesssim \alpha L_1 \omega = n_1 \overline{\varphi}_L$. This resonance is especially dangerous, since it leads to the destruction of a region of the size $r \propto \varepsilon_1^{1/(2n-3)}$ (when $n_1 = 1$). while for peripheric resonances the size of the region destroyed is $\Delta r \propto \sqrt{\varepsilon_1}$.

$$N_r \sim \frac{n_1}{\xi} \qquad (4.2.12)$$

In the stochastic region, when condition (4.2.10) is violated, the diffusion coefficient $D \sim (\xi s/n_1)^2$ and the "lifetime" of the line of force is:

$$N_s \sim \frac{s^2}{D} \sim \left(\frac{n_1}{\xi}\right)^2 \sim N_r^2 \qquad (4.2.13)$$

The estimates obtained cease to be correct in the immediate vicinity of the separatrix where, in particular, the higher harmonics ($k\omega$) play a part. This problem was studied by Zaslavsky, Sagdeev and Filonenko[38]. However, the solution they obtained was not final, namely the dependence of $d\omega/dI$ on ω was not disclosed. In Section 2.6 it was seen that for very general conditions the behaviour of the system near the separatrix is universal and is described by expressions (2.6.7) and (2.6.8). It follows from (2.6.8) that the spatial width of the stochastic layer in the stellarator being proportional to the energy width is always small and is completely negligible in the sense of a limitation of the stable region. It is interesting to note that the width of this stochastic layer is not exponentially small, as in the case of the non-linear resonance (Section 2.6), but simply proportional to the small perturbation parameter. This characteristic was already discovered by Mel'nikov[37]. The explanation is that in the case of the stellarator the perturbation frequency, for example on account of toroidality, $\sim \omega$, whereas the destruction of the separatrix of a resonance some way from the border of stochasticity is usually due to the action of high frequency perturbation.

The frequency width of the stochastic layer (2.6.7) is always great and therefore it is impracticable to rely on the use of a large rotation angle in the immediate vicinity of the separatrix of the stellarator. Figure 4.2.1 gives the results of numerical computation from a paper by Gibson[116] (toroidal perturbation). In the case concerned $\Omega_c \propto \psi_0 - \psi_s$, where $\psi_0 (\propto \Omega_\phi)$ is the rotation angle at the separatrix and ψ_s the rotation angle at the border of stochasticity. The interpolation line equation is given in Fig. 4.2.1 and the expected dependence takes the form (2.6.7):

$$\frac{\psi_0}{\psi_0 - \psi_s} = 1 + \frac{\Omega_\phi}{\mp\Omega_1} \cdot \ell_H \frac{1}{\varepsilon} + \frac{\Omega_\phi}{\mp\Omega_1} \cdot \ell_H \frac{\Omega_1}{\Omega_\phi} \qquad (4.2.14)$$

From the results in Fig. 4.2.1 we obtain: $\Omega_1/\Omega_\phi \approx 1.28$, whence the last term ≈ 0.06, which cannot be regarded as a serious deviation from the interpolation line.

The stochastic instability of the lines of force can be used to create a so-called Skornyakov trap[112]. The distinguishing feature of this trap is the region of "turbulent motion" of the lines of force, in which the lines, at first close together, rapidly diverge considerably. Stochastic instability also has this same property. The reason for using

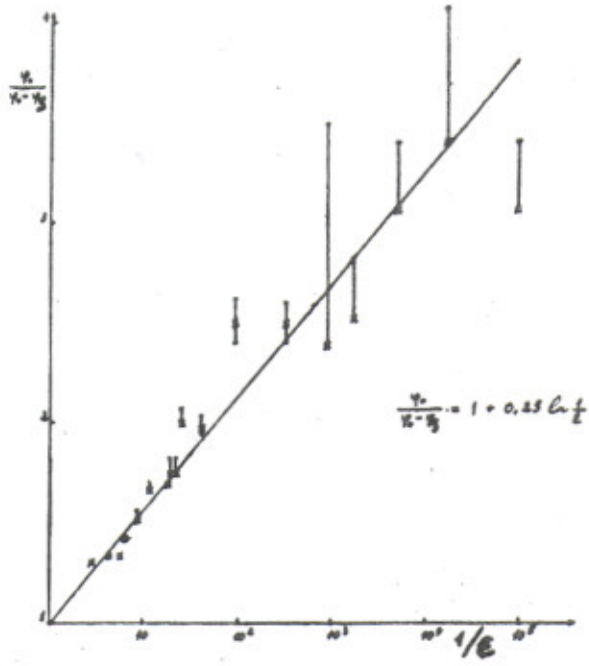

Fig. 4.2.1. Decrease of the rotation angle of a magnetic line of force in dependence on the ratio of the stellarator radii $\varepsilon = r/R$ (toroidal perturbation): φ_0 is the maximum rotation angle at the separatrix; φ_s is the rotation angle at the boundary of the stochastic layer.

such a "turbulent" region is the hope that inside it the development of plasma instabilities will be hampered. Indeed, the spatial non-uniformities (fluctuations) occurring in the plasma, moving along the rapidly diverging lines of force, will spread out and mix, which is equivalent to some damping. The difficulty of creating a Skornyakov trap lies in the fact that the turbulent region must be completely surrounded by a reliable "laminar" layer of regular magnetic surfaces to ensure heat insulation. In particular, the stochastic instability considered in the previous section is completely unsuitable for this purpose, since the turbulent region extends as far as the separatrix.

One of the possible methods of creating a "turbulent" layer in a stellarator by means of an additional short "resonant" winding is described in Ref. 89. Two other methods will be mentioned here.

The first was proposed by Mel'nikov and does not require any additional equipment at all. It is based on the fact that the separatrix of the central resonance $\omega = 0$ (which is always the case for $n > 2$, see note on p. 178) is destroyed by toroidal perturbation, which automatically leads to the formation of a stochastic layer. The width of the layer depends on the ratio of the perturbation frequency [$\omega_1 = 1$ for toroidal perturbation[115]] to that of the phase oscillations Ω_ϕ (4.2.6). For the central resonance the frequency Ω_ϕ can also be estimated from the relation: $\Omega_\phi \sim \dot{s}/s \sim 2\xi/n_1 \sim \xi$, since $\Delta s \sim s$ and $\psi \sim 1$. This estimate is of the same order of magnitude as (4.2.6) on the edge of the resonance: $\alpha L_1 \omega \sim \xi$ (see above). The transition to dimensionless "frequency" is effected by means of the transformation: $\Omega_\phi \to \Omega_\phi/\alpha L$. Whence:

$$\frac{\omega_1}{\Omega_\phi} \sim \frac{\alpha L}{\xi} \sim \omega^{-1} \qquad (4.2.15)$$

In this last estimate we used the above-mentioned condition $\xi \sim \alpha L_1 \omega$ for the size of the central resonance ($n_1 \sim 1$). Since it is desirable for $\xi << 1$, a large width of the stochastic layer, corresponding to the condition $\omega_1 \lesssim \Omega_\phi$, is possible only for a very small α, which leads, in particular, to "discontinuity" of the field when it rotates in the stellarator. For continuity of the field it is necessary for $\alpha L \geq 2\pi/n \sim 1$.

The second method of creating a "turbulent" zone is based on the destruction of the central resonance by a special winding, the pitch angle of which (α_1) is identical to that of the line of force at the edge of the resonance: $\alpha_1 \approx \alpha\omega$. The total rotation angle of the additional winding is then equal to: $\alpha_1 L \approx \alpha\omega L \sim \xi << 1$, so that there are again difficulties with the field continuity, but only for the additional winding.

The entropy in the "turbulent" region characterizing the rate of decrease of the instability[89] will be of the order (per z unit, representing time):

$$h \sim \alpha\omega \sim \frac{\xi}{L} \qquad (4.2.16)$$

This value is smaller (when $\xi < 1$) than in the method described in Ref. 89, where $h = (\ln \Omega_\phi^2)/L \sim L^{-1}$, if the error in formula (15) of this paper is corrected.

At present the possibility of stabilizing plasma instabilities in a Skornyakov trap remains highly problematical. The main difficulty here is due, apparently, to the border between the "turbulent" and "laminar" regions, where large gradients of plasma density may occur, facilitating the occurrence of plasma instabilities. Nevertheless, in view of the simplicity of the additional equipment required for creating a "turbulent" layer, it appears expedient to carry out the corresponding experiment.

4.3 Arnold diffusion in the interaction of colliding beams

Below only the simplest case will be considered -- that known as weak-strong interaction, when the influence of the weak beam on the strong one can be neglected. This is usually the case for colliding electron-positron beams and will be even more so for proton-antiproton beams*). Weak-strong interaction amounts in fact to an interaction between a single particle and a colliding bunch. A convenient model of such an interaction, which is fully acceptable for our estimates, is proposed in Ref. 13.

For proton, and especially antiproton, storage devices even very weak diffusion can be important, since under natural conditions there is absolutely no damping of the oscillations and the necessary lifetime is a few hours[125]. Recently, Budker proposed artificial cooling of protons by means of an accompanying electron beam[126], in which case everything would depend on the damping time in fact realized.

It is convenient to characterize the intensity of the interaction by the frequency shift of the small (linear) betatron oscillations ($\Delta\nu$); as the small dimensionless parameter

---

*) For a description of colliding beam technique see Ref. 80.

let us choose $\varepsilon = \Delta\nu/\nu_0$. When the amplitude of the oscillations is of the order of the transverse size of the bunch the non-linearity reaches a peak, equal to: $\alpha \sim \varepsilon$ [13].

The resonance condition takes the form:

$$n_1 \nu_1 + n_2 \nu_2 + p \nu_0 = 0 \qquad (4.3.1)$$

where all the frequencies are given in units of the revolution frequency ω_0; n_1, n_2, p are integers; ν_0 is the frequency of the external perturbation, which we assume to be δ-shaped (any p). Taking into account that in the present case m = 2, the amplitude of the perturbation harmonic can be written in the form [see (2.12.23)]:

$$\varepsilon_n \sim \varepsilon \cdot e^{-n/n_0} \qquad (4.3.2)$$

The parameter n_0 depends on the shape of the beam and the amplitude of the oscillations a. In particular, for a cylindrical beam shape $n_0 \sim a/r_0$, where r_0 is the transverse dimension of the beam[13]. Let us also introduce a dimensionless parameter of the coupling between the betatron oscillations β^2, which in some cases can be very small[125].

The resonance density can be estimated in the same way as in Section 2.12, taking N = 3, since the external perturbation, as we assumed, has many harmonics. Moreover, the resonance density must be inversely proportional to the constant frequency of the external perturbation ν_0. As a result we obtain from (2.12.27):

$$\Delta_n \sim \frac{\nu_0}{n^3} \qquad (4.3.3)$$

An example of a set of resonances up to and including the fourth order is shown in Fig. 4.3.1. It can be seen that the density of the resonances is very non-uniform. This effect can be included in the parameter ν_0 (4.3.3).

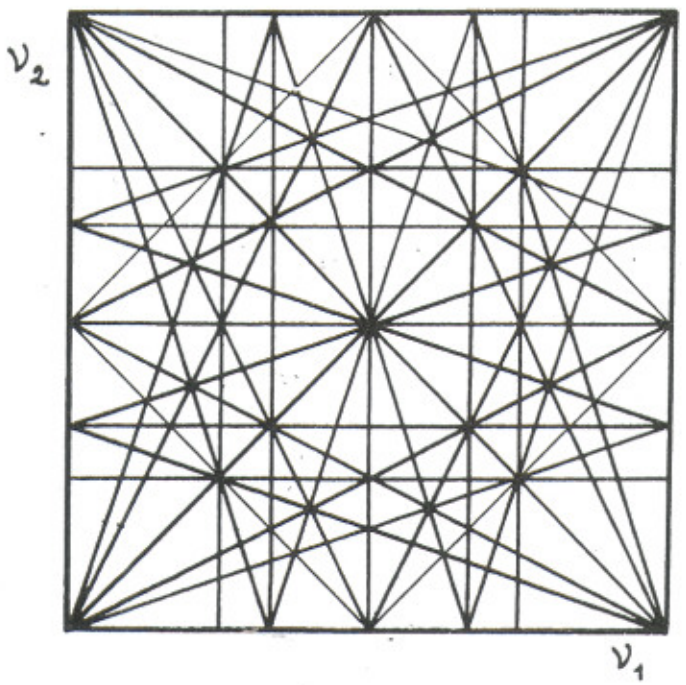

Fig. 4.3.1. Set of resonances $n_1\nu_1 + n_2\nu_2 + p\nu_0 = 0$ for $\nu_0 = 1$; $|n_1| + |n_2| \leq 4$; p is any integer; 40 different resonances in all.

Let us first of all estimate the border of stochasticity, which is determined by the overlapping of the main resonances ($n \lesssim n_0$). Using expression (2.12.29a) in which we put: $\varepsilon \to \varepsilon\beta^2$ (the majority of the resonances are coupling resonances), we obtain:

$$\varepsilon_s \sim \frac{\nu_0}{\nu} \cdot \frac{1}{\beta n_0^{\nu}} \tag{4.3.4}$$

Turning to the estimate of the rate of Arnold diffusion, let us note that in the present case we are interested in the expression for the diffusion coefficient as a function of the number of the resonance harmonic (2.12.29). The point is that the main deleterious result of the interaction of the colliding beams is the "blow-up" of the weak beam, leading to a decrease in the so-called luminosity of the colliding beams[80]. The frequency of the betatron oscillations changes, roughly speaking, by a value $\Delta\nu = \varepsilon\nu$ of the total frequency shift under the action of the oncoming bunch. It is therefore clear that the action of the resonances will be substantial for the majority of the particles, if this frequency change exceeds the mean distance between guiding resonances Δ_n (4.3.3).

When $\varepsilon \ll \varepsilon_s$ expression (2.12.29) can be simplified, neglecting the term $n/2n_0$ in M_n and putting $\left[2n_0^2\, C(N-1)/N^2 n\right]^{1/N} \approx 1$. Further, if one considers the diffusion along coupling resonances under the action of other coupling resonances, D_A is in addition multiplied by a factor β^3 (Section 2.11). This case is typical. Taking into account, finally, that $\alpha \sim \varepsilon$ and $N = 3$, we obtain from (2.12.29) the following estimate for the Arnold diffusion coefficient:

$$D_A(n) \sim I^2 \omega_0 \varepsilon \nu \beta^3 \cdot \exp\left(-3\left(\frac{\varepsilon_s}{\varepsilon}\right)^{\frac{1}{3}} \cdot e^{\frac{n}{6n_0}}\right) \tag{4.3.5}$$

Since Arnold diffusion occurs inside the stochastic layers, the volume of which can be ignored when $\varepsilon \ll \varepsilon_s$ (Section 2.6), in practice it can become substantial only in the presence of additional ("external") diffusion, for instance on account of gas scattering or some other kind of fluctuations in the storage rings. "External" diffusion ensures the entrance of the particle into the nearest stochastic layer and subsequent Arnold diffusion. If the latter is sufficiently great the "blow-up" time of the beam will be determined by the "external" diffusion up to the nearest resonance surface, i.e. by a distance $\sim \Delta_n$, instead of $(\varepsilon\nu)$ in the absence of Arnold diffusion. Since the diffusion time is proportional to the square of the distance, the beam "blow-up" time will then be reduced by

$$k = \left(\frac{\varepsilon\nu}{\Delta_n}\right)^2 \tag{4.3.6}$$

times (see Section 2.12).

By means of (4.3.3) and (4.3.6) we find:

$$\frac{n}{n_0} \sim k^{1/6} \cdot \gamma^{-1/3}; \quad \gamma = \frac{\varepsilon}{\beta \varepsilon_s} \tag{4.3.7}$$

Substituting this in (4.3.5), we obtain:

$$D_A \sim I^2 \omega_0 \varepsilon \nu \beta^3 \cdot \exp\left(-3(\beta\gamma)^{-1/3} \cdot e^{\frac{k^{1/6}}{6\gamma^{1/3}}}\right) \tag{4.3.8}$$

The value of D_A is determined by the required lifetime ("blow up" time) of the beam τ: $D_A \sim I^2/\tau$. Putting: $B = \beta\,(\varepsilon\nu\tau\omega_0)^{1/3}$ and $k = 1$, we arrive at the equation for the lower limit γ_1, determining the region of influence of the Arnold diffusion:

$$6\gamma_1^{1/3} \cdot \ln\left[(\beta\gamma_1)^{1/3} \cdot \ln B\right] = 1 \tag{4.3.9}$$

This expression shows in particular that the threshold of γ_1 depends weakly on the coupling coefficient β^2, provided the latter is not too small: $\beta^2 >> (\ln B)^{-6} = A^{-2}$. The equation for γ_1 can be written in the form:

$$2\gamma_1^{1/3} \cdot \ln(A\beta\gamma_1) = 1 \tag{4.3.9a}$$

Putting $\gamma_1 \approx 1/8$ in first approximation we find:

$$\gamma_1 \approx \left[2 \ln\left(\frac{A\beta}{8}\right)\right]^{-3} \tag{4.3.10}$$

It is evident that the latter expression is valid only for $A\beta >> 8$; if this is not so it is necessary to solve equation (4.3.9) more accurately.

From expression (4.3.10) it can be seen that the critical value of the frequency shift $(\Delta\nu)_1$ depends substantially only on the frequency of the external perturbation ν_0 and the field smoothness parameter of the oncoming beam n_0; dependence on the other parameters is weak, including that on the coupling parameter of the oscillations β^2 and on time τ.

When $(\Delta\nu)$ increases above the threshold it can be considered that $n/n_0 = \text{const}$ (4.3.5), and D_A increases on account of the factor $(\beta\gamma)^{-1/6}$ (4.3.8). Then from (4.3.7) it follows that:

$$k = \left[\frac{(\Delta\nu)}{(\Delta\nu)_1}\right]^2 \tag{4.3.11}$$

Let us also write down the expression for the harmonic number of the resonances determining the Arnold diffusion. From (4.3.5) we have:

$$n_A \approx 6 n_0 \ln\left[(\beta\gamma)^{1/3} \cdot \ln\beta\right] \tag{4.3.12}$$

The estimates obtained were based on formula (2.12.29), which is valid when $n' > n$ (Section 2.12). Let us find the condition under which it is possible for $n' = n$, and the diffusion coefficient is given by the estimate (2.12.26). Using expressions (2.12.25) and (4.3.7) we obtain:

$$\frac{\varepsilon}{\varepsilon_s} > \left(\frac{Q}{6}\right)^3 \approx 0.1 \tag{4.3.13}$$

Estimate (2.12.26) in our case takes the form:

$$\mathcal{D}_A' \sim I^2 \omega_0 \varepsilon \nu \beta^3 \cdot e^{-2n/n_0} \tag{4.3.14}$$

Let us consider the influence of synchro-betatron resonances on Arnold diffusion. The simplest effect is a considerable increase in the density of the resonances. For this it is necessary only for the spectrum of the synchro-betatron resonances to span the distance between resonances (4.3.3). The width of the spectrum depends on the mechanism of synchro-betatron interaction. For colliding beams the main effect is apparently the modulation of the frequency of the betatron oscillations, which takes place for two reasons. Firstly, on account of the modulation of the non-linear frequency shift, when the width of the spectrum may here reach $\Delta_c \sim n \times \Delta\nu_r$, where n is the harmonic number of the betatron resonances, and $\Delta\nu_r$ the total non-linear frequency shift of the radial oscillations; secondly, on account of the modulation of the revolution frequency, the width is $\Delta_c \sim n\nu\nu_c/q$ [q is the high frequency harmonic number[5)]].

The overlapping condition can be found from the following considerations. In the equation of the resonance $\Sigma_i n_i \nu_i = 0$, the term $n_c \nu_c \sim \Delta_c$ should be of the order of the variation of the residual sum between neighbouring resonances, which in its turn $\sim n\Delta_n \sim \nu_0/n^2$ (4.3.3). Hence the overlapping condition: $\Delta_c \gtrsim \nu_0/n^2 \sim n \cdot (\Delta\nu)_1$, where n is determined by the time of the Arnold diffusion and $(\Delta\nu)_1 \equiv (\Delta\nu_z)_1$ is the Arnold diffusion threshold, without taking into account the synchro-betatron resonances. Then the last expression for the width Δ_c leads to the synchrotron frequency limitation:

$$\nu_c \gtrsim \frac{\nu_0 q}{\nu n^3} \qquad (4.3.15)$$

The Arnold diffusion threshold will now be determined by the distance between the synchro-betatron resonances, which is $\sim \nu_c/n$[133], i.e. it decreases by $n\Delta_n/\nu_c$ times, which at the boundary (4.3.15) is $\sim (\nu n/q)$. In fact, the decrease will be even greater, since the rate of the Arnold diffusion also increases on account of the increase in the density of the resonances*) and therefore resonances of much higher harmonics begin to work. The first expression for $\Delta_c \sim n \cdot (\Delta\nu_r)$ leads to the condition $\Delta\nu_r \gtrsim (\Delta\nu)_1$, i.e. it does not lower the threshold.

The modulation of the magnetic field of the storage ring acts in a similar way. Again there is frequency modulation with a spectrum width $\Delta_H \sim n\nu\xi$, where $\xi = \Delta H/H$ is the amplitude of the modulation. From the overlapping condition $\Delta_H \gtrsim n\Delta_n$, we obtain the limit of dangerous modulation:

$$\xi \gtrsim \frac{\nu_0}{\nu n^3} \qquad (4.3.16)$$

In this case the decrease in the Arnold diffusion threshold (by $\nu_0/n^2\nu_m$ times) will be considerably greater on account of the small modulation frequency ν_m and also on account of the increased Arnold diffusion [see above and (4.4.15)].

The action of radio-frequency modulation is considerably more complex. On the one hand it leads to frequency modulation with a threshold (4.3.16) for a quantity $q\xi_\omega = q\Delta\omega/\omega$. It is true that the amplitude of this perturbation may already be considerably smaller than that from the oncoming beam. On the other hand, the perturbation modulation spectrum may span the gap between neighbouring synchro-betatron resonances, which under condition (4.3.15) leads to an even greater lowering of the threshold of Arnold diffusion. The above-mentioned gap is $\sim \nu_c/n$ in betatron frequency[133] or $\sim \nu_c/\nu n$ in revolution frequency. Hence the boundary of dangerous modulation of the radio-frequency is:

$$\xi_\omega \gtrsim \frac{\nu_c}{\nu n q} \sim \frac{\nu_0}{q\nu^2 n^4} \qquad (4.3.17)$$

This last estimate is given in the limit (4.3.15). The amplitude of such perturbation may also be small (see above).

Finally, the effect of modulation of the synchrotron frequency itself is also possible under the action of various factors. However, spanning the gap between the synchro-betatron resonances in this case already calls for rather considerable modulation $\Delta\nu_c/\nu_c \gtrsim n^{-1}$.

---

*) See similar estimate in next Section (4.4.15).

As we saw, the action of (frequency) modulation amounts to splitting up each resonance plane and forming a distinctive multiplet of the parallel planes. When the distance between these resonances is sufficiently small they begin to destroy each other with the formation of a solid stochastic "corridor". It is significant, however, that this phenomenon does not change the Arnold diffusion, since the vectors (n) of all the resonances of the multiplet are parallel (see Section 2.12).

Returning to the synchro-betatron resonances, let us note that they may also lead to a more important effect than a simple increase in the density of the resonances, namely to streamer diffusion (Section 2.12). The high frequency accelerating voltage is here the external perturbation destroying the conservativeness of the system. In other words, this perturbation shifts the system out of a constant energy surface and thus ensures streamer diffusion.

For diffusion to take place over a considerable distance, neighbouring streamers must intersect. This is possible if the dynamic frequency variation

$$\Delta\nu \gtrsim \Delta_n \sim \frac{\nu_0}{n^4} \qquad (4.3.18)$$

Here we are considering four frequencies -- two betatron frequencies, the revolution frequency and the frequency of the external perturbation. The last must have a sufficient number of harmonics ($\sim n$). In the opposite case the necessary ($\Delta\nu$) considerably increases (see below). This requirement is usually not satisfied in storage rings. Firstly, the accelerating voltage, as a rule, has only one harmonic, and secondly, under synchrotron operating conditions the revolution frequency on the average remains constant. Streamer diffusion in this situation is possible only outside the limits of the synchrotron separatrix, which may be of importance for very low energy protons or electrons (see Section 4.4).

Under ordinary conditions it is necessary to bear in mind the synchrotron oscillations, the frequency of which will also be a third dynamical frequency in addition to the two betatron ones.

For considerable streamer diffusion it is necessary, as noted above, for neighbouring streamers to intersect. This is possible precisely on account of the variation of the synchrotron frequency itself $\Delta\nu_c$. If one puts $\Delta\nu_c \sim \nu_c$, the condition for intersection of the streamers proves to be the same as that obtained above for crossing the gap $\Delta_n \sim \nu_0/n^3$ by the synchro-betatron resonances. From the width of the spectrum of the latter, due to the non-linear frequency shift: $\Delta_c \sim n \cdot (\Delta\nu_r)$ (p. 185), we obtain the streamer diffusion threshold in the form

$$(\Delta\nu_r)_1 \sim \frac{\nu_0}{n^3} \qquad (4.3.19)$$

Modulation of the revolution frequency gives a threshold identical to expression (4.3.15).

The harmonic number of the resonances n is determined by the time of the streamer diffusion for which, taking into account "external" diffusion, estimate (2.12.39) should be taken. Let us re-write it for the problem under consideration, taking into account that $N = 3$; $\varepsilon \to \varepsilon \cdot \beta^2$; $\alpha \sim \varepsilon$; $m = 2$; $\omega = \omega_0$; we obtain:

$$\mathcal{D}_c^0 \sim I^2 \omega_0 \nu \left(\frac{\Delta\nu}{\nu}\right)^3 \beta^5 n^2 \cdot e^{-\frac{5n}{2n_0}} \tag{4.3.20}$$

Let us specify this estimate in the simplest case $\beta^2 \sim 1$; $\Delta\nu_r \sim \Delta\nu$. Using estimate (4.3.15) and again introducing the beam "blow-up" time $\tau \sim I^2/D_c^0$, we obtain the equation for the critical value of the synchrotron frequency:

$$(\nu_c)_1 \approx \frac{15}{n_0^3} \cdot \frac{\nu_0 q}{\nu} \cdot \left\{ \ln\left[\omega_0 \tau \nu \left(\frac{\Delta\nu}{\nu}\right)^3 \left(\frac{\nu_0 q}{\nu \nu_c}\right)^{2/3}\right]\right\}^{-3} \tag{4.3.21}$$

This depends weakly on the strong beam current $J \propto \Delta\nu$, provided $(\omega_0 \tau\nu) \cdot (\Delta\nu/\nu)^3 \cdot \beta^5 \gg 1$ (4.3.20). Combining in a similar way (4.3.19) and (4.3.20) we find the streamer diffusion threshold in current from the equation:

$$(\Delta\nu)_2 \approx \frac{15\nu_0}{n_0^3} \cdot \left\{ \ln\left[(\nu\tau\omega_0)\cdot\left(\frac{\Delta\nu}{\nu}\right)^{\frac{7}{3}} \cdot \left(\frac{\nu_0}{\nu}\right)^{\frac{2}{3}}\right]\right\}^{-3} \tag{4.3.22}$$

Effects (4.3.21) and (4.3.22) work independently. The "blow-up" time decreases in approximately inverse proportion to the square of the amount by which the corresponding quantity exceeds the threshold [see (2.12.41) and (4.3.11)].

Modulation of the magnetic field or the high frequency may lead to an increase in streamer diffusion, but it cannot bring this about by itself (without synchrotron oscillations) since the modulation frequency is not a dynamical variable.

As an example let us choose the following parameters for a proton storage ring: $\tau = 10^5$ sec; $\nu = 10$; $\nu_0 = 1$; $\omega_0 = 10^8$ sec^{-1}; $\beta^2 \sim 1$; $(\Delta\nu)_s \sim 1/20$. The last value is taken from numerical experiments[97,127] and from experiments on electron storage rings[127,133]. In all cases the quantity $(\Delta\nu)_s$ lay in the interval 1/10 - 1/40. Hence the parameter $n_0 \sim 2$ (4.3.4) can also be estimated.

Solution of Eq. (4.3.9) by the successive approximation method gives: $\gamma_1 \approx 1/50$ whence $(\Delta\nu)_1 \sim 10^{-3}$, with resonances working up to $n \approx 8$. The streamer diffusion threshold (4.3.22) is $(\Delta\nu)_2 \sim 2 \times 10^{-3}$ ($n \approx 8$), i.e. roughly the same as for ordinary Arnold diffusion. Finally, the synchrotron frequency threshold (4.3.21) is: $(\nu_c)_1/q \sim 5 \times 10^{-4}$ ($n \approx 6$) when $\Delta\nu = 10^{-3}$. In fact the synchrotron frequency should be even smaller: $\nu_c/q \lesssim 2 \times 10^{-4}$, which follows from estimate (4.3.15) with $n = 8$. In the opposite case the ordinary Arnold diffusion threshold decreases in addition by $\sim \nu n/q \approx 80/q$ times. The tolerance is of the same order for both the magnetic field modulation and the frequency modulation $(q\Delta\omega/\omega)$ (4.3.16).

The case of the cylindrical beam which we are considering is probably the worst. An effective way of preventing Arnold diffusion appears to be to decrease the coupling between the betatron oscillations, i.e. the coefficient β^2, and also the anharmonicity parameter n_0. Moreover, the working point of the storage ring (ν_1,ν_2) should be located in the region of minimum density of resonances. The most radical means would be to cut off the high frequency completely, but this might reduce the luminosity of the colliding beams[125]. Increasing the high frequency harmonic number to $q \gtrsim n\nu$ also helps (p. 186).

When the intensity of both colliding beams is comparable the large-size beam plays the role of the weak one, since the parameter n_0 is very small for a narrow beam[13]. When the dimensions of the beams are comparable, their mutual "blow-up" is possible, in which event $(\Delta\nu)$ decreases to the threshold value. In this case the process can be considerably complicated by the coherent oscillations of the beams[127], but these are comparatively easy to suppress, for example by means of a feedback[127].

The estimates obtained above are of course very rough. They can be refined in specific cases by means of a numerical experiment. According to Ref. 76, for this it is sufficient to investigate the local stability of motion in a comparatively short computation.

It would be still better to carry out model experiments on electron storage rings. Although in this case the time of the Arnold diffusion is considerably limited by radiation damping, it can be made long enough to observe this process (up to 1 sec in the rings described in Ref. 133)*).

4.4 Magnetic mirror traps: conservation of the adiabatic invariant

The confinement of a charged particle in an open magnetic system of the type of a magnetic mirror trap is effected, as is known, at the expense of the conservation of the orbital magnetic moment of the particle (μ), which is the adiabatic invariant of Larmor rotation[117]. An adiabatic invariant is not an exact invariant and until recently its conservation conditions were still unclear. In particular, in a paper as early as 1928, Andronov, Leontovich and Mandelstam[119] showed in a simple example of the Mathieu equation that an adiabatic invariant can be destroyed when there is arbitrarily slow but resonant periodic variation of the parameter. For periodic perturbation, Firsov introduced corrections to the adiabatic invariant which made it possible to remove the substantial deviation of the invariant up to increasingly high orders of asymptotic expansion[118]. This direction was pursued by Kruskal in a paper[18] showing that the improved adiabatic invariant is conserved in all orders of the asymptotic expansion. Of course this does not mean rigorous invariance, but it is equivalent to an assertion that the variation of the adiabatic invariant is in any event "exponentially" small (see below and Section 2.2). Only relatively recently Arnold was able to demonstrate the eternal conservation of the adiabatic invariant for a one-dimensional non-linear oscillator and, correspondingly, the eternal stability of motion of a charged particle in an axially-symmetric magnetic trap[120]. The requirement for axial symmetry is essential here and is connected with the topological features of the KAM theory, which were mentioned in Sections 2.2 and 2.12.

As we already know, the KAM theory does not give the critical value of the perturbation. This can be estimated from the numerical experiments in Ref. 123 and from Rodionov's experiments with electrons[121]. In both cases it turned out that the border of instability is

*) There is a unique possibility of experimentation on Arnold diffusion using the proton colliding beams (ISR) now in operation at CERN.

determined approximately by the simple criterion of the overlapping of the resonances[10]. However, it remained unclear whether the stability observed was eternal, in conformity with the KAM theory, or whether the time for the development of instability simply increased. A series of experiments[122,81-83,131] were devoted to this problem. All these papers report the discovery of very weak instability developing during up to 10^9 reflections of the electron by the magnetic mirrors. A particularly thorough investigation of this weak non-adiabaticity was made in Refs. 82 and 83. An example of the dependence of the mean lifetime of an electron in a trap on the strength of the magnetic field is shown in Fig. 4.4.1, taken from Ref. 83. The curves correspond to different pressures of residual gas in the trap and different methods of measuring the lifetime. The non-adiabaticity manifests itself in a more or less sudden reduction of the latter. The formation of a lower "plateau", i.e. independence of the lifetime on the low magnetic field, was completely unexpected.

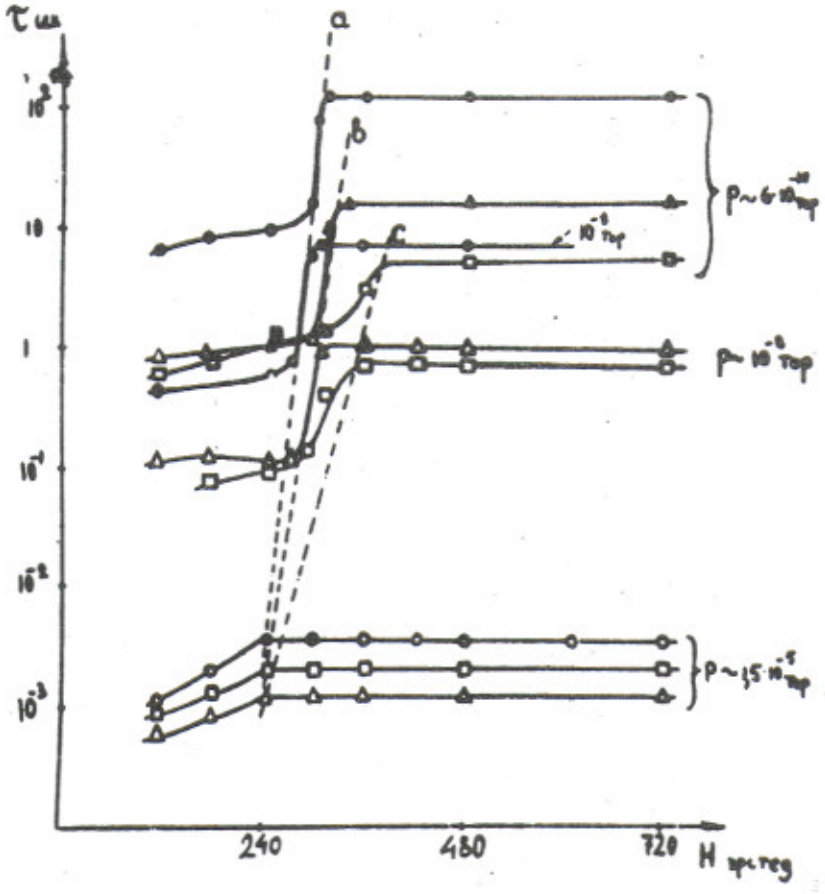

Fig. 4.4.1. Dependence of the lifetime of electrons in a magnetic mirror trap on the strength of the magnetic field H.

The nature of this weak instability has not been clarified experimentally. At present only two hypotheses can be put forward.

According to the first, the instability discovered is due to the fact that the real magnetic field of the trap was not axially-symmetric, in spite of all the measures taken. In this case the system becomes three-dimensional and the KAM theory can no longer guarantee

stable motion, in spite of the invariant tori. Furthermore, Arnold discovered a specific mechanism of instability in this case[21], which in Section 2.12 was called Arnold diffusion. This second hypothesis will be examined thoroughly below.

Let us first of all discuss the second hypothesis, according to which very weak instability is also possible in an axially-symmetric trap on account of the indeterminacy of the border of stochasticity and the penetration of the stochastic sections deep into the region of Kolmogorov stability (Section 2.5).

The motion of the particle in the trap can be described by means of a transformation, if the variation of the magnetic moment during a half-period of the oscillation between the mirrors is integrated (for a trap which is symmetric in relation to the median plane). The result of this integration is presented in the most convenient form in a recent paper by Hastie, Hobbs and Taylor[124]. Their calculations are based on the observation, already made in Ref. 123, that the main variation of μ occurs in the median plane of the magnetic field. This can be explained as follows. If the lines of force diverge without curving, then the magnetic field H is locally axially symmetric. Hence, in this case the magnetic moment is exactly conserved, since it is proportional to the generalized momentum. If the lines of force curve, the axial symmetry is destroyed even locally, the generalized angular momentum is not conserved and only adiabatic invariance of μ is possible. Since the curving of the lines of force is proportional, roughly speaking, to H'' (the prime signifies the differentiation along the lines of force), we arrive at the following expression for the local parameter of the adiabaticity[124]:

$$\varepsilon_a = \frac{3}{2} \cdot \frac{v_\parallel}{\omega_H} \sqrt{\frac{H''}{2H}} \sim \frac{\Omega}{\omega_H} \qquad (4.4.1)$$

Here $\omega_H = eH/mc$ is the Larmor frequency; Ω is the frequency of the longitudinal oscillations; $v_\parallel$ is the particle velocity component along the line of force, and the numerical coefficient is introduced for the sake of convenience. Let us note that the latter expression loses its sense near the axis of symmetry of the trap, over a length of the order of a Larmor radius, because of the conservation of the generalized angular momentum. Above it was mentioned that the variation of μ very strongly depends on ε_a and consequently it is in practice local*) and takes place at the maximum of ε_a. In the simplest case, but of course not always, this maximum coincides with the median plane.

According to Ref. 124, the variation of the magnetic moment after transition through the median plane is given in first approximation by the expression**):

---

*) For a sufficiently smooth (non-resonant) magnetic field configuration. In the opposite case the region where μ is changing and $\Delta\mu$ itself increases considerably, and all expressions of this section become invalid.

**) By using the estimate $\varepsilon_a \sim \Omega/\omega_H$ (4.4.1) we arrive at the typical expression, $\Delta\mu \sim e^{-\omega_H/\Omega}$, for the variation of the adiabatic invariant when there is analytical variation of the parameter, which we repeatedly used in this work (see also Ref. 45).

$$\Delta\mu \approx A \cdot e^{-\frac{1}{\varepsilon_a}} \cdot \cos\psi \qquad (4.4.2)$$

Here ψ is the Larmor phase at the maximum of ε_a and A is a certain complicated expression:

$$A = -\frac{3\sqrt{\pi e}}{8\varepsilon_a} \cdot \mu \cdot \left[\frac{\rho}{R}\left(1+\frac{2v_\parallel^2}{v_\perp^2}\right) - \frac{2H}{H''} \cdot \frac{v_\perp^2 + v_\parallel^2}{v_\perp^2} \cdot \rho \cdot \left(\frac{1}{R}\right)''\right] \sim \frac{r}{\ell}\mu \qquad (4.4.3)$$

where ρ is the Larmor radius; R the radius of curvature of the line of force; r the distance from the axis of the trap; $\ell^2 = H/H''$. Expression (4.4.2) is valid when $r \ll \ell$ [124].

The phase shift between two successive transitions through the median plane in first approximation is:

$$\Delta\psi \approx \int \omega_H(\mu)\,dt = \theta(\mu) \sim \frac{\ell}{\rho} \sim \varepsilon_a^{-1} \qquad (4.4.4)$$

If in the same approximation ε_a and A are considered to be constants, we obtain a transformation of the basic model type:

$$\begin{aligned} \mu' &= \mu + \varepsilon\cos\psi\,; \quad \varepsilon = Ae^{-\frac{1}{\varepsilon_a}} \\ \psi' &= \psi + \theta(\mu') \end{aligned} \qquad (4.4.5)$$

The stochasticity criterion takes the form $(r/\rho)e^{-1/\varepsilon_a} \sim 1$ or $\varepsilon_a \sim 1$.

Taking into account the results of the numerical experiments described in the previous section, one can hardly hope for any kind of residues of stochasticity when the value of the dimensionless small parameter $\varepsilon d\theta/d\mu \lesssim 10^{-4}$ [82,83] ($\varepsilon_a \leq 0.1$: $r \sim \rho$). It is true that the exact equations of motion are more complex than transformation (4.4.5) and it may be thought that it is just these small corrections that lead to slow diffusion. However, according to the KAM theory small perturbation does not destroy the invariant tori. Nevertheless, since the limit of applicability of the KAM theory has been established experimentally only for a very special system (Section 3.3), the question still remains open.

Let us return to the first hypothesis. The resonance condition now has the form:

$$p\Omega_g + q\Omega + \ell\bar{\omega} = 0 \qquad (4.4.6)$$

Here $\Omega_g \ll \Omega \ll \bar{\omega}$ are the frequencies of the drift and the longitudinal oscillations, and the mean frequency of the Larmor rotation, respectively. As in the previous section, we can again use the Arnold diffusion theory developed in Section 2.12.

The mean features of the problem are as follows:

1. An electron in an asymmetrical trap represents a three-dimensional autonomous oscillator with threefold interaction (m = 3). Estimate (4.3.3) for the density of the resonances remains valid:

$$\Delta_n \sim \frac{\omega_0}{n^3} \qquad (4.4.6a)$$

and the parameter $\omega_0 \sim \bar{\omega}$ also takes into account the deviation of the density of the resonances at a given point of the frequency space $(\Omega_g, \Omega, \bar{\omega})$ from the mean ($\langle\omega_0\rangle = \bar{\omega}$).

2. The working point $(\Omega_g, \Omega, \bar{\omega})$ is given by the parameter of adiabaticity

$$\frac{\Omega_g}{\Omega} \sim \frac{\Omega}{\bar{\omega}} \sim \varepsilon_a \qquad (4.4.7)$$

The exponent for ε_n (2.12.23) is now written in the form: $|p|/2n_g + |q|/2n_0 + |\ell|/2n_0$. In (4.4.7) let us put $\ell = 0;1$ so that the term $\ell/2n_0$ can be neglected. Further $p \sim q$ (4.4.7) but probably $n_g \gg n_0$. The latter is due to the fact that the azimuthal non-uniformity is usually also limited along the trap, i.e. it is operative for a time $\lesssim \Omega^{-1}$. Hence $n_g \gtrsim \Omega/\Omega_g \gg 1$. Consequently, only one of the three terms of the exponent remains. Now taking into account the relations (4.4.2) and (4.4.3) we arrive at the estimate:

$$\varepsilon_n \sim \varepsilon_a \cdot e^{-1/\varepsilon_a} \qquad (4.4.8)$$

The numerical coefficient in the exponent was chosen here according to (4.4.2). The frequency of the phase oscillations of the triple resonance [p, q, $\ell \neq 0$ (4.4.6)] is given by the estimate ($\alpha \sim 1$):

$$\Omega_3 \sim \bar{\omega}\beta\sqrt{\varepsilon_a \Omega_g/\Omega} \sim \bar{\omega}\varepsilon_a\beta \qquad (4.4.9)$$

Here the factor Ω_g/Ω (instead of the exponent) takes into account the fact that the azimuthal perturbation, although it is also operative for a short time, is almost repeated through a half-period of the longitudinal oscillations. The stochasticity parameter for an asymmetrical trap can be written in the form:

$$\frac{\Omega_3}{\Delta_n} \sim \left(\frac{\bar{\omega}}{\omega_0}\right)\varepsilon_a\beta n_0^2 n_g \sim \beta n_0^2\left(\frac{\bar{\omega}}{\omega}\right) \sim 3\beta \qquad (4.4.10)$$

The numerical value of the parameters is based on the experimental results of Ref. 82, which show the strong effect of azimuthal non-uniformity when $\beta^2 \sim (\Delta H/H)_{\lambda} \geq 10\%$. In the Arnold diffusion region the dependence $H_{cr}(\beta)$ is very weak (see below).

3. According to (4.4.1) $\varepsilon_a \propto v_{\parallel}/H \propto (\sin\theta)/H$, and the change of the angle of slope of the trajectory to the median plane $\Delta\theta \propto \tau_p^{\frac{1}{2}}$, where τ_p is the time of diffusion due to gas scattering. There is still an angular interval ($\sin\theta \approx 0$), where the Arnold diffusion is not considerable and everything is determined by gas scattering. This region is at least partly responsible, apparently, for the formation of the lower plateau in Fig. 4.4.1. Putting $\Delta\theta \sim \theta$ we can obtain the shape of this plateau from the condition $(\sin\theta)/H = (\sin\theta_c)/H_c$:

$$\tau \approx \frac{\tau_0}{\theta_c^2} \cdot \arcsin^2\left[(H/H_{cr}) \cdot \sin\theta_c\right] \qquad (4.4.11)$$

where H_{cr} is the critical value of the magnetic field above which Arnold diffusion stops playing a part (for a given pressure of residual gas); τ_0 is the lifetime of the electron in the upper plateau and θ_c is the angle of the loss cone. Law (4.4.11) works only for particles in the region $\theta \approx 0$, the number of which depends on the method of injection. The lifetime of the remaining particles is determined by the diffusion up to the nearest resonance as in the problem in the previous section. In this case, as we know, two plateaux are also formed (Sections 2.12 and 4.3). Let us estimate the step between them. For this let us compare the distance in frequency to the nearest resonance Δ_n and to the exit from the trap $\Delta\Omega \sim \Omega$. Using (2.12.36) and (4.4.6a) we find:

$$k \sim \left(\frac{\Delta\Omega}{\Delta_n}\right)^2 \sim \varepsilon_a^{-4} \qquad (4.4.11a)$$

where we put $\omega_0 \sim \omega \sim \varepsilon_a\Omega$; $n \sim \varepsilon_a^{-1}$. The shape of the curves in Fig. 4.4.1 is determined by a complex combination of both processes (4.4.11) and (4.4.11a).

Additional information about the structure of Arnold diffusion in a magnetic trap from the point of view of the hypothesis under consideration can be obtained from the very interesting results of Ref. 83 shown in Fig. 4.4.2.

This is a diagram showing an example of trapped electron distribution (spectrum) in μ in units of the maximal μ_{max}. The point $\mu/\mu_{max} = 1$ corresponds to the motion in the median plane ($\theta = 0$). The point on the extreme right of the spectrum ($\mu/\mu_{max} \approx 0.4$) lies on the loss cone. The upper spectrum (a) was plotted immediately after injection (10^{-3} sec after) and represents some kind of fast processes in the trap. The picture of Arnold diffusion is comparable to the lower spectrum (b), plotted 3.4 sec after injection. The most interesting feature of this spectrum is the minimum, which is identical to one of the main resonances $n\Omega = \bar{\omega}$ ($n = 7$), whose position is marked by an arrow. The presence of a minimum in the spectrum testifies to particle losses, probably due to the diffusion along the stochastic layer of resonances. Similar losses occur also in the resonances $n = 6;8$ (Fig. 4.4.2b).

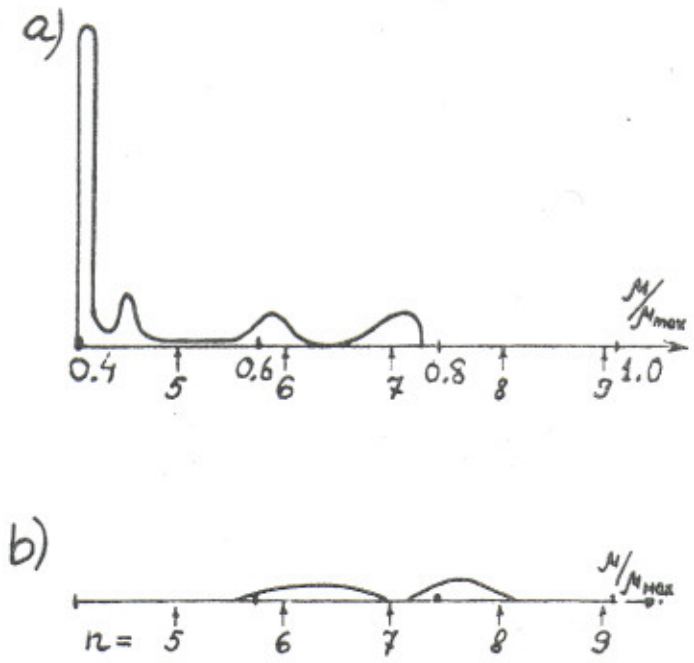

Fig. 4.4.2. Electron distribution in the trap in magnetic moment μ;
a) 10^{-3} sec after injection;
b) 3.4 sec after; μ_{max} is the maximum value of μ.

A slight disagreement with the calculated position of the resonances can easily be explained by experimental errors, since the spectrum in Fig. 4.4.2 was obtained by differentiation of the directly measured integral spectrum.

According to the results in Fig. 4.4.2 one can determine the reduction in the lifetime of the electrons as compared to the upper plateau:

$$k \sim \left(\frac{\bar{\mu}-\mu_c}{\Delta\mu/2}\right)^2 \approx \left(\frac{0.3}{0.06}\right)^2 = 25$$

(Δμ is the distance between resonances), which agrees in order of magnitude with the value $k \approx 16$ from the results in Fig. 4.4.1. However, it is substantially different from estimate (4.4.11a), which in this case gives: $k \sim 10^3$. The reason for the difference is obvious -- in the case in Fig. 4.4.2 the lifetime is determined by the diffusion up to the nearest main resonance $n\Omega = \bar{\omega}$, and not the three-frequency resonance $n\Omega + \ell\Omega_g = \bar{\omega}$ as assumed in (4.4.11a).

A possible explanation of the peculiarity noted is connected with the structure of the transitional region in the $\Theta(\mu)$. As already noted above, for sufficiently high $\mu \to \mu_{max}$ Arnold diffusion is absent ($\varepsilon_a \to 0$). Therefore in the transitional region only the strongest resonances can manifest themselves. At the same time in this region there are generally quite a number of particles, since it corresponds to a large solid angle (small Θ). Therefore the measured lifetime of the electrons in the trap depends essentially on the processes in this region. Three-frequency resonances operate effectively, apparently, only in the

region $\mu/\mu_{max} \lesssim 0.6$ (Fig. 4.4.2), where the lifetime therefore sharply decreases, which leads in practice to the absence of particles in this region (Fig. 4.4.2). The formation of a stochastic layer near the loss cone coinciding with the separatrix of the particle oscillations in the trap might be a competing process here. However, the width of this layer according to the estimates of Section 2.6 is negligibly small: $\Delta\mu_s \sim e^{-1/\varepsilon_a} \sim 1/400$ (4.4.2).

It remains for us to estimate the rate of Arnold diffusion. For this it is necessary once more to obtain an estimate of D_A (Section 2.12) taking into account the remarks made above. The exponential factor takes the form (2.12.29):

$$\mathcal{M}_n = n^{-1} \cdot \exp\left(-3 \cdot \left(\frac{C\omega_0}{4\bar{\omega} n_0^2}\right)^{1/3} \cdot (\varepsilon_a \beta)^{-\frac{1}{3}} \cdot e^{\frac{1}{6\varepsilon_a}}\right) \qquad (4.4.12)$$

It is difficult to find the exact value of the numerical factor in the first exponent ($B \sim 3$); it is obtained below from experimental results. Let us find the diffusion coefficient in a similar way to that used in Section 4.3:

$$D_A \sim \mu^2 \bar{\omega} \varepsilon_a \beta^3 \cdot \exp\left(-\frac{\beta \cdot e^{1/6\varepsilon_a}}{(\beta\varepsilon_a)^{1/3}}\right) \qquad (4.4.13)$$

The results of Ref. 83 lead to the following values of the parameters for $\Theta = \Theta_c \approx 50°$ (on the loss cone): $\varepsilon_a = 0.18$; $\bar{\omega} = 3.5 \times 10^9$; $\tau \approx 100$ sec. The most indefinite quantity is the azimuthal non-uniformity. As already noted above, in the majority of experiments no special non-uniformity was introduced and according to measurements with an accuracy of 0.5% the field was uniform. On the other hand, in special experiments increasing the non-uniformity up to 10% did not change H_{cr} within the limits of experimental errors of ±20% [82]. On the basis of these results one can apparently put: $(\Delta H/H)_\phi = \beta^2 \sim 10^{-2}$. Fortunately the value B, which we want to determine, depends weakly on the non-uniformity: $B \propto (\Delta H/H)_\phi^{1/6}$.

Before calculating B, let us find the relation between τ and D_A. Since D_A very sharply depends on ε_a, i.e. on μ, the diffusion time will be considerably less than the quantity μ^2/D_A. As a rough estimate one can assume that $\tau \sim (\Delta\mu)^2 D_A$, where $\Delta\mu$ is determined from the condition that the exponent in (4.4.13) $\Pi = B(\beta\varepsilon_a)^{-1/3} \cdot e^{1/6\varepsilon_a}$ is reduced by a unity. Putting: $\Delta\varepsilon_a/\varepsilon_a \sim \Delta\mu/\mu$ and $6\varepsilon_a \approx 1$, we obtain: $\mu/\Delta\mu \sim \Pi \sim \ln(\mu^2\bar{\omega}\varepsilon_a\beta^3/D_A) \approx \ln(\varepsilon_a\bar{\omega}\tau\beta^3)$. Assembling all the relations, we find: $B = 2.0$. The difference from the expected value $B \sim 3$ cannot be considered serious in view of the roughness of the estimates. If one attempts to take into account the factor neglected in the exponent: $(C\omega_0/4\bar{\omega}n_0^2)^{1/3} \approx 0.62$, putting $\omega_0 \sim \bar{\omega}$; $C \sim n_0 \sim 1$, then $B \approx 1.9$. Although this already agrees better with the experimental results, one should not attach much importance to this in view of the arbitrary choice of some parameters. It can only be asserted, apparently, that our hypothesis does not contradict the experimental results.

The Arnold diffusion coefficient depends very strongly on the parameter of adiabaticity (4.4.13). This leads to a rather sharp fall in the lifetime for $H \approx H_{cr}$ (Fig. 4.4.1).

Even in a semi-logarithmic scale the dependence of $\ln \tau$ on ε_a is exponential and may give the impression that there is a limit of absolute stability[82].

Estimate (4.4.13) shows how difficult it is in such experiments to escape from the influence of azimuthal non-uniformity. Thus, for instance, decreasing the non-uniformity 100 times, from 10% to 0.1%, leads to reducing H_{cr} by only 46%.

Of course, for serious confirmation of the above-mentioned hypothesis on the nature of the weak instability of particles in a magnetic trap, additional special experiments are necessary.

In conclusion let us consider what effects the variation of the magnetic field of the trap in time may lead to. With continuous growth of the magnetic field the transverse energy of the particle increases $\propto H(\mu \approx \text{const.})$, and the longitudinal energy only as $\sqrt{H}$, since the square of the frequency of the longitudinal oscillations is proportional to the effective "potential" energy of the trap μH. As a result the pitch angle of the velocity of the particle to the line of force increases, i.e. the particle is dragged deep into the "potential" well. The stability of motion naturally increases.

The most interesting case is the periodic variation of the magnetic field, which can take place, for example, on account of the residual pulsations of the rectified current feeding the magnet coils. Thus in experiments described in Refs. 82 and 83 the field pulsations reached a magnitude of 0.1% in the centre of the trap and about 0.03% in the magnetic mirrors. The pulsation frequency was 300 cps. Since under the conditions of these experiments the pulsation period is much smaller than the lifetime of the particles in the trap, new resonances appear. On account of the spatial non-uniformity of the pulsations, frequency modulation can be assumed to occur at all degrees of freedom. As is known[75], the spectrum of the frequency-modulated oscillations is equidistant, the distance between the lines being equal to Ω_0 (modulation frequency) and the total width of the basic part of the spectrum $\sim \Delta\bar{\omega}$ -- the total interval of frequency variation. For $\Delta\bar{\omega} \gg \Omega_0$ -- a condition that is generally satisfied -- each resonant plane splits into a multiplet of $N_\omega \sim \Delta\bar{\omega}/\Omega_0$ parallel planes $\sim \Omega_0/n$ apart, where $n^{-1} \sim \Omega/\bar{\omega} \sim \varepsilon_a$ (4.4.6). The origin of this small factor is easy to imagine from geometrical considerations (see also Section 4.3).

If now $\Delta\bar{\omega}/n \gtrsim \Delta_n$ (.4.46a), the mean density of the resonances sharply increases and at the same time also the Arnold diffusion. Putting $n \sim 1/\varepsilon_a$, we find the tolerance on the field modulation:

$$\xi_{cr} = \left(\frac{\Delta H}{H}\right)_{cr} \sim \varepsilon_a^2 \gtrsim 3\% \qquad (4.4.14)$$

The numerical estimate is obtained from the condition $6\varepsilon_a \sim 1$, determining the boundary of the region in which Arnold diffusion may in practice be important (4.4.13). For $\xi \gtrsim \xi_{cr}$ the increase of the diffusion can be estimated as follows. First there is an increase in the density of resonances: $\omega_0/\bar{\omega} \sim (\Delta\bar{\omega}/\Omega_0)^{-1} \sim (\xi\bar{\omega}/\Omega_0)^{-1}$ (4.4.12). Furthermore, the width of each resonance decreases by $(\Delta\bar{\omega}/\Omega_0)^{\frac{1}{4}}$ times owing to the reduction of the amplitude of the perturbation of the resonant harmonic by $(\Delta\bar{\omega}/\Omega_0)^{\frac{1}{2}}$ times as a result of the splitting of the resonance. The diffusion coefficient consequently becomes:

$$\mathcal{D}_A \sim \mu^2 \bar{\omega}\, \varepsilon_a \beta^3 \cdot \exp\left(-2\left(\frac{\Omega_0}{\bar{\omega}}\right)^{\frac{1}{4}} \frac{e^{\frac{1}{6\varepsilon_a}}}{(\beta\varepsilon_a)^{1/3}}\right) \qquad (4.4.15)$$

where we used the value $B \approx 2$, obtained above (4.4.13). The main new factor in the exponent $(\Omega_0/\Delta\bar{\omega})^{\frac{1}{4}}$ is in the typical case ~ 10.

If the magnetic field modulation is in resonance with particle oscillation in a trap, streamer diffusion may occur. The process is exactly similar to the case in the previous section, where in fact we studied the same problem of particle motion in a magnetic trap of special configuration. Streamer diffusion will not be thoroughly studied here. Let us only note that for this the frequency of the external perturbation (modulation) should be sufficiently high, at least of the order of the drift frequency Ω_g.

4.5 Stability of the Solar System

The problem of the stability of motion of the planets, although not a pressing one from a practical viewpoint, has long attracted the attention of astronomers, mathematicians and students of mechanics by its beauty and difficulty (see for instance Ref. 129). From the very beginning it was clear that very fine effects of the mechanical motion of a conservative system are important here. Even the simplest non-trivial case of two planets leads to the well-known and still completely unsolved three-body problem. Stability means here the absence of any significant and, what is more important, cumulative energy exchange between planets. As is known, in another similar system -- an excited multi-electron atom -- this energy exchange occurs in the relatively short time of $\sim 10^4$ turns and leads to so-called auto-ionization[145]. It is clear that these two systems differ essentially by the perturbation strength ($\varepsilon \sim 10^{-3}$ for planets and $\varepsilon \sim 1$ for the atom, see below). However, the question arises as to whether the apparent stability of the Solar System during $\sim 10^{10}$ turns is rigorous stability or only very slowly developing instability. Like other similar questions (see for example Section 4.4) this problem was solved to some extent only by the KAM theory[20]. The peculiarity of the problem under consideration, unlike, for instance, the motion of a particle in a magnetic trap (Section 4.4) lies in the fact that even in the simplest case of two planets with nearly circular coplanar orbits (known as the plane three-body problem) the system is many-dimensional in the sense of the KAM theory (Section 2.2), i.e. the four-dimensional tori do not divide a six-dimensional surface of constant energy and angular momentum in phase space. This means that in spite of the invariant tori, Arnold diffusion and slow instability are possible along the everywhere dense system of stochastic layers of resonances (Section 2.12). Only in the case of two planets of substantially different mass, when one can neglect the reaction of the light planet on the heavy one, under the additional condition of the co-planarity of both orbits and the circular orbit of the heavy planet (so-called restricted circular three-body problem), does the KAM theory lead to the result of the eternal stability of such motion. Below we give some preliminary estimates of the rate of Arnold diffusion for planetary and similar systems.

Let us once more recall in order to avoid misunderstandings that the actual lifetime of a planetary system may be considerably longer depending on the initial conditions and the additional "external" diffusion (Section 2.12). To take into account the effect of these latter factors would be outside the scope of this paper. In this section we will thus give a lower estimate of the lifetime of the solar system. However, taking into account the fact that in the process of evolution of the system the planetary orbits could vary considerably (see, for example, Ref. 141), this estimate will probably not be too far from reality.

The main peculiarity of the system under consideration is so-called Coulomb degeneracy, meaning that the unperturbed motion of a planet has only one ("fast") frequency instead of three (in non-relativistic approximation). This degeneracy is removed by interaction with other planets, and therefore the other two frequencies are always small ("slow"). Having used the result of Ref. 144, let us re-write the non-resonant averaged equations for the variation of the parameters of the unperturbed orbit, mainly for the variation of its frequencies. We shall restrict ourselves to the case of small eccentricities and inclinations ($e, i \ll 1$), which is the second characteristic feature of the Solar System; this is valid even for the majority of asteroids, not to mention the large planets. We have:

$$\begin{aligned}
\frac{de}{dt} &= -\varepsilon\omega \cdot \frac{ei^2}{2} \cdot \sin 2\omega' \\
\frac{di}{dt} &= -\varepsilon\omega \cdot \frac{ie^2}{2} \cdot \sin 2\omega' \\
\frac{d\Omega'}{dt} &= -\varepsilon\omega \left(1 - \frac{i^2}{2} + \frac{e^2}{2}\left(10\sin^2\omega' - 1\right)\right) \\
\frac{d\omega'}{dt} &= 2\varepsilon\omega \left(1 - \frac{e^2}{2} + \frac{5}{2}\left(e^2 - \frac{i^2}{2}\right)\sin^2\omega'\right) \\
\varepsilon &= \frac{3}{4} \cdot \frac{m}{M} \cdot \left(\frac{a}{a_0}\right)^3
\end{aligned} \qquad (4.5.1)$$

Here Ω', ω' are the longitude of the ascending node and the angular position of the perihelion measured from this node, respectively[139]; m, a_0 are the mass of the perturbing planet and the semimajor axis of its orbit; ω, a are the frequency and semimajor axis for the perturbed planet ($a_0 \gg a$); ε is the small parameter of the problem. From the equations written it can be seen that one slow frequency is connected with the precession of the eccentricity ($\dot{\omega}'$) and angular momentum ($\dot{\Omega}'$) vectors; it has an order $\Omega \sim \varepsilon\omega$. The second slow frequency depends on the difference $\dot{\omega}' + 2\dot{\Omega}'$ and is $\sim \varepsilon\omega e^2 \sim \varepsilon\omega i^2$ ($e \sim i$).

For the Solar System the latter frequency can be neglected, in view of its smallness ($\sim 10^{-5}\ \omega$). Therefore streamer diffusion (Section 2.12) is possible only for $N_0 = 3$ planets, taking into account one slow frequency Ω, or for $N_0 = 4$ in the fast frequencies. Ordinary Arnold diffusion can occur for $N_0 = 2$ (taking into account Ω) and for $N_0 = 3$ in the fast frequencies.

Let us estimate the amplitude of the various resonances. The Hamiltonian of the interaction of two planets is m/r, where

$$r^2 \approx r_1^2 + r_2^2 - 2 r_1 r_2 \cos(\varphi_2 - \varphi_1)$$
$$r \approx \frac{r_0}{1 + e \cos\varphi} \qquad (4.5.2)$$

r, φ are the coordinates of the planet in the plane of its unperturbed orbit with a parameter r_0 [143]. After expansion of 1/r in powers of cos $(\varphi_2 - \varphi_1)$ the harmonics of the difference frequency $n(\omega_2 - \omega_1)$ appear, the higher the nearer the planet orbits. The power expansion coefficients for $n \gg 1$ take the form

$$b_n \approx \left(\frac{2 r_1 r_2}{r_1^2 + r_2^2}\right)^n = \left(\frac{2 (\omega_1 \omega_2)^{2/3}}{\omega_1^{4/3} + \omega_2^{4/3}}\right)^n \qquad (4.5.2a)$$

where we used the relation $\omega_i \propto r_i^{3/2}$. All these harmonics give one and the same resonance: $\omega_1 = \omega_2$. In order to obtain the other resonances $n_1\omega_1 = n_2\omega_2$ $(n_1 \neq n_2)$, it is necessary to expand r_1, r_2 in (4.5.2) in powers of eccentricity, or take into account the frequency modulation $\varphi(t)$ for motion in an elliptical orbit. Both effects turn out to be of the same order and give a small factor e^q, where $q = |n_1 - n_2|$ is the so-called order of commensurability (of the frequencies)[139] *). The total number of two-frequency resonances $\approx nq$.

Resonances with slow frequency Ω appear as a result of eccentricity modulation in (4.5.2). The amplitude of this modulation $\sim i^2$ (4.5.1) and the harmonic number (p) of the frequency Ω does not exceed the order of commensurability: $p \leq q$. An additional small factor $\sim i^{2p}$ appears. If $e, i \ll 1$, the "slow" resonances (including the frequency Ω) cannot fill the distance between the "fast" resonances, since this would require too high harmonics p. Therefore Arnold diffusion over considerable distances is impossible under these conditions. However, such diffusion may begin after a considerable increase of e,i as a result of Arnold diffusion along resonances with a small $p \sim 1$. We shall estimate it later.

According to the above estimates the amplitude of the resonant harmonics for two planets turns out to be of the order of:

$$\varepsilon_n^{(2)} \sim \varepsilon e^q i^{2p} \cdot \exp\left(-\frac{n}{n_0}\right) \qquad (4.5.3)$$

---

*) In this section the letter e always signifies eccentricity, whereas the symbol exp will be used for the exponential.

where the parameter n_0 can be estimated from the power expansion coefficients of the perturbation m/r (4.5.2a):

$$n_0^{-1} \approx \ln \frac{2(n_1 n_2)^{2/3}}{n_1^{4/3} + n_2^{4/3}} \tag{4.5.3a}$$

With regard to the harmonic number in (4.5.3), $n = n_1$, if the expansion is taken in e_2 and inversely.

Let us now consider three planets. Their combined resonances are possible only in second approximation in the small parameter ε, since direct gravitational interaction is two-particle. In order to estimate the amplitude of the resonances let us note that in the case of three planets the quantities r_1, r_2 in (4.5.2) in first approximation contain small perturbations due to the interaction with the third planet. In second approximation this leads to three-planet resonances. When the perturbation m/r is expanded two independent frequency differences appear (for example $\omega_1 - \omega_2$ and $\omega_2 - \omega_3$). Their harmonics are simply multiplied, which leads to a set of resonances with two independent harmonic numbers. This gives $\sim n^2$ resonances even for circular orbits. When ellipticity is taken into account additional resonances appear as in the previous case. As it is easy to verify, the order of commensurability is now: $q = |n_1 + n_2 + n_3|$ $(n_1 \omega_1 + n_2 \omega_2 + n_3 \omega_3 = 0)$; the total number of resonances $\sim n^2 (q + 1)$. The corresponding small factor in the amplitude of the resonance remains as previously e^q, like the factor i^{2p} for the p^{th} harmonic of the slow frequency. The resulting estimate of the amplitude will contain an extra factor ε and $\exp(-n/n_0)$ owing to the appearance of a second frequency difference. The exponent in estimate (4.5.3) takes the form $(n_1 + n_2)/n_0 = 2\bar{n}/n_0 = n/n_0$, where n is now the maximum value of the harmonic number [compare (2.12.23)]. The final estimate for the three planets gives:

$$\varepsilon_n^{(3)} \sim \varepsilon^2 e^q i^{2p} \cdot \exp\left(-\frac{n}{n_0}\right) \tag{4.5.4}$$

In a similar way one can obtain an estimate of the amplitude of the resonance for an arbitrary number of planets:

$$\varepsilon_n^{(N_0)} \sim \varepsilon^{N_0 - 1} e^q i^{2p} \cdot \exp\left(-\frac{N_0 n}{2 n_0}\right)$$
$$q = \left| \sum_{i=1}^{N_0} n_i \right| \tag{4.5.5}$$

Here it is assumed that the masses of all the planets and the parameters of their orbits are of the same order.

The total number of resonances is now $\sim n^{(N_0 - 1)} \times (q + 1)$ and the mean distance between them:

$$\Delta_{nq} \sim \frac{\omega_0}{n^{N_0-1}\cdot(q+1)} \tag{4.5.6}$$

Let us first consider the case of $N_0 \geq 3$ planets, when Arnold diffusion may occur in fast resonances. Moreover, we can put $q = 0$, since $e \ll 1$ [(4.5.5) and (4.5.6)]. Let us first find the border of stochasticity, for which (2.12.29a) can be used. Putting: $\alpha \sim 1$; $m = N_0$; $N = N_0 - 1$; $\varepsilon^{(N_0)} \sim \varepsilon^{N_0-1}$ we obtain:

$$\varepsilon_s \sim \left(\frac{N_0}{2n_0}\right)^{\frac{2N_0}{N_0-1}} \tag{4.5.7}$$

The minimum is reached for the smallest $N_0 = 3$: $\varepsilon_s \sim n_0^{-3}$.

This estimate was obtained taking into account only N_0 frequency resonances. They are in fact the majority, but they are very weak on account of the reduction of the effective interaction parameter (4.5.5). For $N_0 \gg 3$, it is therefore reasonable to consider the opposite limiting case of pair resonances, the number of which is obviously equal to $N_0 - 1 \approx N_0$. Then the stochasticity criterion (2.12.29a) becomes:

$$\varepsilon_s \sim N_0^{-2} \tag{4.5.8}$$

Hence it follows that for a sufficiently large N_0 the system necessary becomes stochastic. This applies, for example, to star clusters[174]. If one considers that the masses of the stars in a cluster are of the same order, then $\varepsilon \sim 1/N_0$, since each star moves in the field of all the others. From estimate (4.5.8) it then follows that the border of stochasticity corresponds to $N_0 \sim 3$. A double star, of course, is absolutely stable in the absence of external perturbations. A multiple star with $N_0 > 2$ may also be stable if the masses of its components or the distance between them are substantially different, which further reduces the interaction parameter ε (4.5.1). Our Solar System is like this.

A many-electron excited atom behaves in a similar way, which leads in particular to auto-ionization, which was mentioned at the beginning of this section. Also in this case the stochasticity may be violated if the interacting electrons are at a considerable distance (in different shells).

Actually the picture is the same for the nucleus, since in estimate (4.5.8) the specific nature of Coulomb interaction was not used. Furthermore, the Bohr statistical model, assuming stochasticity of motion, can be invalid, particularly when a small number of nucleons are excited. This effect has been observed experimentally[146].

Let us return to the Solar System and estimate Arnold diffusion, first in fast resonances. Let us divide the resonances into guiding and perturbing (see Section 2.12).

For the former, the effective perturbation parameter can be written in the form: $\varepsilon_1 \sim \varepsilon^{N_0-1}$ [(4.5.5), p = q = 0], and one should have: $N_0 \geq 3$; for the second, let us express the perturbation parameter through the number to independent frequencies $N = N_0' - 1$ (4.5.6): $\varepsilon_2 \sim \varepsilon^N$; the quantities N_0, N_0' can be different. In the estimate for the diffusion coefficient (2.12.29) let us put $\exp(mn/4n_0N) \sim 1$, since we want to estimate the maximum diffusion rate in the lower resonances $n \sim 1$. Moreover, let us assume that the factor $[2N/n_0(N-1)]\,(\ldots)^{1/N} \sim 1$ (2.12.29). Introducing the diffusion time τ over $\Delta I \sim I$, we obtain the estimate:

$$(\tau\omega) \sim \sqrt{\varepsilon_1}\,\varepsilon_2^{-2} \cdot \exp\left(\varepsilon_1^{-\frac{1}{2N}}\right) \sim \varepsilon^{\frac{N_0+1}{2}-2N} \cdot \exp\left(\varepsilon^{-\frac{N_0-1}{2N}}\right) \tag{4.5.9}$$

If one assumes that for the Solar System $\varepsilon \sim 10^{-3}$, the last expression reaches a minimum for $N_0 = N = 3$, equal to: $(\tau\omega_0) \sim 10^{16}$ (years)*). This is considerably greater than the time of existence of the Solar System ($\sim 10^{10}$ years).

In fact the diffusion time will be still considerably greater, since there are only two large planets for which $\varepsilon \sim 10^{-3}$, whereas for the above-mentioned estimate four planets are required (N = 3).

In the case of two planets, as already noted above, it is necessary for Arnold diffusion to take into account a slow frequency, which is too small to span the gap between the fast resonances (see above). Nevertheless the diffusion may occur by resonances of the first harmonic in slow frequency: $n_1\omega_1 + n_2\omega_2 + p\Omega = 0$; $(p = 0, \pm 1)$. There are thus three resonances forming an intersection, exactly the minimum necessary for Arnold diffusion (Section 2.12). The eccentricity and inclination of the orbits increase, the orbits come together and as a result the interaction between planets considerably increases. If the initial distance between the planets was not too great, intersection of the orbits is even possible, and this will certainly lead to stochasticity. The latter is connected with the fact that arbitratily close encounters are possible, which means that the parameter $n_0 \to \infty$ (4.5.3a) and the density of the resonances increases infinitely (see also Fig. 4.5.1).

The width of the resonances under consideration and the distance between them is of the order [see (4.5.3) and (4.5.1)]:

$$\Omega_n \sim \omega \cdot i^p \sqrt{\varepsilon e^q} \cdot \exp\left(-\frac{n}{2n_0}\right)$$
$$\Delta_n \sim \varepsilon\omega \tag{4.5.10}$$

---

*) The frequency $\omega_0 \approx 0.53$ year^{-1} is taken for Jupiter.

In the case when the masses of the two planets are substantially different, the motion of the heavy planet can be considered to be given (restricted three-body problem). If, moreover, the eccentricity of the heavy planet $e_0 = 0$, in the rotating frame of reference of the heavy planet the total energy of the light planet is conserved -- the so-called Jacobi integral, which can be written approximately in the form[147]:

$$\frac{1}{a} + \frac{2\cdot\cos i}{a_0^{3/2}}\cdot\sqrt{a(1-e^2)} \approx \text{const}. \qquad (4.5.11)$$

Hence it is seen that if, as proposed above for the resonances chosen, a = const in the Arnold diffusion process, $e^2 + i^2 = \text{const}$ also ($e,i \ll 1$). This diffusion cannot substantially change the orbit if initially $e,i \ll 1$. Therefore, it is necessary to take into account the eccentricity of the heavy planet, i.e. to expand the perturbation m/r over both eccentricities. Since for the heavy planet the eccentricity is usually small, we shall restrict ourselves to the first power of it. Then estimate (4.5.3) takes the form:

$$\varepsilon_n^{(2)} \sim \varepsilon(e_0 n)\, e^{q-1} i^{2p} \cdot \exp\left(-\frac{n}{n_0}\right) \qquad (4.5.12)$$

where n now relates to the heavy planet. Instead of (4.5.10) we obtain, respectively:

$$\Omega_n \sim \omega \cdot i^p \sqrt{\varepsilon(e_0 n) e^{q-1}} \cdot \exp\left(-\frac{n}{2n_0}\right) \qquad (4.5.13)$$

$$\Delta_n \sim \varepsilon\omega$$

The diffusion mechanism indicated above is operative for $q \geq 2$, since for $q = 1$ there are no lateral resonances with slow frequency, i.e. $p = 0$.

In order to estimate the rate of Arnold diffusion it is necessary to use the original formula (2.12.22). Since the diffusion rate strongly depends on e, the diffusion time will be determined in order of magnitude by the duplication of e from the initial value or the quadrupling of the energy of the radial oscillations, which is $\Delta I/I \sim e^2$ of the total energy of the planet. Estimating the time necessary for this as $\tau \sim (\Delta I)^2/D_A$, we obtain from (2.12.22) for case (4.5.13):

$$(\tau\omega) \sim \left(\varepsilon e_0 n e^{q-1}\right)^{-\frac{3}{2}} \cdot \left(\frac{e}{i}\right)^{\gamma} \cdot \exp\left(2\sqrt{\frac{\varepsilon\cdot\exp(n/n_0)}{e_0 n e^{q-1}}}\right) \qquad (4.5.14)$$

Let us apply this estimate to the Solar System. Let us first consider a set of large planets, the characteristics of which according to the data of Ref. 139 are given in Table 4.5.1, including a hypothetical Olber's planet (No.5) between Mars and Jupiter, disintegrated into asteroids[147]. The quantity ξ is equal to the ratio of the frequencies

Table 4.5.1

No.	Name of Planet	m*)	a	ω_i	$\xi = \frac{\omega_{i+1}}{\omega_i}$	$\xi_0 = \frac{n_1}{n_2}$	$\frac{\xi - \xi_0}{\xi_0}$ %	e	i
1	Mercury	0.036	0.39	4.16	0.3915	2/5	0.85	0.21	0.12
2	Venus	0.82	0.72	1.63	0.6152	3/5	1.5	0.007	0.059
3	Earth	1.00	1.00	1.00	0.5317	1/2	3.2	0.017	-
4	Mars	0.11	1.52	0.53	0.4014	2/5	0.14	0.093	0.032
5	Asteroids**)	< 0.1	(2.8)	0.21	0.3848	2/5	0.52	-	-
6	Jupiter	310	5.2	0.084	0.4028	2/5	0.28	0.048	0.023
7	Saturn	94	9.5	0.034	0.3504	1/3	1.7	0.056	0.043
8	Uranus	14	19	0.012	0.5098	1/2	1.0	0.047	0.013
9	Neptune	17	30	0.0061	0.6599	2/3	0.68	0.009	0.031
10	Pluto	0.94	40	0.0040	-	-	-	0.25	0.30

*) Mass of the sun $M = 3.3 \times 10^5$.

**) Hypothetical Olber's planet, decomposed into asteroids[147].

of neighbouring planets, and ξ_0 indicates the "closest" resonance. The choice of this resonance is rather arbitrary and is determined by a compromise between the q value and the accuracy of the resonance $(\xi - \xi_0)$.

Let us begin with the last pair of the Solar System, Neptune-Pluto. In this case, as noted above, it is not the resonance 2/3 (q = 1) that is operative but the resonance 4/6 (q = 2), which is identical to it. Putting $\varepsilon \sim 5 \times 10^{-5}$ we obtain by means of estimate (4.5.14): $\tau \sim 5 \times 10^{10}$ years, which is comparable with the lifetime of the Solar System. It is possible, therefore, in view of the roughness of the estimate, that the anomalously large eccentricity and orbit inclination of Pluto is explained just by Arnold diffusion. On the other hand, the reverse influence of Pluto over Neptune is considerably weaker on account of the small mass of Pluto ($\tau \sim 4 \times 10^{12}$ years). A similar anomaly for Mercury apparently cannot be explained by Arnold diffusion on account of the small mass of Venus ($\tau \sim 7 \times 10^{11}$ years) *). Let us note, however, that if the order of commensurability of the frequencies of Mercury and Venus were not q = 3 but q = 2, even for e = 0.1 we should obtain $\tau \sim 10^{10}$ years, i.e. Arnold diffusion would already be appreciable. It is possible, therefore, that this diffusion played some part in the process of formation of the Solar System, limiting the distance between the planets from below. This is connected with the fact that over small distances there are many resonances of the form (n - 2)/n (q = 2; $n_0 \approx n^2$).

*) This anomaly is possibly explained by the small mass of Mercury itself[141].

Evidently, one must have a clear understanding of how controversial and unconvincing such hypotheses may be, which, by the way, is necessarily rather typical of astronomy[147]. Nevertheless, when a new phenomenon is discovered, such as Arnold diffusion in the present case, it is useful to imagine, although this enters the world of fantasy, all its possible manifestations.

Let us now turn to another resonant pair Jupiter-Saturn, for which: $q = 3$; $\varepsilon \sim 10^{-3}$; $n/n_0 \approx (2/9) \times (q^2/n) = 2/5$. In this case we have to use (4.5.10), since the masses of both planets are of the same order. This, by the way, does not give a great disparity since the values of eccentricity of their orbits are also close. From estimate (4.5.14) we obtain a sufficiently long time $\tau \sim 10^{12}$ years on account of the small eccentricity. Again, for $q = 1$ it would be $\tau \sim 3 \times 10^6$ years and even for $q = 2$ it would still be $\tau \sim 10^9$ years. For the other pairs of planets Arnold diffusion is negligibly small on account of the small masses of the planets except for the Saturn-Uranus pair. In this case $\tau \sim 3 \times 10^{10}$ years, i.e. of the same order as for the Neptune-Pluto pair. The difference between these pairs lies in the fact that the first of them is considerably further from the resonance. It is also possible that the estimate of τ for the latter pair is considerably reduced, since the anomalously small eccentricity of Neptune's orbit may have been substantially greater in the past.

Finally the resonance of Jupiter with the hypothetical Olbers' planet was also possible (see table). Let us assume that this planet, having a small mass, had considerable eccentricity, say the same as Mercury: $e = 1/5$ ($\sim i$). Then estimate (4.5.14) gives: $\tau \sim 10^8$ years. This result, in our opinion, enables us to overcome the difficulties in explaining the mechanism of the rupture of Olbers' planet and the formation in this way of a belt of asteroids. As far as can be judged from the literature[147] the hypothesis of the rupture of the original planet is the most probable for explaining the origin of the asteroids. From our point of view, the destruction of Olber's planet could have been the result of its close encounter with Jupiter. The rupture (or several ruptures) proper of the planet could also have occurred later, for example, under the influence of planet rotation[147]. With regard to the distribution of the asteroids, at present it may be considerably different from the original distribution as a result of the evolution of the orbits.

In this connection let us note that the classical perturbation theory generally used to analyse such evolution is not applicable near resonances[129] for $t \gtrsim t_s$, where t_s is the time of development of instability in the stochastic layer, which can be estimated as (4.5.13):

$$t_s \sim \Omega_n^{-1} \sim 10^3 \text{ years}. \qquad (4.5.15)$$

The numerical value is taken for resonance 2/5 with Jupiter. Therefore the "unchanged" or eigen parameters of the orbits of the asteroids introduced by Hirayama[148,147] have sense only far away from the main resonances. In particular, Arnold diffusion violates the Laplace-Poisson theorem on the absence of secular perturbations in the semimajor axis of the orbit. It is interesting to note that the five main families of asteroids with close values of "unchanged" elements, discovered by Hirayama, lie just between the main resonances (Fig. 4.5.1).

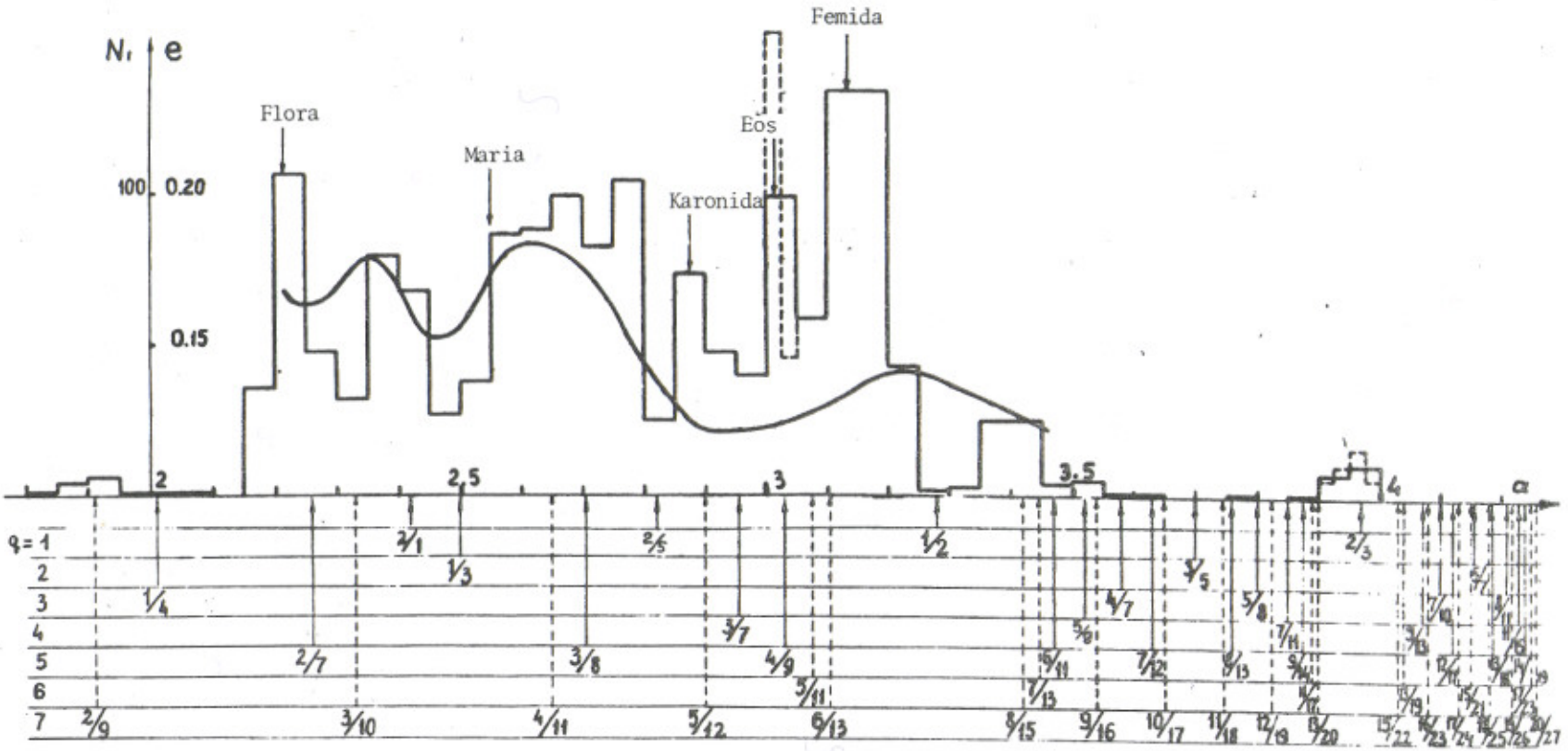

Fig. 4.5.1 Frequency spectrum of 1641 asteroids (angular line) and correlations with the eccentricity e (curve): N_1 is the number of asteroids in the interval $\Delta a = 0.05$: the dotted line gives the distribution (×2) in the interval $\Delta a = 0.025$.

Figure 4.5.1 gives a histogram of the distribution of the asteroids in the semi major axis (a) of their orbit, or, in other words, the frequency spectrum of the asteroids. The interval represented: $1.8 < a < 4.0$, covers 1641 asteroids out of 1660, the parameters of which are given in Ref. 149. The arrows denote resonances with Jupiter, which are divided into seven groups according to the value of the order of commensurability $q = 1\text{-}7$ *).

For all resonances with $q \leq 5$ in the distribution, there are so-called "gaps", i.e. clear decreases in the number of asteroids. Slightly less definite "gaps" are also observed for resonances with $q = 6$, but they are completely absent for $q = 7$. Resonances 2/3 and 4/9 appear to be an exception; they correspond to the distribution maximum instead of "gaps". However, a more detailed distribution (dotted line) shows that near these resonances the number of asteroids decreases also (compare with resonance 2/7). Sometimes a "maximum" is mentioned near resonance 3/4 ($a = 4.2949$) implying a single asteroid Tule ($a = 4.2829$; $e \approx 0.032$; $i \approx 0.041$) [147]. However, a single case cannot constitute a serious objection to general regularity, and all the more since in the present case the quantities e and i are anomalously small [$\langle e \rangle = 0.141$; $\langle i \rangle = 0.166$ [147]].

Finally, there is yet another exception -- this time an undoubted one -- the so-called Trojan group (15 asteroids) [147] situated inside resonance 1/1 ($a = 5.2028$), the relative width of which $\sim \sqrt{\varepsilon} \approx 3\%$. The reason why this resonance is an exception is because it is inside the stochastic ring, since the distance between resonances with a given q [$\omega_1/\omega_2 = (n - q)/n$] vanishes when $\omega_1/\omega_2 \to 1$: $\Delta_n \approx q/n^2$. However, these resonances, the width of which $\sim \sqrt{\varepsilon e^q}$ [(4.5.13), $n_0 \simeq (2/9)/(q/n)^2$, see above] cannot completely destroy resonance 1/1, the width of which is substantially greater ($\sim \sqrt{\varepsilon}$). Therefore, a stable region forms inside resonance 1/1, in which the Trojan group is located. Similar stable regions are also possible for the other resonances, since the neighbouring resonances with slow frequency producing Arnold diffusion are considerably weaker and cannot destroy a two-frequency resonance completely. This effect also apparently explains, at least in part, the conservation of a certain number of asteroids in "gaps".

Let us estimate the Arnold diffusion rate for asteroids, putting for the sake of simplicity in (4.5.14): $e_0 n \sim e \sim i \sim 1/5$; $n \sim n_0$. Then for $q = 2$ we obtain: $\tau \sim 4 \times 10^6$ years. The limitation of the operating resonances can be found if one takes as the maximum observable $\tau \sim 10^{10}$ years. We obtain $q_{max} = 4 (\tau_4 \sim 3 \times 10^9$ years). Agreement with the experimental results in Fig. 4.5.1 may be regarded as satisfactory, taking into account the roughness of the estimates.

Figure 4.5.1 also shows the dependence of the mean eccentricity of the orbits of the asteroids on their semi-major axis [according to Putilin[147]], which is clearly correlated with the resonances in accordance with estimate (4.5.14). The exception is resonance 1/2, the distinguishing feature of which is the equality of the rotation frequency of the asteroid and that of the radial oscillations of Jupiter in the frame of reference spinning with the latter. The oscillations may be so phased that the distance between two planets would be maximal.

---

*) Sometimes one denotes also a "gap" connected with Mars (resonance 2/1), also shown in Fig. 4.5.1. However, the fall in the distribution function in this place certainly does not go beyond the limits of statistical error.

The width of the majority of the "gaps" is $\sim 1\%$ (Fig. 4.5.1) and weakly depends on the order of the resonance. Its lower limit is determined by the width of the resonance and is $\sim 10^{-2}$-10^{-3} (q = 2-5). The upper limit depends on the additional diffusion, for example due to the interaction of the asteroids between themselves or with interplanetary matter. Besides the diffusion, systematic variation of the orbit also plays a part. In this connection let us point out that some of the "gaps" (2/7; 3/8; 4/9; 2/3, see drawing) are displaced in relation to the resonance to the side of greater energies (a), which corresponds to an increase of the size of the orbit with time. In any event, it can be expected that if the distance between the working resonances becomes smaller than the width of the "gap", the majority of the asteroids will be destroyed. Apparently just this is observed in the section a > 3.2 (Fig. 4.5.1). There are only 16 asteroids with a > 4.0 and with special parameter values; the rest, if they existed initially, must have come too close to Jupiter, entered the stochastic ring and been captured by Jupiter. It is possible that the explanation of the almost complete absence of asteroids near Mars (there are in all three asteroids with a < 1.8) is similar.

As far as we know, the only competing hypothesis is the Brouwer hypothesis[151], which explains the appearance of the "gaps" simply by phase oscillations in the resonances, on the assumption of uniform or, at least, sufficiently smooth distribution of asteroids in the integrals of motion. This effect undoubtedly exists, but the above-mentioned independence of the width of the "gap" from q is unclear, as well as the limitation of the operating resonances by the condition $q \leq 6$ (Fig. 4.5.1). In order to clarify this question, more accurate estimates of Arnold diffusion in the Solar System are necessary.

4.6 Non-linear waves; turbulence

In this section, we shall endeavour to apply to the motion of a continuous medium the notion of stochasticity that has been developed. In exactly this case we have a well-known and extremely clear picture of stochastic motion -- turbulence. Moreover, turbulent motion is a typical example of a system with divided phase space (Section 2.5) (laminar and turbulent zones), a fact which seems so surprising for a discrete dynamical system. There also exist critical values of the parameters, for example the flux velocity giving the border of turbulence (stochasticity). For analytical calculation of this border, the criterion of local instability is used[164], which in discrete systems is equivalent to stochasticity (Section 2.4). There is thus a close analogy between the motion of a discrete and a continuous dynamical system. This analogy can be fully understood if it is recalled that under ordinary conditions, for instance when the dimensions of the medium are restricted, its motion may be decomposed into some discrete modes ("quasi-particles"), weakly interacting with each other, at least for some values of the parameters of the problem. Moreover, in a series of cases the spectrum of such modes is limited, for instance, by dispersion, so that only a finite number of modes effectively interact. In this case there is complete analogy with a discrete system.

The distinctive feature of the methods of investigating stochasticity developed in the present paper lies in the use of the properties of non-linear resonance. Therefore, at the present time, it is not clear how these methods can be applied (and if they can be applied at all) for investigating classical turbulence in hydrodynamics. However, there are also the specific oscillatory problems of the motion of a continuous medium.

These are non-linear waves interacting with each other. Similar problems have been studied from different angles by many authors. It is not possible for us to analyse all these papers thoroughly here, so we shall mention only two effects, in our opinion the most beautiful. The first, the stability on non-linear modes, discovered by Fermi, Pasta and Ulam[165] is similar to Kolmogorov stability for a continuous system. Going further in this direction Kruskal and Zabusky discovered specific non-linear formations -- solitons -- possessing remarkable stability, or in other words so-called reversible shock waves[166]. The second effect -- collisionless (and, as usual, irreversible) shock waves -- was predicted in theory by Sagdeev[175].

Below we shall restrict ourselves to the study of the Fermi-Pasta-Ulam problem[165] and as a model of the system we will not take a continuous medium but, as in Ref. 165, a chain of coupled non-linear oscillators approximately representing it, or for the sake brevity, a non-linear chain, the motion of which is described by a set of ordinary differential equations:

$$\ddot{x}_\ell = (x_{\ell+1} - 2x_\ell + x_{\ell-1}) + \beta\left[(x_{\ell+1} - x_\ell)^3 - (x_\ell - x_{\ell-1})^3\right] \qquad (4.6.1)$$

$\ell = 1, 2, \ldots, N-1$; $a = 1$; $L = N$. Here a is the unperturbed distance between neighbouring masses ($m = 1$), coupled by a non-linear spring; L is the total length of the chain.

This model is very convenient in the first place for numerical experiments, since it does not call for the integration of partial differential equations. Moreover, such a relatively simple model makes it possible to trace the transition from a discrete system to a continuous medium.

Set (4.6.1) is related to the second order wave equation[165]:

$$\frac{\partial^2 x}{\partial t^2} = \frac{\partial^2 x}{\partial z^2}\left(1 + 3\beta\left(\frac{\partial x}{\partial z}\right)^2\right) + \gamma^2 \frac{\partial^4 x}{\partial z^4} \qquad (4.6.2)$$

where $z \approx \ell a$ is the coordinate along the chain. The last term was introduced by Zabusky[167] and characterizes the dispersion due to the discreteness of the chain:

$$\gamma^2 = \frac{a^2}{12} = \frac{1}{12}\left(\frac{L}{N}\right)^2 \qquad (4.6.3)$$

In the absence of dispersion the solution of the non-linear wave equation, after a short time becomes singular and then multivalued.

For a wave of one direction one can also write a first order equation[167]:

$$u_\tau + u^2 u_z + \delta^2 u_{zzz} = 0 \qquad (4.6.4)$$

where $u = \partial x/\partial z$; $\delta^2 = 2\gamma^2/3\beta$; $\tau = (3/2)\,\beta\,(t - z)$ and the index denotes the differentiation with respect to the corresponding argument. In this form the equation is valid only when $\beta \to 0$ (see below).

As follows from Eqs. (4.6.1), (4.6.2) and (4.6.4), we will restrict ourselves here to the (simpler) case of cubic non-linearity (in force). Quadratic non-linearity ($u^2 \to u$) has been studied in detail by Israelev[186].

The statistical properties of a non-linear chain (4.6.1) are explained more or less thoroughly in Ref. 168. The main thing here is the border of stochasticity, which provided an explanation of the result of Fermi, Pasta and Ulam which was paradoxical in its time -- the absence of equipartition of energy among the modes of a non-linear chain.

Let us first find the position of the border of stochasticity. As an unperturbed system let us take a linear chain ($\beta = 0$), the motion of which can be represented in the form of a superposition of normal oscillations $Q(t)$*):

$$x_\ell = \sqrt{\frac{2}{N-1}} \sum_{k=1}^{N-1} Q_k \cdot \sin \frac{\pi k \ell}{N} \tag{4.6.5}$$

with frequencies:

$$\omega_k = 2 \cdot \sin \frac{\pi k}{2N} \tag{4.6.6}$$

As the small perturbation parameter let us take the quantity:

$$\epsilon = 3\beta u^2 = 3\beta w \tag{4.6.7}$$

where w is the density of the energy of the oscillations per unit of chain length. Let us restrict ourselves to the case of $k \ll N$, which gives the possibility of transition to a continuous medium ($N \to \infty$). Then the distance between resonances in first approximation is:

$$\Delta = \omega_{k+1} - \omega_k \approx \frac{\pi}{N} \tag{4.6.8}$$

This expression is valid if the number of perturbed modes (N_0) is small. In the opposite case it is necessary to use estimate (2.12.15), which in the present case [four-phonon interaction (4.6.2)] leads to the expression:

---

*) Here we are studying the oscillations of a chain with fixed ends: $x_0 = x_N = 0$, i.e. standing waves; for travelling waves, see below.

$$\Delta \sim N_0^{-3} \tag{4.6.9}$$

The preceding formula is thus applicable under the following condition:

$$N_0 \lesssim N^{1/3} \tag{4.6.10}$$

The non-linearity coefficient of the chain $\alpha \sim \varepsilon$, since the unperturbed system is linear and cubic non-linearity shifts the frequency already in first approximation[3]. This is why the problem is simpler for cubic non-linearity than for quadratic, for which frequency shift appears only in second approximation. Finally, the phase oscillation frequency is of the order:

$$\Omega_\varphi \sim \varepsilon \omega_k \approx \frac{\varepsilon \pi k}{N} \tag{4.6.11}$$

Whence the border of stochasticity is determined by the estimate[168]:

$$\varepsilon_s \sim \frac{1}{k} \sim \frac{\lambda}{L} \tag{4.6.12}$$

where λ is the wave length of the oscillations. It can be seen that when the lower modes are excited the stochasticity threshold is raised; this explains the result of Fermi, Pasta and Ulam[165].

In fact in estimate (4.6.10) it is necessary to put the maximum value of k reached in the process of evolution of the non-linear wave. The evolution amounts, mainly, to the disintegration of the initial wave into so-called solitons[166]. The quantity k_m is determined by the width of the soliton and can easily be estimated from (4.6.4)[166]:

$$k_m \sim L \cdot \left(\frac{u}{\delta}\right) \sim \sqrt{\varepsilon} \cdot N \tag{4.6.13}$$

This estimate is valid if the initial $k_0 \lesssim k_m$; in the opposite case the disintegration into solitons does not take place[169]. For (4.6.13) the border of stochasticity (4.6.12) takes the form:

$$\varepsilon_s' \sim N^{-2/3} \tag{4.6.14}$$

In the following approximation in k/N the frequency $\omega_k \approx \pi k/N - (\pi^3/24)\cdot(k/N)^3$, so that a denser system of resonances is possible, with a minimum distance of:

$$\Delta_1 \sim \frac{k^2}{N^3} \tag{4.6.15}$$

This gives a border of stochasticity of the form:

$$\varepsilon_s^{(1)} \sim \frac{k}{N^2} \tag{4.6.16}$$

The total width of this system of resonances is: $\Delta\omega \sim (k/N)^3$, which corresponds to an energy exchange:

$$\frac{\Delta E_k}{E_k} \sim \frac{\Delta\omega}{E_k \cdot \omega'_E} \sim \frac{k^2}{\varepsilon N^2} \tag{4.6.17}$$

Comparing with (4.6.16) we find that in the interval:

$$\frac{k}{N^2} \lesssim \varepsilon \lesssim \frac{k^2}{N^2} \tag{4.6.18}$$

developed stochasticity must occur.

Finally, stochasticity is also possible owing to the non-linear spread of the frequencies ω_k, which is of the order of:

$$\Delta\omega_k \sim \Delta E_k \cdot \omega'_E \sim \varepsilon\omega_k \cdot \frac{\Delta E_k}{E_k} \sim \Omega_4 \frac{\Delta E_k}{E_k} \tag{4.6.19}$$

since for sufficiently large N_0 each resonance of the unperturbed frequencies, generally speaking, has a few corresponding combinations of modes. Non-linear perturbation removes this degeneracy and leads to strong destruction of resonances when $\Delta E_k \sim E_k$.

Let us now consider the case of a travelling wave, which is described by a first order equation (4.6.4) in the frame of reference moving with the velocity of an unperturbed (linear) wave. The outstanding feature of equation (4.6.4) is its indepedence of the perturbation parameter β, which simply changes the time scale. From this it follows directly that in this case a stochasticity criterion of the (4.6.12) type is impossible. This in its turn means that the behaviour of standing and travelling non-linear waves may differ considerably. The other alternative is pointed out below.

The sole parameter of Eq. (4.6.4) is the relation:

$$R = \left(\frac{uL}{k\delta}\right)^2 \sim \varepsilon\left(\frac{N}{k}\right)^2 \qquad (4.6.20)$$

which also determines the condition for the disintegration of the wave into solitons ($R \geq 1$)[169]. The question as to whether the latter inequality is also a condition of instability still remains open, although some numerical experiments[166] encourage the idea that this is not so.

It was noted above that the first order equation (4.6.4) is valid only in first approximation for $\beta \to 0$. The following approximations were obtained by H. Krushkal; for instance with an accuracy $\sim \beta^2$ the equation takes the form:

$$u_\tau + u_z u^2\left(1 - \frac{9}{16}\beta u^2\right) + \delta^2 u_{zzz} = 0 \qquad (4.6.21)$$

It is not possible by any scale transformation to get rid of β here, which means that this parameter must also enter into the criterion of stochasticity.

Let us now describe a few numerical experiments with a non-linear chain, which were carried out in cooperation with Israelev and Khisamutdinov[187].

As noted above, a set of ordinary differential equations (4.6.1) with boundary conditions $x_0 = x_N = 0$ was integrated. The initial conditions were given through normal coordinates $Q(0)$ $[\dot{Q}(0) = 0]$ (4.6.5). Computation errors were checked by conservation of the total energy of the chain; their values are given in the captions to the diagrams. The time of motion and step of integration (h) are given in natural units (4.6.6).

The main problem when processing the computation results was the choice of a clear and convenient criterion to show that the motion was actually stochastic. The following methods were used in different cases.

1. Visual estimate from the curves of the energy dependence of a few modes on time, and also from the spectrum at different moments in time $[E_k(t)]$. This method gives a sufficiently clear result, if only one mode is initially excited, as happened in the majority of cases in Ref. 165. An example of such a case for our computations is given in Fig. 4.6.1. The lower curve (b) shows clear almost-periodical energy oscillations of the first mode. Unfortunately, such initial conditions are possible only for the very lowest modes. The point is that the mode $k << N$ can directly exchange energy only with the modes 3k, 5k, 7k, etc. In the case of excitation of a single sufficiently high mode its energy remains practically unchanged. Figure 4.6.2 gives an example of the excitation of a single mode $k_0 = 15$. Small energy oscillations are due to interaction through higher modes. The reasons for the intensive energy exchange after $t = 5000$ will be discussed below.

2. Autocorrelations (Section 2.3) were computed for the displacement of a definite oscillator x_j and for the energy of a definite mode of oscillations E_k according to the following formula:

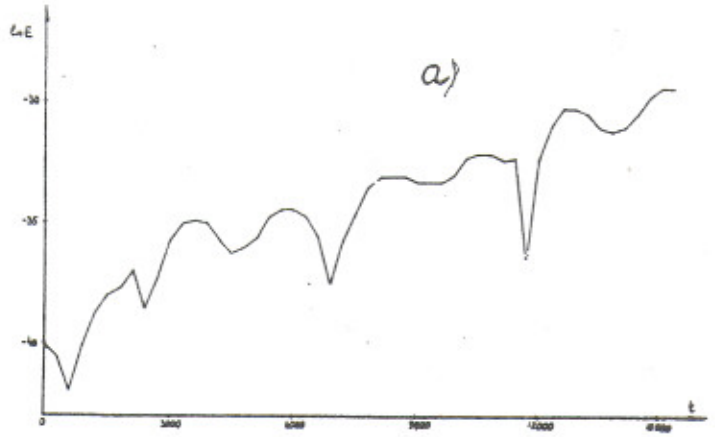

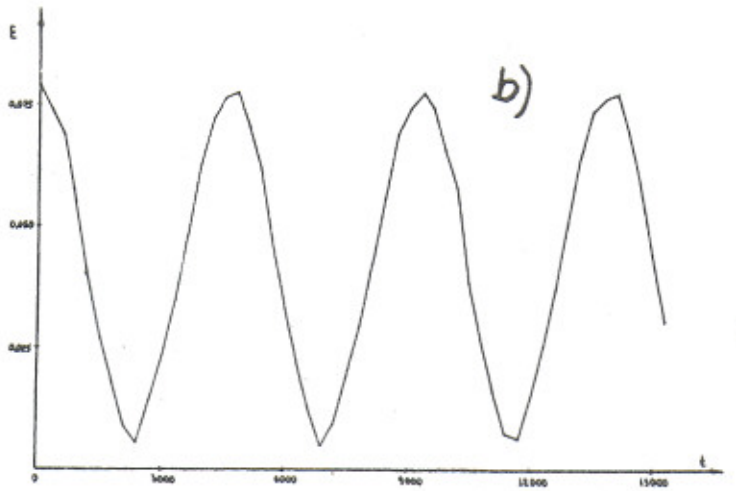

Fig. 4.6.1 Weak stochasticity: $E_1(0) \approx 0.0788$; $E_2(0) \approx 5.3 \times 10^{-18}$; $\beta = 8$; $\varepsilon \approx 0.06$; $t_{max} \approx 15300$; $h = 1/2$; $\Delta E/E \approx 0.15\%$; a) the increase of $E_2(t)$; b) the dependence $E_1(t)$.

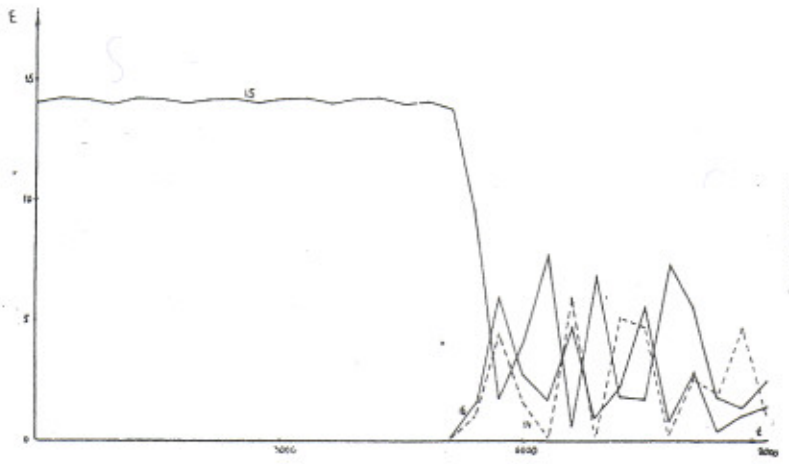

Fig. 4.6.2 Excitation of single (15th) mode: $E_{15} \approx 14.1$; $\beta \approx 0.0314$; $\varepsilon \approx 0.04$; $t_{max} = 9000$; $h = 1/6$; $\Delta E/E \approx 1.5\%$.

$$\rho(x_j, T) = \frac{\overline{x_j(t) \cdot x_j(t-T)}}{\overline{x_j^2(t)}}$$

$$\rho(E_\kappa, T) = \frac{\overline{E_\kappa(t) E_\kappa(t-T)} - \overline{E_\kappa(t)}^2}{\overline{E_\kappa^2(t)} - \overline{E_\kappa(t)}^2} \qquad (4.6.22)$$

Here the bar signifies averaging over t in equal intervals Δt; T is the time shift. In all cases for $\rho(x_j,T)$ $j = 16$, which with N chosen as 32 corresponds to the middle oscillator of the chain.

3. Correlations between modes were computed according to the formula:

$$\rho(E_\kappa, E_\ell) = \frac{\overline{E_\kappa E_\ell} - \overline{E_\kappa} \cdot \overline{E_\ell}}{[(\overline{E_\kappa^2} - \overline{E_\kappa}^2)(\overline{E_\ell^2} - \overline{E_\ell}^2)]^{1/2}} \qquad (4.6.23)$$

where the values E_k and E_ℓ are taken at the same moment of time in Δt, and the bar, as in (4.6.22) represents averaging over t. As a result of the law of conservation of the total energy of the system, the correlation coefficient (4.6.23) is different from zero even for stochastic motion. It is easy to show that in the latter case it is:

$$\rho(E_\kappa, E_\ell) = -\frac{1}{\nu - 1} \qquad (4.6.24)$$

Thus knowledge of this coefficient makes it possible to determine the effective (mean) number of interacting modes ν.

4. Local instability of the oscillations, which means that almost any of the trajectories that are close together at first diverge exponentially fast in the process of motion. In order to investigate local instability we used the spatial symmetry property of our system, according to which the even modes cannot appear in the process of motion, if they were not initially excited[165]. Therefore there is an exact solution $E_{2k}(t) = 0$ and it is sufficient for us to follow the growth of the even modes, if at the beginning they are given very low energy. We discovered this peculiar instability of the even modes by chance. When the excitation of a single mode was investigated, it was found, in the process of computation, that the energy of the even ("forbidden") modes increases from computer zero ($\sim 10^{-19}$) to a considerable quantity and even becomes comparable with the energy of the uneven modes. This means that from the very beginning there was asymmetry in $x_\ell(t)$ with respect to the middle of the chain. The "culprit" turned out to be the computing of the sine entering into the transformation formula (4.6.5). It was discovered that there was an error in computing the sine, depending on the number of the mode k, as a result of which weak asymmetry also occurred, corresponding to slight excitation of the even modes. Subsequently, when it was necessary, special symmetrization of $x_\ell(t)$ was carried out immediately after the transition from $Q_k(t)$ to $x_\ell(t)$.

This very effect was used as the basis of the method of local instability.

Figure 4.6.2 shows just such a case, when as a result of fast developing instability the energy, previously concentrated in one mode (k_0 = 15), after some time strongly goes over to the neighbouring modes. This method enabled us to discover weak instability also for the case when k_0 = 1. The parameters are taken from Ref. 165, whose authors considered the motion in this case to be quasi-periodical. Indeed Fig. 4.6.1b gives no reason to doubt this. Nevertheless Fig. 4.6.1a shows that, although weak, instability does exist, and can influence the general behaviour (for example, of the first mode) after a sufficiently long time. Figure 4.6.3 again shows the growth of the even modes (k_0 = 15, 17) and it is

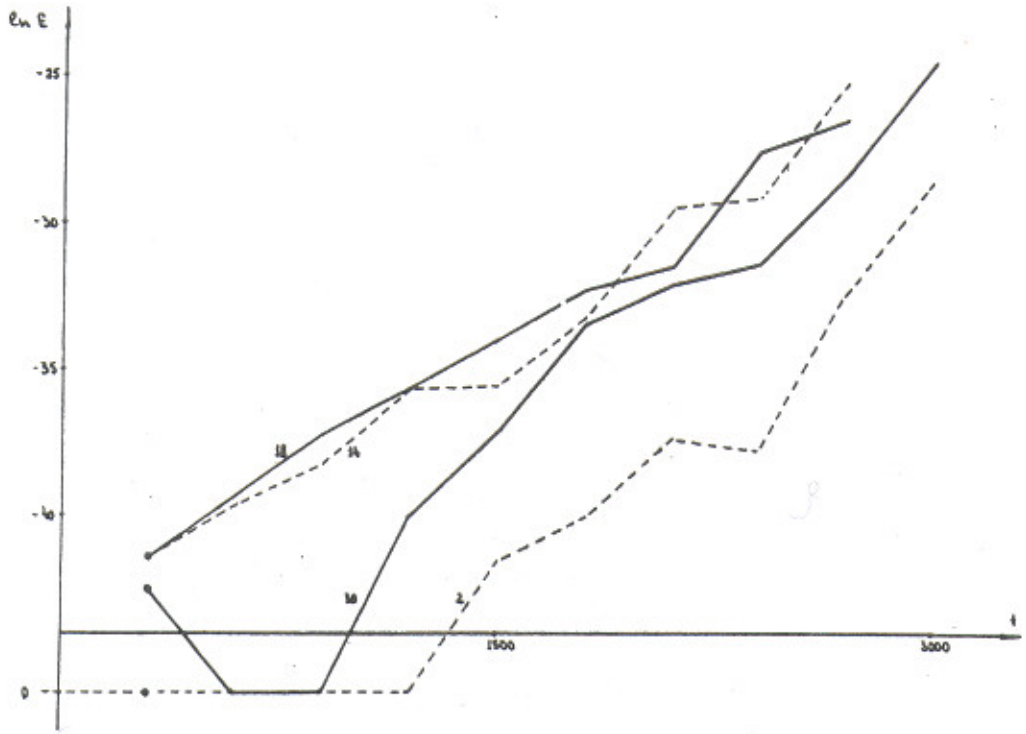

Fig. 4.6.3 Exponential increase of even modes for initial excitation of uneven modes (k_0 = 15; 17): the figures indicate the number of the mode; zero on the graph is the computer zero, corresponding to $E_k \sim 10^{-20}$; $E \simeq 20$; $\beta = 0.0314$; $\varepsilon \approx 0.06$; $t_{max} = 3000$; $h = 1/6$; $\Delta E/E \approx 3.5\%$.

clear that the distant (k = 2, 30) modes "grow" later than the closer ones (k = 14, 18), although the rate of growth of all the modes is approximately identical. Let us also note that the energy transition to the higher modes (k = 30) occurs faster than that to the lower ones (k = 2). This effect was also mentioned in Ref. 168.

Using this same method and giving the initial perturbation of the even modes ($\sim 10^{-14}E$) at a certain moment in time, the border of stochasticity was investigated. The excitation was in three odd modes and the growth rate of the energy of the adjacent even modes was determined.

The method described is extremely convenient, firstly on account of its clearness, and secondly because it does not require long computation times. Moreover, one computation promptly gives the distance between two neighbouring trajectories.

A summary of the results is given in Fig. 4.6.4 in the form of vertical segments giving the experimental interval of the values of the growth rate $1/\tau$. The groups of results I, II, III and IV, were obtained from the growth of even modes with initial excitation of three neighbouring uneven modes in different parts of the spectrum. Groups V

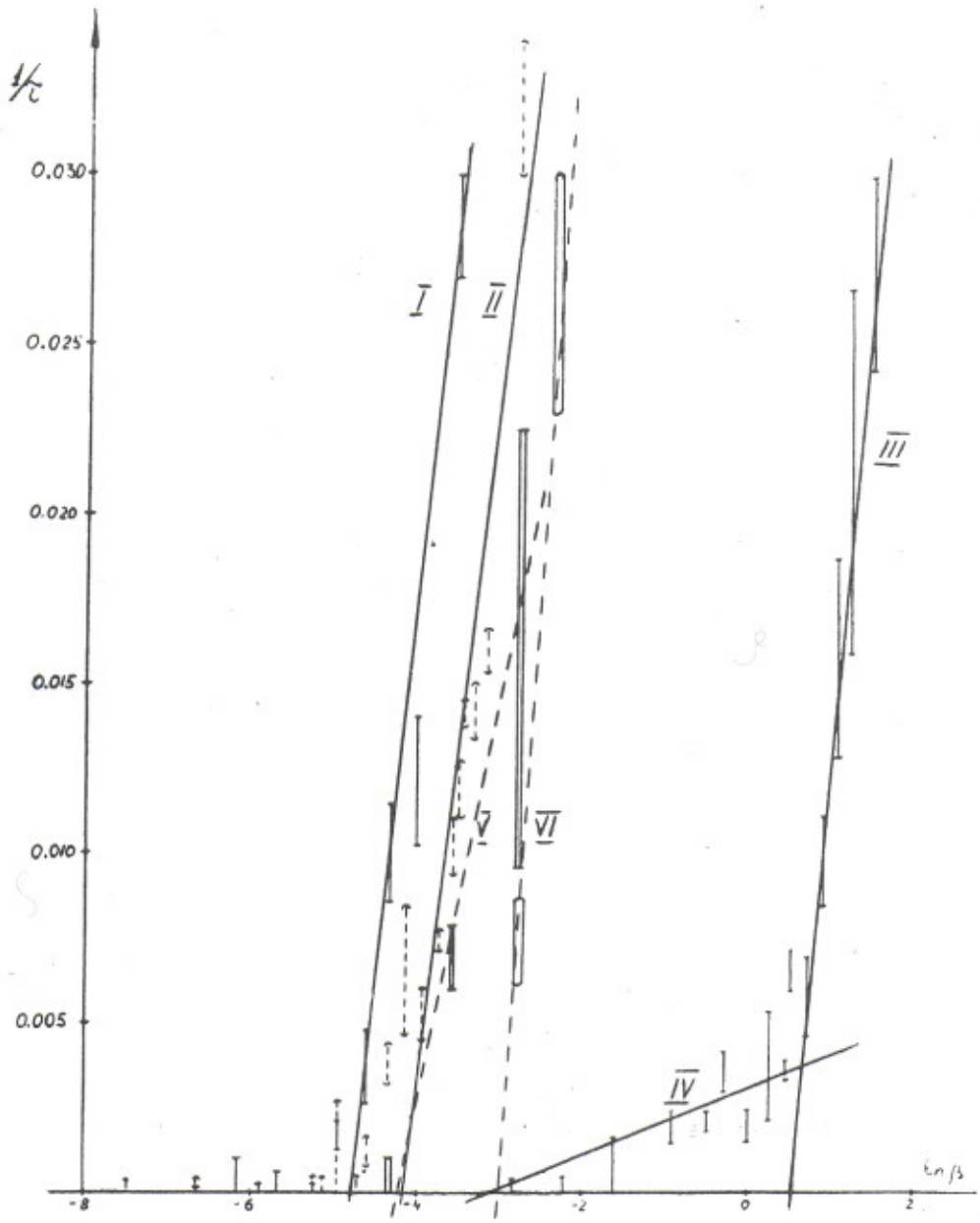

Fig. 4.6.4 Dependence of the rate of development of local instability on the parameter β. Initial conditions: k_0 = 27, 29, 31 (I), E ≈ 30; k_0 = 15, 17, 19 (II), E ≈ 17; k_0 = 1, 3, 5 (III and IV), E ≈ 0.95; k_0 = 27, 29, 31 with symmetrization (V), E ≈ 30; k_0 = 28, 29, 30 (VI), E ≈ 35.

and VI were obtained from the divergence of nearby trajectories, and in the first case (V) the same modes were excited as for (I), but with symmetrization, i.e. complete elimination of the even modes; in the second case (VI) both even and uneven modes were excited (k_0 = 28, 29 and 30).

A semi-logarithmic scale is used in Fig. 4.6.4, corresponding to the expected dependence (2.11.4)*):

$$\frac{1}{\tau} = \frac{\Delta}{\pi} \cdot \ln \frac{\beta}{\beta_{cr}} \qquad (4.6.25)$$

where β_{cr} lies on the border of stochasticity and Δ is the order of magnitude of the distance between resonances. In fact for large β the experimental results lie in straight lines within the limits of error. However, for small β there are considerable deviations and in order to explain them we put forward the hypothesis that these deviations, always to larger $1/\tau$, are connected with other denser systems of resonances. This leads simultaneously both to a decrease of β_{cr}, which is determined by the intersection of the interpolation line in Fig. 4.6.4 with the horizontal coordinate axis, and to a lessening of the slope of the line.

Qualitatively this is just what is observed. The effect is especially clearly seen when the lower modes are excited, where besides the "main" line (III) a second line (IV) can be drawn with equal confidence.

A quantitative comparison can be made by measuring the slope of the interpolation lines. The mean value of this slope for all the groups except (IV) is : $\langle\Delta\rangle \approx 8.2 \times 10^{-2}$, which agrees well with the expected quantity: $\Delta \approx \pi/N \approx 0.1$ (4.6.8). For line IV: $\Delta \approx 3 \times 10^{-3}$. This can be compared with the dense system of resonances (4.6.15), predicted by theory: $\Delta_1 \sim k^2/N^3 \sim 10^{-3}$. In this case β_{cr} ($\propto\Delta$) should decrease by the same amount. This is in fact confirmed in order of magnitude:

$$\Delta(\mathrm{III})\Delta/(\mathrm{IV}) \approx 25; \quad \beta_{cr}(\mathrm{III})/\beta_{cr}(\mathrm{IV}) \approx 37 \quad .$$

The question arises as to what is the difference in this case between both borders of stochasticity from the point of view of the behaviour of the system as a whole. The answer is that a denser system of resonances may be insufficiently wide (see above). Therefore the overlapping of the resonances of such a system does not lead, generally speaking, to complete stochasticity; instead of this a more or less narrow band of stochasticity is formed with limited variation of the energy of the interacting modes (4.6.17).

---

*) The function $\tau(\beta)$ depends, as we know, on the phase relations between the resonances, and law (4.6.25) is in a sense "atypical" (Section 2.11). The justification for the choice of such a law is finally a comparison with the experiment (see below). Let us only note that in the case under consideration there may actually be special phase relations due to the special initial conditions: $\dot{Q}_k$ (0) = 0 (see above).

Apparently this is the effect that explains the behaviour of the system, which at first glance appears strange, for the case shown in Fig. 4.6.1. The upper curve in this diagram clearly indicates local instability of motion. However, this instability does not develop, apparently, to any appreciable level, since it does not appear at all in the lower curve. In particular, the successive maxima on this curve differ from each other by a few per cent but this difference does not grow exponentially as on the upper curve.

An even more important question arises as to whether such a stochastic layer can lead to a considerable redistribution of energy between modes after a sufficiently long time. Although we now have no experimental results on this subject, we know that generally speaking this is possible, owing to Arnold diffusion (Section 2.12). However, this instability develops extremely slowly and therefore it is reasonable to consider it apart from strong instability, due to the overlapping of a wide (and less dense) system of resonances.

The results given in Fig. 4.6.4 satisfactorily agree with the estimates of the position of the border of stochasticity [(4.6.12), (4.6.14)]. Thus for case II the experimental value $\varepsilon_{cr} \approx 0.03$, and estimate (4.6.12) gives: $\varepsilon_s \sim 0.06$; for case III: $\varepsilon_{cr} \simeq 0.17$; $\varepsilon_s' \sim 0.1$ [in this case it is necessary to take into account the formation of solitons (4.6.13)]. Our estimates do not extend to the remaining cases because $k_0 \approx N$ (see Ref. 168).

Let us note that the position of the border of stochasticity depends substantially on the "details" of the initial state. This effect is demonstrated by lines V and VI in Fig. 4.6.4. Thus for line V, β_{cr} is approximately twice as large as for line I, and the only difference between them is the complete absence of even modes for case V. An even more important difference occurs in the case of excitation of modes of mixed parity (VI), where β_{cr} exceeds the value for the comparable case (I) by almost an order. It is difficult to say now what this is due to; perhaps, for example, to a reduction of the number of modes of identical parity. In any case this again demonstrates the very complex structure of the transitional zone.

It is known that local instability does not necessarily signify strong stochasticity (although apparently it necessarily leads to real instability). Therefore it is desirable to use other methods to convince oneself that for sufficiently large β, E our system (4.6.1) actually is stochastic. Three check runs were carried out for the utmost possible time under our conditions $t_{max} \sim 10^4$.

In the first case three uneven modes were excited ($k_0 = 15, 17, 19$), as for case II in Fig. 4.6.4, but with symmetrization. The value $\beta \approx 0.0314$ was chosen approximately twice as great as β_{cr}. The autocorrelations of the 15th mode and the shift of the central oscillator were measured, and also the correlations between modes 15 and 17. The results are given in Fig. 4.6.5. It can be seen that the correlations are of an almost periodical nature and the number of interacting modes practically does not change: $\nu = 4 \pm 1$ (4.6.23).

This result does not necessarily contradict the results on the position of the border of stochasticity in Fig. 4.6.4. The point is that the conditions for the appearance of stochasticity are determined in reality by the energy of the interacting modes[168] and not only the total energy, as assumed for the sake of simplicity above (4.6.12). Therefore, firstly, the energy cannot extend to a large number of modes and, secondly, the energy of

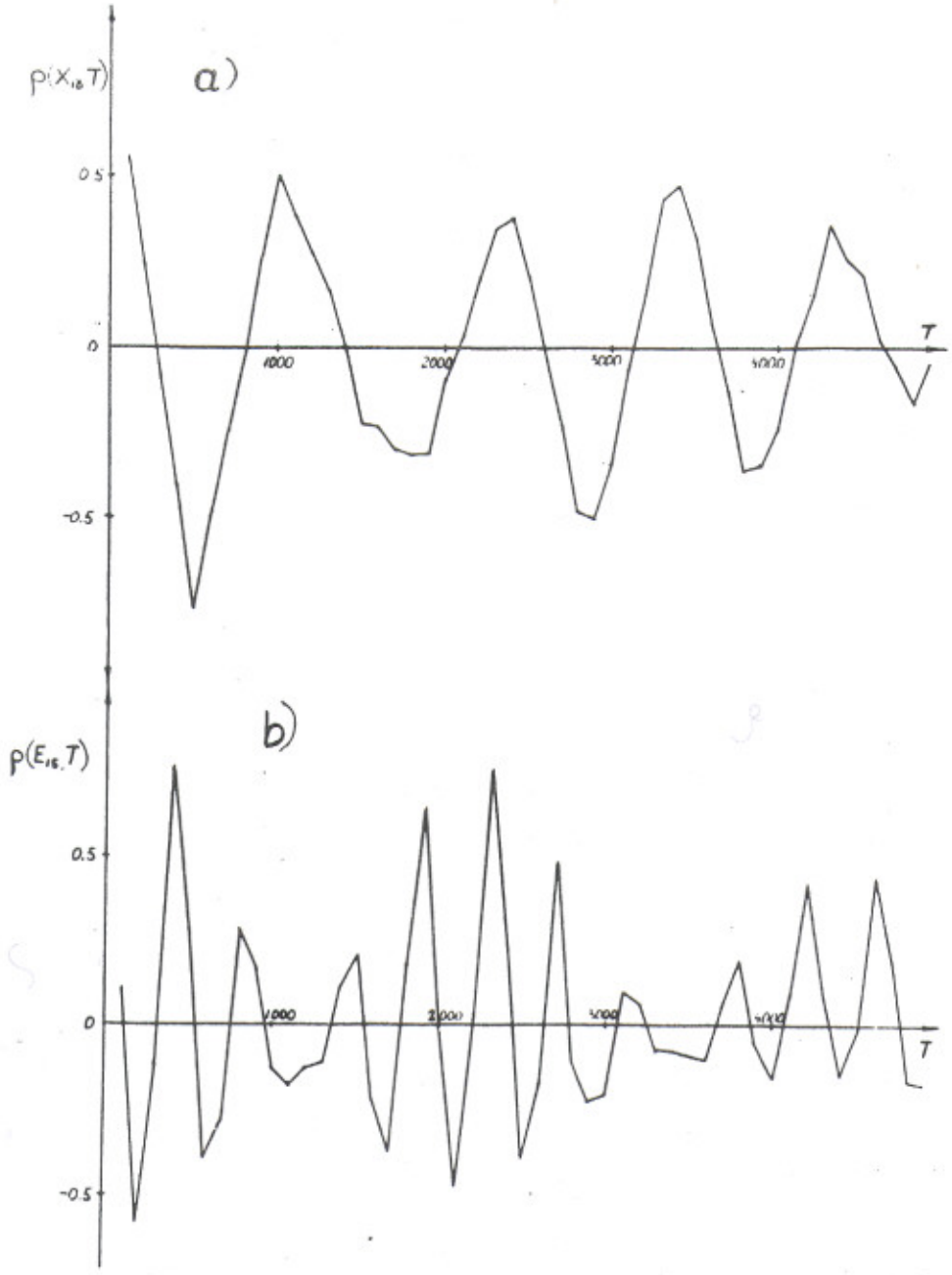

Fig. 4.6.5 Correlations for case II in Fig. 4.6.4 with symmetrization: $E \approx 17$; $\beta \approx 0.0314$; $\varepsilon \approx 0.05$; $t_{max} \approx 18300$; $\Delta T = 100$; $\Delta t = 1$; $h \approx 1/3$; $\Delta E/E \approx 3\%$; $\rho(E_{15}, E_{17}) = -(0.30 \pm 0.07)$.

each mode cannot decrease considerably near the border of stochasticity, since the stochasticity conditions are also destroyed. This means that only a partial energy exchange between modes is possible, which in its turn leads to the residual correlations.

If, however, one takes $\beta \gg \beta_{cr}$ we should already obtain "true" stochasticity. The second control computation exactly corresponds to $\beta/\beta_{cr} \approx 28$ (Fig. 4.6.6). Here the energy

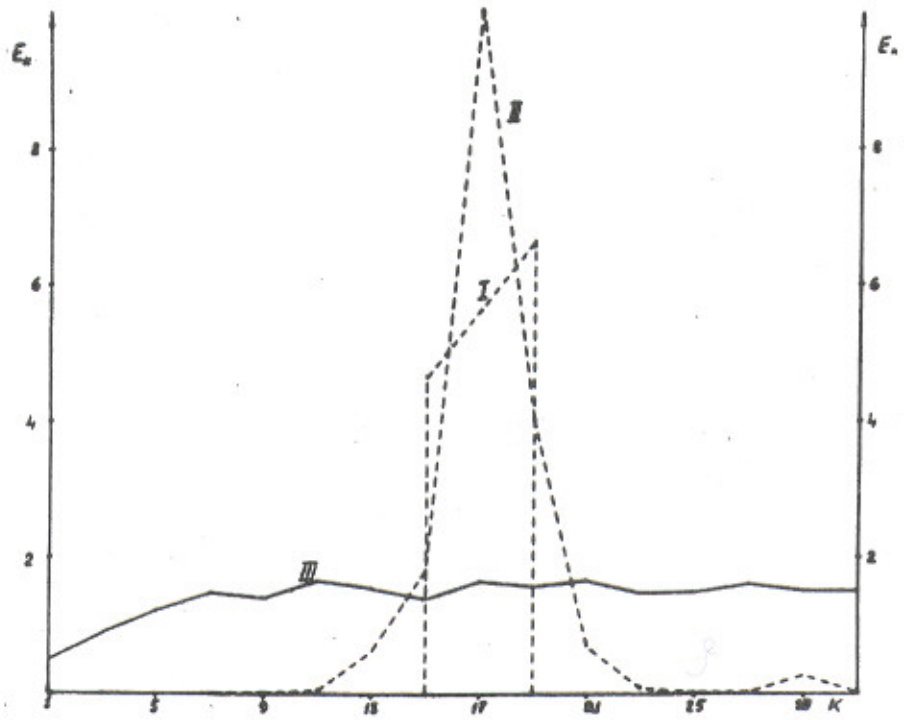

Fig. 4.6.6 Energy spectrum for initial excitation of three modes (k_0 = 15, 17, 19) with symmetrization (curve I); curve II corresponds to the mean energies of the modes for the results given in Fig. 4.6.5; curve III for the results given in Fig. 4.6.7.

in fact spreads between almost all the modes, excepting only the lowest, for which it is difficult to satisfy the stochasticity criterion. This result is also confirmed by the value $\rho(E_{15}, E_{17})$ (Fig. 4.6.7). On account of the large experimental error, only the lower limit can be estimated for the number of interacting modes: $\nu > 8$. From the results in Fig. 4.6.7 it can also be seen that within the limits of statistical error (±0.1) the correlations of the 15th mode are absent. With regard to the x correlatious, they are connected mainly with the fact that stochasticity does not reach the first mode. It is interesting to note that the correlations slowly fade. It is not out of the question that this is in some way due to the influence of computation errors (see below) but in that case why is there no fading in Fig. 4.6.5? Another possible explanation is that the motion of the first mode, responsible for the x correlations, is nevertheless stochastic but for a considerably longer time, since this mode lies in the transitional zone.

To sum up, it can be said that the totality of the experimental results confirm the hypothesis put forward in Ref. 168 concerning the presence of a border of stochasticity for system (4.6.1) and, moreover, confirm the order of magnitude of estimate (4.6.12) for the position of this border. The weakest point is the substantial computation errors,

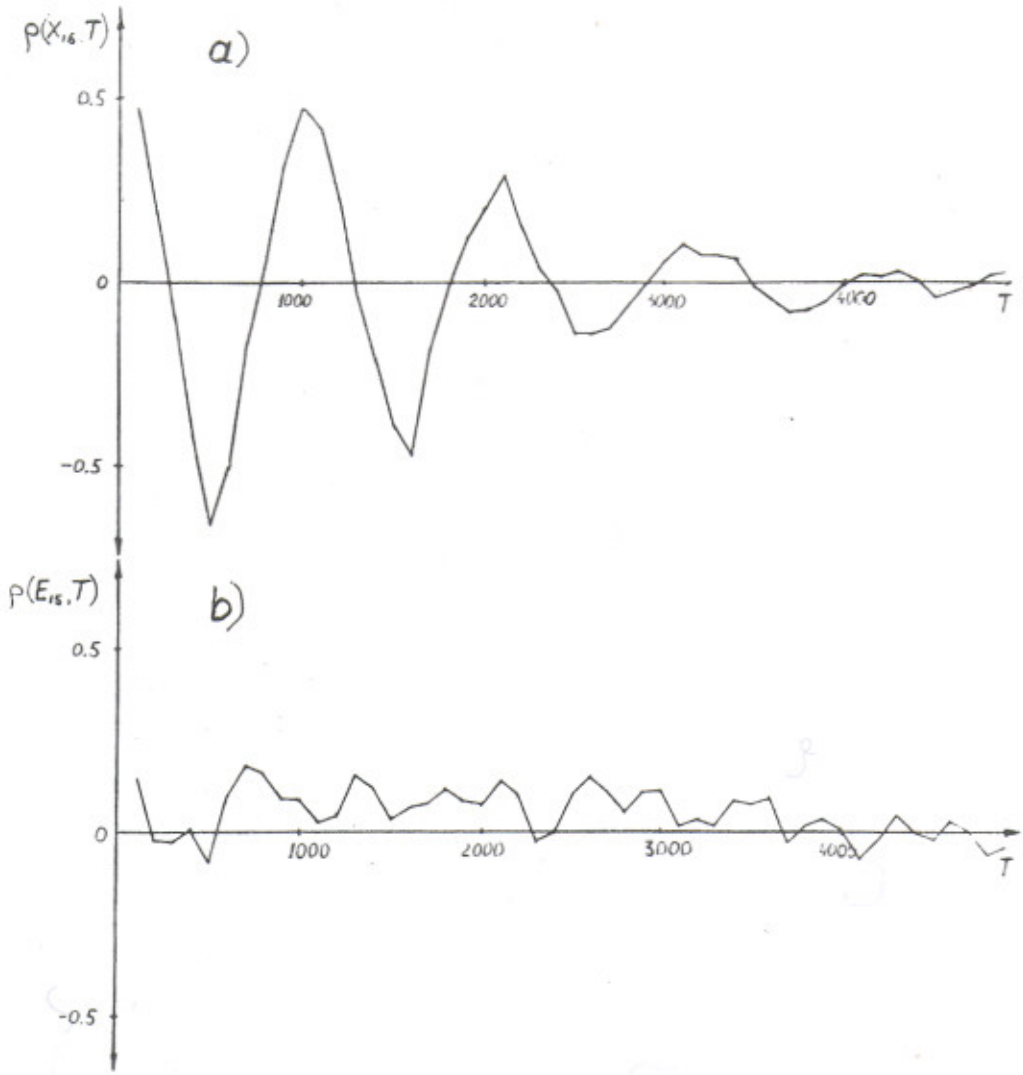

Fig. 4.6.7 Correlations for case II in Fig. 4.6.4 with symmetrization:
$E \approx 24$; $\beta \approx 0.314$; $\varepsilon \approx 0.75$; $t_{max} \approx 16050$; $\Delta T = 100$; $\Delta t = 1$;
$h \approx 1/6$; $\Delta E/E \approx 2\%$; $\rho(E_{15}, E_{17}) = -(0\text{-}0.13)$.

which were checked by variation of the total energy of the system (see captions to figures). This particularly concerns the above-mentioned check experiments, where $\Delta E/E$ reaches 3%. Can these errors by themselves produce stochasticity? We think not. This is confirmed by the considerable residual correlations (Fig. 4.6.5) and the absence of energy exchange (Fig. 4.6.6) for small β. Another check on the influence of the errors was carried out for the experiment with local instability. When the integration step was reduced by a factor of two $\Delta E/E$ decreased from 3% to 0.03%, and the curves of the exponential growth of the even modes changed slightly, but the value of the parameter of interest to us $1/\tau$ remained as before within the limits of experimental error.

Nevertheless it seems to us useful to continue numerical experimentation with a non-linear chain, with a higher accuracy, and with a larger number of oscillators.

Recently Hirooka and Saito carried out similar experiments with a two-dimensional lattice with cubic non-linearity, and also obtained a border of stochasticity[170]. In fact, they also used the local instability method, measuring the duration (T) of the "induction period" in the development of instability. An example of this phenomenon is given in Fig. 4.6.2 and its mechanism is explained in the text. The quantity 1/T is proportional to the K-entropy h. It turned out that the dependence $h(\beta)$ is nearly linear: $h \propto (\beta - \beta_{cr})$. It can probably be compared to the "typical" estimate (2.11.3): $h \propto \beta^{4/3} (\beta >> \beta_{cr})$. Let us note that the computing accuracy in Ref. 170 was very high ($\Delta E/E \approx 0.01\%$).

A more thorough analytical investigation of the stochasticity of non-linear waves is reported in papers by Zaslavsky, Sagdeev and Filonenko[104,105,150].

4.7 Pseudo-random number generators

The problem in this final section is essentially different from the other applications of the theory developed that are described above. Here we shall try not so much to investigate the statistical properties of any practical dynamical system as to construct the simplest system simulating a "random" process. The need for such simulation arises in many cases, but perhaps most of all when using the so-called Monte Carlo method (statistical test method) proposed by Metropolis and Ulam (see Ref. 95)*). The idea of this method is to abandon, in research into the kinetics of molecular processes, the equations in partial derivatives, approximating this kinetics which are very inconvenient to solve in a computer, and to go back to dynamical molecular processes. Of course, a complete return to the solution of exact dynamical equations for all molecules is absolutely impossible, but one can choose an intermediate, coarse dynamical model with a relatively small number of particles, which nevertheless reproduces the properties of the original system relatively well. In particular, the "random" element itself of the motion of a molecular system is not obtained automatically by the dynamical equations and is introduced artificially from outside by means of so-called random number generators. These generators can also be of a physical nature, for example radioactive decay or electrical noise. In this case the term random number can be used without inverted commas, if we believe that "true" randomness exists in nature**).

From the practical point of view, however, a generator using a certain computing algorithm in the computer itself is considerably more convenient. In this case one is already obliged to put the word "random" (number) in inverted commas or substitute the word pseudo-random. The point is that the axiomatic (empirical) definition of a random sequence carries a requirement for so-called "irregularity", i.e. the absence of the

---

*) Of the other problems let us mention the computation of many-dimensional integrals[95], and stochastic cybernetic machines[130].

**) To avoid misunderstanding it should be recalled that we are speaking only of statistical physics. In particular, quantum randomness may be of a completely different nature and does not have any direct bearing here (see Section 2.13).

algorithms for obtaining a sequence. It is evident that this requirement can be verified only in a negative sense, i.e. it is in a certain sense unobservable. So it is evident that in the present case of algorithmic pseudo-random generators it is not satisfied by definition. However, according to all the other criteria the pseudo-random numbers are in no way different from "true" random numbers (see Ref. 95 and below). According to the ideas developed in this paper, this is the result not so much of the fact that so far no effective method of verifying "randomness" has been found, as the fact that in nature there is no "irregularity" (Section 2.13). Moreover, if one chooses as an algorithm, for example, a transformation describing a stochastic dynamical system, one can assert that such an algorithm will in a sense be the best random number generator. The point is that very often we do not know exactly which properties of random numbers are important in one or another specific problem. Under these conditions it appears wisest to follow nature, i.e. to obtain random numbers by means of the stochastic dynamical process. From the point of view of the Monte Carlo method this will be one more step in the same direction of a return to molecular dynamics.

For such simulation there is apparently no need to use a Hamiltonian system, it is sufficient to take the simplest ergodic transformation with mixing and K-entropy, for example (see Section 2.3):

$$x_{n+1} = \{k x_n\} \tag{4.7.1}$$

This is in fact probably the simplest transformation of this type. The corresponding transformation in integers is written in the form:

$$r_{n+1} \equiv k r_n \pmod{2^p} \tag{4.7.2}$$

Among others, such a random number generator was devised by Lehmer as long ago as 1951[132], two years after the appearance of the Monte Carlo method. However, if this generator was so far distinguishable from a series of others, it was only because of the drawback it involves due to the multiplication operation, which consumes a relatively large amount of computer time.

Although the transformation for real numbers (4.7.1) has been fully investigated analytically (Section 2.3) the transition to integers in the computer (4.7.2) may lead to the appearance of anomalies, since the theorems of the ergodic theory are valid, except the set of zero measure. A well-known example of such anomalies is the existence of a period of pseudo-random sequence. However, finer violations of statistical properties are also possible. Therefore it is necessary to verify the generator (4.7.2). Such checking has already been reported in a series of papers[95]. Below we give some results of a further test in which the unique facilities of the BESM-6 were used. The checking was carried out in co-operation with Israelev and Antipov[188].

According to Ref. 135 the maximum period (2^{p-2}) of sequence (4.7.2) is reached for:

$$k \equiv 3;\ 5 \pmod 8; \tag{4.7.3}$$

r_0 is uneven), and the pair correlation coefficient of neighbouring pseudo-random numbers is[136]:

$$\rho \approx \frac{1}{k} \tag{4.7.4}$$

Since integral multiplication modulo 2^p by k and $(k - 2^p)$ is equivalent, for $k \gtrsim 2^{p-1}$ the correlations will increase as compared to (4.7.4). According to Ref. 136 an increase of the correlations is possible even for $k > 2^{p/2}$ depending on the specific value of k.

In order to test the quality of the pseudo-random sequence the following generator parameters were chosen (in octal representation of a BESM-6 word):

$$\begin{aligned} \langle k \rangle &: 4013064256500425 : \\ \langle r_0 \rangle &: 4013543660414035 : \end{aligned} \qquad \frac{k}{2^p} \approx \frac{11}{16} \tag{4.7.5}$$

Accurate parameter values are unimportant when the conditions in (4.7.3) are satisfied. Even a very "round" constant <k>: 4000000000200003 does not impair the statistical properties of the generator. Let us note that this is apparently not always so[137]. Therefore it is better to choose "non-round" parameters (4.7.5).

Three tests were used: uniformity (16384 bins); pair correlations r_{n+1}, r_n (128 × 128 bins) and 14-fold correlations of neighbouring numbers by one binary digit ($2 \times 2 \ldots = 2^{14}$ bins).

The main results are given in Table 4.7.1. The randomness criterion for all three methods was the deviation from uniform distribution in the whole array of $2^{14} = 16384$ bins. The deviation characteristic is the ratio of the dispersion (D) to the mean value (M) of the amount of pseudo-random numbers in one bin. The expected value of the ratio for a random sequence is (with a confidence of 95%):

$$\frac{D}{M} = 1.0 \pm 0{,}022 \tag{4.7.6}$$

Table 4.7.1 also gives the values $\sqrt{D}/M$ of the statistical accuracy of the test.

As an additional test of the statistical properties a count was made of the number of empty bins of the array of 512 × 1024 for pair correlations. The array is logical and each element occupies one binary digit (compare Section 3.2). The results are given in Table 4.7.2, where m and m_{theor} are the actual and the expected number of empty bins in the array.

Table 4.7.1

	N	10^3	10^4	10^5	10^6	10^7	10^8
Uniformity	$\sqrt{\mathcal{D}}/M$ %	405	128	40	13	4.0	1.3
	$\mathcal{D}/M$	1.003	1.003	1.003	1.006	1.000	0.977
	$\bar{m}$	15415	8911	27	0	0	0
Pair correlations	$\sqrt{\mathcal{D}}/M$ %	407	128	40	13	4.0	1.3
	$\mathcal{D}/M$	1.013	1.000	0.998	0.983	0.987	1.004
	$\bar{m}$	15420	8905	38	0	0	0

Table 4.7.2

	N	10^3	10^4	10^5	10^6	10^7
Pair correlations	$\bar{m}$	523288	514376	433175	77852	0
	$\bar{m}_{Teor}$	522700 ± 700	514300 ± 700	433600 ± 650	78000 ± 280	0

Table 4.7.3

	N	10^3	10^4	10^5	10^6	10^7	10^8
1st digit	$\sqrt{\mathcal{D}}/M$ %	412	127	41	13	4.0	1.3
	$\mathcal{D}/M$	1.037	0.982	1.008	0.997	0.974	1.002
	$\bar{m}$	15431	8848	31	0	0	0
14th digit	$\sqrt{\mathcal{D}}/M$ %	414	128	41	13	4.0	1.3
	$\mathcal{D}/M$	1.045	1.006	1.013	0.994	0.989	1.008
	$\bar{m}$	15431	8889	33	0	0	0

Table 4.7.3 gives the results of the test of the statistical properties for the 14-fold correlations of the first and 14th binary digits. In order to increase the period in the latter case perturbation of the constant k was applied (4.7.7).

Finally, for the pair correlations a secondary distribution of the deviations from the mean value was plotted, which is a finer method of checking statistical properties. The random quantity here is the deviation of the number of entries into a bin of the

two-dimensional array from the mean value, normalized by the square root of dispersion. The distribution was plotted in the interval (-4, 4) divided into 128 bins. A graph of the distribution obtained and a comparison with the Gaussian curve are given in Fig. 4.7.1. The dispersion of the points is due to two reasons: the statistical dispersion of ±5%, which agrees well with the majority of points in the diagram, and the dispersion due to the integral nature of the random quantity. The minimum value of the random quantity is approximately 1/5 of the size of a distribution bin, which may cause an oscillation of ±20%.

To sum up, it can be said that in none of the tests both ours and those of other writers, was any deviation of the properties of the sequence (4.7.2) form the random observed. With regard to the length of the period, there are several ways of increasing it. One was proposed by Sobol[138]) and uses perturbation of the constant k in (4.7.2) during L steps:

$$k_{\ell+1} \equiv k_\ell + C \pmod{2^P} \tag{4.7.7}$$

where C = 8 is the minimum constant, for which $k_\ell \equiv 3 \pmod 8$ for all ℓ. According to Ref. 138 the period is then increased by $\sqrt{L}$ times

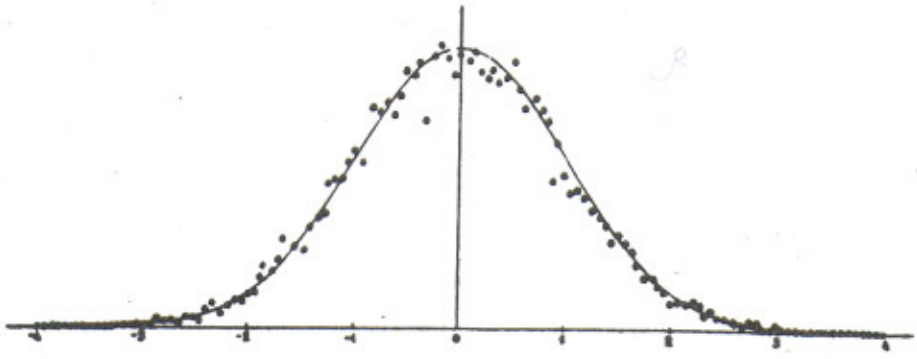

Fig. 4.7.1

Another method uses more complex generators, for example of the type of the elementary model (2.4.16) with a linear function of $f(\psi) = \psi - \frac{1}{2}$. In this case in order to start repetition of the pseudo-random sequence it is necessary to have exact coincidence of the two numbers φ, ψ with one of the previous pairs (φ, ψ).

Another problem is connected with the choice of the initial value of r_0 (4.7.2), especially for multiple calls of the generator. Here again it is important to exclude exact coincidence of the initial conditions for two calls. Apparently the best method is to give r_0 from another more complex generator with a practically infinite period, and this latter should operate continuously, never returning to its initial conditions.

Another approach to solving the problem of the arithmetical simulation of random processes was developed by Postnikov[24,33]. He also rejects the requirement for irregularity of the sequence, replacing it with a requirement for completely uniform distribution, i.e. the absence of correlations of any multiplicity (see Section 2.3). From our point of view this requirement is not sufficient for good simulation of the random process, since it does not guarantee the positive K-entropy of the process (Section 2.3), and if the K-entropy is equal to zero, the mixing may run very slowly and non-uniformly, which in a practical respect is not permissible.

A specific problem of the study of pseudo-random number generators is the accumulation of round-off errors in computation. This problem can be split into two. The first part (the over-all error accumulation) is connected with the dynamical computing algorithm, mainly with its stability. For example, when computing the trajectory of a stochastic system the errors grow exponentially with time. The second part of the problem -- local (in time) accumulation of errors -- is determined by the round-off process. As already noted in Section 3.3 this process is equivalent to the work of a pseudo-random number generator, the algorithm of which is determined by the computation algorithm. The distinctive feature of the error accumulation process lies in the fact that the mean error (drift) is generally speaking not equal to zero. Therefore the main problem is to find this drift. If it is equal to zero, for example from the symmetry condition of the computation algorithm, then we have exactly the pseudo-random number generator. In particular, if the computation algorithm contains multiplication by a constant, then the generator is "good", as shown above, and the round-off errors accumulate according to a random law. Examples of random and non-random accumulation of errors are given in Section 3.3.

It can be hoped that the detailed study of such "round-off" generators will finally enable us to obtain the reliable estimates of computation errors which are so desirable for work with a computer.

REFERENCES

1) G. Goldstein, Classical mechanics.

2) V.M. Volosov, Doklady Akad. Nauk SSSR 121, 22 (1958).

3) N.N. Bogolyubov and Yu.A. Mitropolsky, Asymptotic methods in non-linear oscillation theory (Fizmatgiz, 1958).

4) Yu.F. Orlov, Zh. Eksper. Teor. Fiz. 32, 316 (1957).

5) A.A. Kolomensky and A.N. Lebedev, Theory of cyclic accelerators (Fizmatgiz, 1962).

6) B.V. Chirikov, Dokl. Akad. Nauk SSSR 125, 1015 (1959).

7) V.I. Veksler, Dokl. Akad. Nauk SSSR 43, 346; 44, 393 (1944).

8) E.M. McMillan, Phys. Rev. 68, 143 (1945).

9) P.A. Sturrock, Ann. Phys. (USA) 3, 113 (1958).

10) B.V. Chirikov, Atomnaya Energiya 6, 630 (1959).

11) K. Symon and A. Sessler, Proc. CERN Symposium 1956 (CERN, Geneva, 1956), vol. 1, p. 44.

12) H. Weyl, Math. Annalen 77, 313 (1916).

13) Ya.S. Derbenev, S.I. Mishnev and A.N. Skrinsky, Atomnaya Energiya 20, 217 (1966).

14) A. Schoch, CERN 57-21 (1958).

15) E.L. Burstein and L.S. Solov'ev, Dokl. Akad. Nauk SSSR 139, 855 (1961).

16) D.D. Birkhoff, Dynamical systems.

17) Ya.G. Sinai, Izv. Akad. Nauk Mat. 30, 15 (1966).

18) M. Kruskal, Asymptotic theory of Hamiltonian and other systems with all solutions nearly periodic, Conference of Plasma Physics and Controlled Nuclear Fusion Research, Salzburg, 1961.

19) A.N. Kolmogorov, Dokl. Akad. Nauk SSSR 98, 527 (1954).

20) V.I. Arnold, Uspekhi Mat. Nauk 18, No. 6, 91 (1963).

21) V.I. Arnold, Dokl. Akad. Nauk SSSR 156, 9 (1964).

22) V.A. Rokhlin, Izv. Akad. Nauk Mat. 25, 499 (1961).

23) N.M. Korobov, Izv. Akad. Nauk Mat. 14, 215 (1950).

24) A.G. Postnikov, Arithmetical simulation of random processes, Proceedings of the V.A. Steklov Mathematical Institute, LVII, 1960.

25) A.N. Kolmogorov, Dokl. Akad. Nauk SSSR 119, 861 (1958).

26) P.R. Halmos, Lectures on ergodic theory, The Mathematical Society of Japan, Tokyo, 1956.

27) L.D. Landau and E.M. Lifshits, Statisticheskaya Fizika (Gostekhizdat, 1951).

28) J. Moser, A rapidly convergent iteration method and non-linear differential equations, II, Annali della Scuola Normale Superiore di Pisa, Serie III, vol. XX, Fasc. III, 1966.

29) E. Hopf, Statistik der geodätischen Linien in Mannigfaltigkeiten negativer Krümmung, Ber. Verh. Sächs. Akad. Wiss. Leipzig 91, 261 (1939).

30) N.S. Krylov, Papers on foundation of statistical physics, Izd. Akad. Nauk SSSR, 1950.

31) D.V. Anosov, Dokl. Akad. Nauk SSSR 145, 707 (1962); 151, 1250 (1963).

32) G.V. Chester, The theory of irreversible processes, Rep. Progr. Phys. 26, 411 (1963).

33) A.G. Postnikov, Ergodic questions in the congruence theory and the diophantine approximation theory, Proceedings of the V.A. Steklov Mathematical Institute, LXXXII, 1966.

34) Ya.G. Sinai, Probability notions in ergodic theory, Proceedings of the International Congress of Mathematicians, 1962.

35) G. Hedlund, Bull. Amer. Math. Soc. 45, 241 (1939).

36) H. Poincaré, Les méthodes nouvelles de la mécanique céleste, vols. I, II, III (Paris, 1892, 1893, 1899).

37) V.K. Mel'nikov, Dokl. Akad. Nauk SSSR 139, 31 (1961); 142, 542 (1962); 148, 1257 (1963).

38) N.N. Filonenko, R.Z. Sagdeev and G.M. Zaslavsky, Nuclear Fusion 7, 253 (1967).

39) A.N. Kolmogorov, General theory of dynamical systems and Classical Mechanics, International Mathematical Congress in Amsterdam, 1954 (reports) (Fizmatgiz, 1961).

40) Ya. G. Sinai, Izv. Akad. Nauk Mat. 30, 1275 (1966).

41) V.A. Rokhlin, Uspekhi Mat. Nauk 22, No. 5, 3 (1967).

42) D.V. Anosov and Ya. G. Sinai, ibid. p. 107.

43) S. Chandrasekhar, Stochastic problems in physics and astronomy, Rev. Mod. Phys. 15, 1 (1943).

44) A.N. Kolmogorov, Uspekhi Mat. Nauk, No. 5, 5 (1938).

45) A.M. Dykhne and A.V. Chaplik, Zh. Eksper. Teor. Fiz 40, 666 (1961).

46) M.N. Rosenbluth, R.Z. Sagdeev, J.B. Taylor and G.M. Zaslavsky, Nuclear Fusion 6, 297 (1966).

47) J.M. Greene, J. Math. Phys. 9, 760 (1968).

48) J. Ford, Phys. Rev. 188, 416 (1969).

49) I. Prigogine, Non-equilibrium statistical mechanics (New York - London, 1962).

50) H. Grad, Levels of descriptions in statistical mechanics and thermodynamics, Report on Delaware Seminar on the Foundations of physics, 1967.

51) M.A. Leontovich, Zh. Eksper. Teor. Fiz. 5, 211 (1935).

52) Ya. G. Sinai, Funktsional'ny Analiz 2, 64, 70 (1968).

53) P.G. Saffman, Proc. Roy. Soc. 299, 101 (1967).

54) N.N. Bogolyubov, Problems of dynamical theory in statistical physics (Gostekhizdat, 1946).

55) K.P. Gurov, Fundamentals of kinetic theory (N.N. Bogolyubov's Method) (Nauka, 1966).

56) A.A. Vedenov, E.P. Velikov and R.Z. Sagdeev, Uspekhi Fiz. Nauk 73, 701 (1961); Nuclear Fusion 1, 82 (1961).

57) Yu.L. Klimontovich, Statistical theory of non-equilibrium processes in plasma (MGU, 1964).

58) S.L. Sobolev, Mathematical physics equations (Nauka, 1966).

59) M.M. Lavrent'ev, On the formulation of some improper problems in mathematical physics, Collection: Nekotorye voprosy vychislitel'noj matematiki (Nauka, Novosibirsk, 1966).

60) A.N. Tikhonov, Dokl. Akad. Nauk SSSR 153, 49 (1963).

61) E. Schroedinger, Preuss. Akad. Wiss., Berlin 9, 144 (1931).

62) A.N. Kolmogorov, Math. Ann. 113, 766 (1937).

63) G. Sandri, Ann. Phys. (USA) 24, 332, 380 (1963).

64) Yu. L. Klimontovich and Yu. A. Kukharenko, Fiz. Metal. Metalloved 19, 161 (1965).

65) S.T. Belyaev, Kinetic equation for rarefied gases in strong fields, Collection: Fizika Plazmy i problema uprovlyaemykh termoyadernykh reaktsij, vol. III, p. 50 (1958).

66) L.D. Landau, Zh. Eksper. Teor. Fiz. 7, 203 (1937).

67) Ya.I. Frenkel, Statisticheskaya Fizika (Moscow - Leningrad) (1948).

68) V.M. Alekseev, Dokl. Akad. Nauk SSSR 177, 495 (1967).

69) R. Balescu, Physica 36, 433 (1967).

70) L. Brillouin, Scientific uncertainty and information (Academic Press, New York and London, 1964).

71) N.N. Bogolyubov, On some statistical methods in mathematical physics (Akad. Nauk SSSR, 1945).

72) M. Kac, Statistical independence in probability, analysis and number theory (The Mathematical Association of America, 1959).

73) M. Kac, A few stochastic problems of physics and mathematics (Nauka, 1967).

74) F.G. Bass, Ya.B. Feinberg and V.D. Shapiro, Zh. Eksper. Teor. Fiz. 49, 329 (1965).

75) E. Madelung, Die mathematischen Hilfsmittel des Physikers (Springer-Verlag, Berlin, 1957).

76) B. Chirikov, E. Keil and A. Sessler, Stochasticity in many-dimensional non-linear oscillating systems, CERN Internal Report ISR-TH/69-59 (1969).

77) V.I. Arnold, Dokl. Akad. Nauk SSSR 137, 255 (1961).

78) J. Moser, On the theory of quasiperiodic motions, SIAM Rev. 8, 145 (1966).

79) V.I. Arnold, The problem of stability and ergodic properties of classical dynamical systems, Report of International Congress of Mathematicians, Moscow, 1966.

80) G.I. Budker, Uspekhi Fiz. Nauk, 89, 533 (1966).

81) G. Gibson, W. Jordan and E. Lauer, Phys. of Fluids, 6, 116, 133 (1963).

82) A.N. Dubinina and L.S. Krasitskaya, Zh. Eksper. Teor. Fiz. Pis'ma, 5, 230 (1967); A.N. Dubinina and Yu. N. Yudin, Zh. Eksper. Teor. Fiz. 53, 1206 (1967).

83) V.G. Ponomarenko, L. Ya. Trajnin, V.I. Yurchenko and A.N. Yasnetsky, Zh. Eksper. Teor. Fiz. 55, 3 (1968).

84) A.A. Andronov and L.S. Pontryagin, Dokl. Akad. Nauk SSSR 14, 247 (1937).

85) A.A. Andronov, A.A. Vitt and S.E. Khajkin, Oscillation theory (Fizmatgiz, 1959).

86) W.B. Riley, Electronics, No. 10, 141 (1967).

87) E.V. Evreinov and Yu. G. Kosarev, Izv. Akad. Nauk SSSR, tekhn. kibern., No. 4, 3 (1963).

88) Yu. M. Voloshin, A.P. Ershov and G.I. Kozhukhin, Input language for programming automation systems, Izd. SO Akad. Nauk SSSR, 1964.

89) B.V. Chirikov, Dokl. Akad. Nauk SSSR 174, 1313 (1967).

90) B.V. Chirikov, When does the dynamical system turn into the statistical one? Communication at International Congress of Mathematicians, Moscow, 1966.

91) L.J. Laslett, A computational investigation of a non-linear algebraic transformation, 1967 (unpublished).

92) M. Hénon and C. Heiles, Astron. J. 69, 73 (1964).

93) S.M. Ulam, A collection of mathematical problems, Los Alamos Scientific Laboratories, New Mexico.

94) N.J. Zabusky, A synergetic approach to problems of non-linear dispersive wave propagation and interaction, University of Delaware, 1965.

95) N.P. Buslenko, D.I. Golenko, I.M. Sobol, V.G. Sragovich and Yu.A. Schreider. Statistical test method (Monte Carlo Method) (Fizmatgiz, 1967).

96) D.I. Golenko, Simulation and statistical analysis of pseudo-random numbers in computers (Fizmatgiz, 1965).

97) E. Courant, IEEE Trans. Nuclear Sci. NS-12, No. 3, 550 (1965).

98) M.G.N. Hine, private communication, 1967.

99) E. Fermi, Phys. Rev. 75, 1169 (1949).

100) E.L. Burstein, V.I. Veksler and A.A. Kolomensky, The stochastic method of particle acceleration, Collection: Nekotorye Voprosy teorii tsiklicheskykh uskoritelej (Akad. Nauk SSSR, 1955).

101) V.N. Tsytovich, Statistical acceleration of particles in Plasma, Tr. Fiz. Inst. Akad. Nauk SSSR 32, 130 (1966).

102) S. Ulam, Proc. 4th Berkeley Symposium on Mathematical Statistics and Probability, 1961, vol 3, p. 315;

103) G.M. Zaslavsky and B.V. Chirikov, Dokl. Akad. Nauk SSSR 159, 306 (1964).

104) G.M. Zaslavsky and R.Z. Sagdeev, Zh. Eksper. Teor. Fiz. 52, 1083 (1967).

105) G.M. Zaslavsky and N.N. Filonenko, Zh. Eksper. Teor. Fiz. 54, 1590 (1968).

106) Ya. G. Sinai, Dokl. Akad. Nauk SSSR 153, 1261 (1963).

107) V.I. Volosov and A.I. Komin, Zh. Tekh. Fiz. 38, No. 5, 846 (1968).

108) V.N. Bocharov, V.I. Volosov, A.V. Komin, V.M. Panasyuk and Yu.N. Yudin, Confinement of plasma in a stellarator under different values of mean free path, Fusion III, D-7 (Novosibirsk, 1968).

109) C.J.H. Watson, The thermonuclear prospects of various confinement schemes, Preprint, Culham Lab., 1968.

110) A.P. Popryadukhin, Atomnaya Energiya 18, 96 (1965).

111) D.K. Akulina, G.M. Batanov, M.S. Berezhetsky, S.E. Grebenshchikov, M.S. Rabinovich, I.S. Sbitnikova and I.S. Spiegel, External injection and confinement of plasma in a stellarator with a double helical field, II, CN-21/244 (Culham, 1965).

112) G.V. Skornyakov, Zh. Tekh. Fiz. 32, 261, 777 (1962).

113) L.M. Kovrizhnykh, Zh. Tekh. Fiz. 32, 526 (1962).

114) F.K. Goward, Lectures on the theory and design of an alternating-gradient-proton synchrotron, CERN, Geneva, October 1953;
M.G.N. Hine, ibid.

115) A.I. Morosov and L.S. Solov'ev, Magnetic field geometry, Voprosy teorii plazmy, Issue 2 (Gosatomizdat, 1963).

116) A. Gibson, Phys. of Fluids 10, 1553 (1967).

117) G.I. Budker, Thermonuclear reactions in a system with magnetic mirrors: Concerning the question of the direct conversion of nuclear energy into electrical power, Collection: Fizika Plazmy i problema upravlyaemykh termoyadernykh reaktsii, Vol. III, p. 3, 1958.

118) O.B. Firsov, Repulsion of a charged particle from a region with a strong magnetic field (On the accuracy of the adiabatic invariant), ibid., Vol. III, p. 259, 1958.

119) A.A. Andronov, M.A. Leontovich and L.I. Mandelstam, Zh. Russ. Fiz.-Khim. Obshch. 60, 413 (1928).

120) V.I. Arnold, Dokl. Akad. Nauk SSSR 142, 758 (1962).

121) S.N. Rodionov, Atomnaya Energiya 6, 623 (1959).

122) G. Gibson, W. Jordan and E. Lauer, Phys. Rev. Letters 5, 141 (1960).

123) A. Garren et al., Proc. 2nd Int. Conf. Peaceful Uses of Atomic Energy (1958), Vol. 31, p. 65.

124) R.J. Hastie, G.D. Hobbs and J.B. Taylor, Non-adiabatic behaviour of particles in inhomogeneous magnetic fields, Fusion III, C-6, (Novosibirsk, 1968).

125) Report on the design study of intersecting storage rings for the CERN PS, CERN, 1964.

126) G.I. Budker, Atomnaya Energiya 22, 346 (1967).

127) Proposal for a high-energy electron-positron colliding beam storage ring at the SLAC, 1966.

128) R.S. Mulliken, Spectroscopy, molecular orbitals, and chemical bonding, Nobel Lecture.

129) A. Poincaré, Lectures on celestial mechanics (Nauka, 1965).

130) S. Beer, Cybernetics and management (London, 1959).

131) V. Balbekov and N. Semashko, Nuclear Fusion 7, 207 (1967).

132) D.H. Lehmer, Annals Comp. Laboratory, Harvard University 26, 141 (1951).

133) G.N. Kulipanov, S.I. Mishnev, S.G. Popov and G.M. Tumajkin, Experimental research into the effects of beam interactions in storage rings, Report at the All-Union Accelerator Conference, Moscow, 1968.

134) V.L. Auslender, G.N. Kulipanov, S.I. Mishnev, A.A. Naumov, S.G. Popov, A.N. Skrinsky and G.M. Tumajkin, Atomnaya Energiya 20, 213 (1966).

135) E. Bofinger and V. Bofinger, J. Assoc. Comp. Mach. 10, 131 (1963).

136) M. Greenberger, ibid. 8, 163 (1961).

137) J. Allard, A. Dobell and T. Hull, ibid. 10, 131 (1963).

138) I.M. Sobol, The theory of probability and its applications 9, 367 (1964).

139) G.A. Chebotarev, Analytical and numerical methods in celestial mechanics (Nauka, 1965).

140) A.M. Molchanov, Dokl. Akad. Nauk SSSR 168, 284 (1966); Collection: Problemy dvizheniya iskustvenykh nebesnykh tel, Akad. Nauk SSSR, 1963, p. 42.

141) O.Yu. Schmidt, Four lectures on the theory of the earth's origin, 1949.

142) An. M. Leontovich, Doklady Akad. Nauk SSSR 143, 525 (1962).

143) L.D. Landau and E.M. Lifshits, Mekhanika (Fizmatgiz, 1958).

144) M.L. Lidov, Collection: Problemy dvizheniya iskustvenykh nebesnykh tel, Akad. Nauk SSSR, 1963, p. 119.

145) E.V. Spolsky, Atomnaya Fizika, vol. II (Gostekhizdat, 1950).

146) V.F. Weisskopf, Phys. Today 14, No. 7, 18 (1961).

147) I.I. Putilin, Malye Planety (Gostekhizdat, 1953).

148) K. Hirayama, Ann. Tokyo Astron. Obs. No. 4, 1918.

149) Efemeridy malykh planet (ezhegodnik), 1965.

150) G.M. Zaslavsky, Statistical irreversibility in non-linear systems (Nauka, 1970).

151) D. Brouwer, Astron. J. 68, 152 (1963).

152) J. Moser, Commun. Pure Appl. Math. 8, 409 (1955).

153) L.D. Landau, Phys. Z. Sowjet. 10, 67 (1936).

154) L.S. Kassel, Kinetics of homogeneous reactions (1937).

155) N.B. Slater, Theory of unimolecular reactions (London, 1959).

156) D.L. Bunker, J. Chem. Phys. 40, 1946 (1964).

157) Ya.B. Zel'dovich and I.D. Novikov, Relativistic astrophysics (Nauka, 1967).

158) L.D. Landau and E.M. Lifshits, Field theory (Fizmatgiz, 1960).

159) E.M. Lifshits, V.V. Sudakov and L.M. Khalatnikov, Zh. Eksper. Teor. Fiz. 40, 1847 (1961).

160) L.B. Okun, Uspekhi Fiz. Nauk 95, 402 (1968).

161) Ta You-Wu, Kinetic equations of gases and plasmas, 1966.

162) G. Ludwig, Z. Phys. 135, 483 (1953).

163) P.C. Hemmer, L.C. Maximon and H. Wergeland, Phys. Rev. 111, 689 (1958).

164) A.N. Kolmogorov, Doklady Akad. Nauk SSSR 30, 299 (1941);
L.D. Landau, Doklady Akad. Nauk SSSR 44, 339 (1944);
C.C. Lin, The theory of hydrodynamic stability (Cambridge, 1955).

165) E. Fermi, J. Pasta and S. Ulam, Studies of non-linear problems I, Los Alamos Scientific Report LA-1940, 1955.

166) N.J. Zabusky and M.D. Kruskal, Phys. Rev. Letters 15, 240 (1965).

167) N.J. Zabusky, Phenomena associated with the oscillations of a non-linear model string (The Problem of Fermi, Pasta and Ulam), Proc. Conf. on Math. Models in the Physical Sciences (Prentice Hall, Englewood Cliffs, New Jersey, 1963).

168) F.M. Israelev and B.V. Chirikov, Dokl. Akad. Nauk SSSR 166, 57 (1966).

169) Yu.A. Berezin and V.I. Karpman, Zh. Eksper. Teor. Fiz. 51, 1557 (1966).

170) H. Hirooka and N. Saito, Computer studies on the approach to thermal equilibrium in coupled anharmonic oscillators, I, J. Phys. Soc. Jap. 26, 624 (1969); II, ibid, 27, 815 (1969).

171) M.D. Kruskal and N.J. Zabusky, J. Math. Phys. 5, 231 (1964).

172) P.L. Kapitsa, Uspekhi Fiz. Nauk 44, 7 (1951).

173) E.D. Courant, M.S. Livingston and H.S. Snyder, Phys. Rev. 88, 1190 (1952).

174) V.A. Ambartsumyan, Evolyutsiya sbezd i astrofizika (Erevan, 1947).

175) R.Z. Sagdeev, Collective processes and shock waves in rarefied plasma, Collection: "Voprosy teorii plasmy" (Atomizdat, 1964).

176) V.K. Mel'nikov, Dokl. Akad. Nauk SSSR 165, 1245 (1965); 181, 546 (1968).

177) P.C. Hemmer, L.C. Maximon and M. Wergeland, Phys. Rev. 111, 689 (1958).

178) V.D. Fedorchenko, B.N. Rutkevich and B.M. Cherny, Zh. Tekh. Fiz. 29, 1212 (1959).

179) J.R. Rees, Private communication, 1966.

180) J. Orban and A. Bellemans, Phys. Letters 24 A, 620 (1967).

181) G.N. Kulipanov, S.I. Mishnev and A.N. Skrinsky, Studies of stochastical instability of electron beam betatron oscillations in a storage ring, Report at International Accelerator Conference, Erevan, 1969.

182) E.M. Moroz, Thesis, Moscow, 1957.

183) H.M. Krushkal, Some estimates of separatrix destruction, Preprint, Novosibirsk, 1971.

184) G.V. Gadiyak and F.M. Israelev, Transitional zone of non-linear resonance, Preprint, Novosibirsk, 1970.

185) J. Ford and G.M. Lungsford, Phys. Rev. A1, 59 (1970).

186) F.M. Izraelev, Stochasticity investigations of oscillations of a string with quadratic non-linearity, Preprint, Novosibirsk, 1966.

187) F.M. Izraelev, A.I. Khisamutdinov and B.V. Chirikov, Numerical experiments with a non-linear chain, Preprint, Novosibirsk, 1968.

188) M.B. Antipov, F.M. Izraelev and B.V. Chirikov, Statistical test of a pseudo-random number generator, Preprint, Novosibirsk, 1967.

189) Ya.G. Sinai, Uspekhi Mat. Nauk 25, No. 2, 141 (1970).